Calibration Method for Space Charge Measurement of Ultra-High Voltage Insulating Systems

(超高圧絶縁系の空間電荷測定のための校正法)

January, 2025

Doctor of Philosophy (Engineering)

LI XIAOXIN

李　曉欣

Toyohashi University of Technology

別紙４－１（課程博士（英文））

Date of Submission（month day, year）: 1/6, 2025

Department of Electrical and Electronic Information Engineering	Student ID Number	D 205205	Supervisors	Yoshinobu Murakami(academic supervisor) Tomohiro Kawashima（co-supervisor)
Applicant's name	LI XIAOXIN			

Abstract（Doctor）

Title of Thesis	Calibration Method for Space Charge Measurement of Ultra-High Voltage Insulating Systems

The construction of long-distance power grids connecting large-scale renewable energy sources with demand areas is gaining momentum in Europe and Asia, increasing the demand for ultra-high-voltage DC cables to carry the submarine portion of the lines. When DC voltage is applied to insulators for a long period of time, an internal charge is generated, which becomes a space charge and distorts the internal electric field, which should be uniform, leading to dielectric breakdown in the worst case. In quality assurance testing at the final stage of manufacturing and development, evaluation has been based mainly on the presence or absence of dielectric breakdown, since there was no technology to measure the space charge of thick insulators. The pulsed electro-acoustic method uses an external sensor to detect acoustic signals generated by the interaction of a pulsed electric field and space charge, but has been used only for the evaluation of basic physical properties of thin samples, mainly due to sensitivity issues. The purpose of this paper is to construct a measurement system and develop a calibration method for charge and electric field distribution to realize space charge measurement in full-scale ultra-high voltage insulation systems.

Chapter I describes the background and purpose of the study. Chapter II describes the construction of the measurement system using a polymer insulator with a thickness of about 10 mm or more, which is similar to an ultrahigh-voltage insulation system. The conventional metallic acoustic coupler was replaced with a polymer one to improve the acoustic matching, and the sensitivity was increased about 5 times. The space charge of an 88 mm polyethylene sample, the thickest in the world in this category, was successfully measured.

In Chapter III, we developed a method for calibrating the charge distribution and electric field distribution of practical insulating systems. In the past, a bias voltage was applied to a sample with no internal space charge, and the acoustic signal generated from the electrodes alone was used as a reference waveform for calibration. However, in many cases, it is impossible to obtain a reference waveform for practical insulating systems because space charge is already present due to the manufacturing process and charging history. Therefore, we proposed a method of applying a time variation to the bias voltage and extracting only the components correlated with the bias voltage from the response signal to obtain a reference waveform. In addition, since the space charge may follow the bias voltage as the sample temperature increases, we proposed a method to decompose the bias voltage and response signal variations into frequencies and correlate them using only the frequency components that the space charge cannot follow. These methods enable calibration at arbitrary times, even for samples with inherently mobile space charge.

In Chapter IV, we examined the effects of baseline and sensitivity fluctuations, which are problematic when actual measurements are made over long periods of time, and discussed how to compensate for these fluctuations. We have shown that the signal intensity is low in measurements of thick insulators and that calculation errors due to fluctuations in the waveform baseline and sensitivity become apparent and uncalibratable, and we have proposed a method to correct all measured acoustic signals so that the fundamental theorem of electrostatic fields holds true. This method is shown to be capable of displaying the electric field distribution with an accuracy of about

0.1 kV/mm, or 0.5% of the average electric field of practical ultrahigh-voltage insulation systems.

Chapter V describes the results of space charge measurements on a cable with an insulation thickness of 10 mm as a demonstration of the proposed method. It is shown that stable analysis results can be obtained by frequency-resolved analysis even when the space charge fluctuates.

In Chapter VI, as a result of this thesis, it is shown that accurate space charge measurement is now possible in any phase during quality assurance testing of full-scale extra-high voltage insulation systems, and application developments are discussed.

別紙４－２（課程博士（和文））

2025 年 1 月 6 日

電気・電子情報工学専攻	学籍番号	第 205205 号
氏名	LI XIAOXIN	

指導教員	村上　義信(主指導教委員) 川島　朋裕(副指導教員)

論文内容の要旨　(博士)

博士学位論文名	超高圧絶縁系の空間電荷測定のための校正法

(要旨　1,200 字程度)

大規模再生エネルギー源と需要地を結ぶ長距離電力連系線の建設が欧亜で活発化しており，海底線部分を担う超高圧直流ケーブルの需要が増大している。絶縁体に長時間の直流電圧を印加すると内部帯電を生じ，空間電荷となって均一であるべき内部電界を変歪させ，最悪の場合絶縁破壊に至る。製造開発の最終段階で行う品質保証試験では，厚い絶縁体の空間電荷を測定する技術がなかったため，主として絶縁破壊の有無のみによる評価が行われてきた。パルス静電応力法は，パルス電界と空間電荷の相互作用で生じる音響信号を外部のセンサで検出するが，主に感度の問題から，薄い試料による基礎物性評価への利用に留まっていた。本論文は，実規模の超高圧絶縁系の空間電荷測定を実現するための測定系の構築と，電荷および電界分布の校正方法の開発を目的としている。

第I章は研究背景および目的を述べている。第II章では，超高圧絶縁系に近い10 mm程度以上の厚さを有する高分子絶縁体を試料とした測定系の構築を述べている。従来の金属製音響結合器を高分子に変更して音響整合を改善し，約5倍の感度を得た。また，この範疇としては世界最厚となる88 mmポリエチレン試料の空間電荷測定に成功した。

第III章では，実用絶縁系の電荷分布および電界分布の校正方法を開発している。従来は内部に空間電荷がない試料にバイアス電圧を印加し，電極のみから発生する音響信号を参照波形とした校正を行ってきたが，実用絶縁系では製造過程や課電履歴から，すでに空間電荷が内在し，参照波形の取得が不可能となることが多かった。そこで，バイアス電圧に時間変動を与え，応答信号の中からバイアス電圧と相関をもつ成分のみを抽出して参照波形を得る方法を提案した。加えて，試料温度が高くなるとバイアス電圧に追従して空間電荷が変動する可能性があるため，バイアス電圧と応答信号の変動を周波数分解して，空間電荷が追従できない程度の周波数成分のみを利用して相関させる方法を提案した。これらにより，移動しやすい空間電荷が内在する試料でも，任意の時刻に校正を実施できるようになった。

第IV章では，実際に長時間に亘る測定を行ったときに問題となる基線と感度の揺らぎの影響を調べ，その補正方法について検討している。厚い絶縁体の測定では信号強度が低く，波形の基線と感度の揺らぎによる計算誤差が顕在化して校正不可能となることを示し，測定した全ての音響信号について，静電界の基礎定理が成立するように補正する方法を提案している。これにより，実用超高圧絶縁系の平均電界の0.5%にあたる0.1 kV/mm程度の精度で電界分布を表示できることを示した。

第V章では，提案法の実証実験として，絶縁厚10 mmを有するケーブルの空間電荷測定を行った結果を述べている。空間電荷が変動する場合でも，周波数分解解析により安定した解析結果が得られることを示した。

第VI章では，本論文の成果として，実規模超高圧絶縁系の品質保証試験中のどのような局面においても正確な空間電荷測定が可能となったことを述べ，応用展開について論じている。

Contents

Calibration Method for Space Charge Measurement of Ultra-High Voltage Insulating Systems（超高圧絶縁系の空間電荷測定のための校正法）

Chapter I

Introduction

In Chapter I, the background of this research will be discussed. The chapter starts with Positioning of space charge measurement in electrical insulation, followed by a brief introduction about the development of HVDC cable and the reasons behind space charge generation inside insulation materials and its effects on these insulation materials. In addition, the historical development of space charge measurement methods with spatial resolution is presented, as well as an overview of the pulsed electroacoustic (PEA) method and issues related to the use thereof, followed by the practical issues related to space charge measurement on thick insulating systems.

1.1 Positioning of space charge measurement in electrical insulation

In recent years, the dramatic growth in demand for electricity and the expanding range of human activities have also accelerated the need for long-distance power transmission, power trading between asynchronous AC grids, and the integration of renewable energy sources. In this context, high voltage direct current transmission (HVDC),which is used for high-power transmission utilizing stable direct current, which has advantages in long-distance, high-capacity transmission, asynchronous interconnection and long-distance traversal of submarine cables due to its non-inductive and non-capacitive reactance, as well as the advantages of large line transmission capacity, low loss, asynchronous operation of AC systems on both sides, has been steadily researched and developed over the past century and is now recognized as a viable option. In recent years, an increasing number of high-voltage direct current transmission projects have been commissioned or are under consideration around the world [1]-[5].

For example, the Hokkaidō–Honshū HVDC Link, Japan's first direct current transmission facility, directly interconnects the Hokkaido and Honshu power grids to form the Kanto Regional Power Circle and to achieve stable operation over a large area of Japan. The Hokkaidō–Honshū HVDC Link is especially significant in Hokkaido, where electricity consumption is high in winter, and in Honshu, where electricity consumption is high and peaks are unstable in summer [6].

Another HVDC transmission system in Japan, the Kii Channel HVDC system, connects Shikoku with Honshū. As both Electric Power Transmission and Distribution of Kansai and Shikoku use a 60 Hz power frequency, AC transmission is also possible. However, DC transmission is used as AC transmission can create loops in the power system, leading to some control problems. In addition, DC transmission is less expensive to construct [7].

For example, outside of Japan, in a country as vast as China, most of the centers of economic development are currently located in the eastern coastal regions, where electricity consumption is much higher than in the central and western regions. This uneven distribution of electricity use has caused localized power shortages, leading to shutdowns at many companies, including, for example, Japanese-owned factories. In order to improve this situation, China has developed a transmission program called “West-East Power Transmission. The western region contains a large amount of hydroelectric and coal resources, and has a low demand for energy due to its small population and relatively underdeveloped economy. Therefore, developing the hydropower and coal resources in the western region for the purpose of generating and transmitting electricity to the eastern region will not only alleviate the problem of power shortage in the eastern region, but also help to alleviate the pressure of the increasing environmental pollution in the eastern coastal region, and make full use of the natural resources in the western region [8].

As a key part of the long-distance power transmission mentioned in the above example, insulation materials play a vital role in ensuring the safe operation of DC high-voltage cables. Generally speaking, the higher the transmission voltage, the lower the power transmission loss in a particular transmission situation. However, the higher the transmission voltage, the higher the requirements for cable insulation materials. Compared to low-voltage cables, high-voltage cable insulation materials need to withstand higher electric field strengths and be less sensitive to space charge buildup and temperature dependent resistivity.

Cross-linked polyethylene (XLPE), as a cable insulation material suitable for power transmission, transforms the molecular structure of polyethylene into a meshed molecular structure. For this purpose, thermoplastic polyethylene is crosslinked through chemical or physical methods, which greatly improves its heat resistance and mechanical properties, reduces its shrinkage and increases its maximum operating temperature, and maintains its excellent electrical properties. XLPE has the advantages of simple structure, light weight, good resistance, high load capacity and high mechanical strength.

In addition, the magnitude of the local electric field strength in XLPE insulation is also affected by the space charge density. As shown in Fig. 1-1, when there is space charge inside the cable insulation, or when space charge is easily generated due to defects in the insulation material, the electric field distribution will be significantly distorted. When the charge density in XLPE insulation is too high, the local field strength will be higher than the breakdown field of XLPE, resulting in local bond breaking, and the accumulation of space charge will eventually cause insulation aging at low field strengths, resulting in insulation defects and possibly electrical breakdown.

From a technical point of view, the generation and accumulation of space charge in XLPE insulated cables during HVDC transmission is the most important problem to be solved.

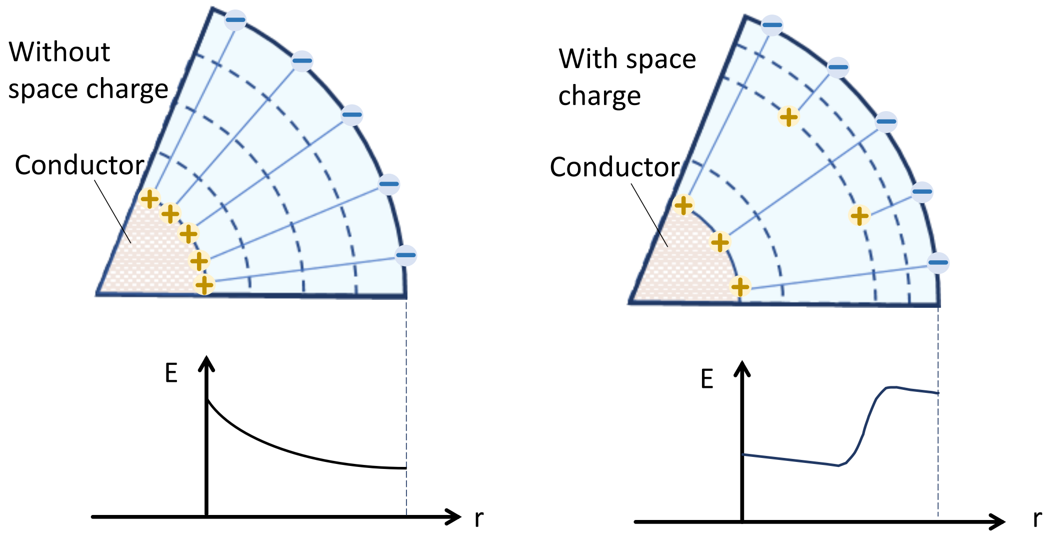

Fig. 1-1 Conceptual illustration of the distortion of the electric field distribution. The broken lines are equipotential lines.

The problem of space charge in cable insulation first arose in 1978 during a submarine cable project in Japan, when excessive space charge build-up led to cable insulation breakage and an electrical accident [9], Space charge is usually defined as the free charge that is trapped locally in the polymer, or the interfacial polarization charge that results from uneven polarization.

There are reasons for space charge to be generated, which are shown in the following.

A. Space charge formed by electrode injection under high electric field

Due to the influence of the applied electric field and polarization, the potential barrier for electrons or holes to escape from the electrode is lowered, causing electrons or holes to migrate under the action of the electric field. During this migration, they can be captured by traps, forming space charge. Traps, acting as centers of attraction for charges, can form anywhere in the molecular structure where there is a local minimum in the potential energy, such as due to impurities, chain breaks, or bonds composed of different atoms. Typically, at electric field strengths above 10 kV/mm, charge injection occurs on almost all the conductor-insulation interfaces, and the accumulation of space charge increases with the field strength and duration of application. This type of space charge, which usually occurs under high electric field applications, is typically homopolar charge [10] - [11].

B. Space charge formed by dissociation of impurity ions such as cross-linked by-products

XLPE, which is often used as cable insulation material, contains impurities such as catalysts, antioxidants and voltage stabilizers, as well as cross-linking agents and cross-linking byproducts. These impurities decompose into positive charges and electrons under the action of an external electric field, move to the cathode and anode respectively, and form space charges in the insulation material. This space charge formed by cross-linking byproducts and impurities is a heterogeneous charge [12].

C. Polarized charge due to dipole turning

The dipoles tend to disperse on the surface of the insulation material and form bound charges, which induce an equal amount of anisotropic charge on the electrode surface, changing the local electric field at the interface between the insulation material and the electrode. Noting that it is noy space charge according to most definitions but bound charge. But during the PEA measurement, the signal causing by it seems to have a similar shape with the space charge [13].

It can be seen that in DC voltage transmission, the accumulation of space charge is common in cable insulation materials. This leads to local field distortion, and the strength of the distorted electric field can be as high as several times that of the external electric field, which is an important reason for the breakdown of cable insulation at rated voltage and causing serious accidents. In addition, space charge is considered to be one of the causes of polymer aging. During the operation of the cable, the participation of electrical aging and thermal aging makes it easier for space charge to accumulate inside the cable. With the increase of aging time, the space charge injected and accumulated in the insulation material gradually migrates into the insulation and causes distortion of the internal field strength [14].

1.2 Historical development of space charge measurement methods with spatial resolution

Space charge limits the application of polymer insulation materials in high-voltage DC cables. Therefore, the accumulation mechanism and suppression strategies of space charge, including the interface properties of semiconductor-insulating materials, the interface properties of semiconductor-insulating materials in corresponding polymer insulated cables, the influence of temperature gradient on the generation of space charge and the accumulation process of space charge, have been the focus of research [15]-[16]. Among them, the measurement of space charge is regarded as a key link in improving the properties of insulation materials.

Considering the relevance of the space charge phenomenon, many space charge measurement methods have been developed and practiced since 50 years ago. At first, most of the measurement methods were destructive to the insulating material because they needed to be cut mechanically before measuring the internal space charge [17].

Over the past 40 years, methods have been developed to measure space charge in solid insulating materials using, electron beams, thermal pulse method, pressure wave method and voltage wave method. Compared to the earliest sectioning methods, these latest techniques can be used to quantitatively measure space charge distribution in insulating materials non-destructively [18].

The electron beam method was proposed in the late 1970s. It uses an electron beam as an excitation source to irradiate solid samples with a stepped energy level electron beam. In the irradiated area of the material, the conductivity of the sample increases, and the space charge in this area is compensated. The electron beam acts as a virtual probe. Under short-circuit conditions or when a biased DC voltage is applied, the induced charge on the back electrode will be released with each increase in the electron beam energy. Depending on the thickness of the sample penetrated by the electron beam, the distribution of the space charge in it can be measured.

The thermal pulse method was proposed in the mid-1970s. By irradiating a metallized sample with a light pulse, the light pulse is absorbed by the sample surface and converted into heat energy. The heat energy diffuses into the sample body, generating a temperature distribution on the sample that varies with time. The thickness and dielectric constant of the sample also vary with temperature. Since the surface potential on the metallized sample electrode varies with time, the spatial charge distribution in the sample can be obtained by deconvolution [19].

The pressure wave method was proposed in the late 1970s [20]. Pressure waves can be generated by lasers, shock wave tubes or piezoelectric devices. When pressure waves propagate in the sample, the material will locally experience uneven deformation, the space charge will undergo a slight displacement, and the dielectric constant will also change. The charge distribution density can be calculated by using the relationship between the voltage and current measurements applied to the sample and the internal field strength using deconvolution [21].

The thermal step method (TS) was used for the measurement of full-scale cable. This method relies on applying a thermal step to the insulator to temporarily maintain the charge still, which affects the amount of charge on the interface, and leads a current signal occur. The current signal is used in the deconvolution process and being amplified, for the acquisition of the connection between the space charge density and cylindrical coordinates [22].

The thermal step method (TS method) was used to measure full-scale cables. In this method, a thermal step is applied to the outside of the cable to produce thermal diffusion and the displacement of charge due to thermal expansion is measured as a current flowing in an external circuit. This current signal is subjected to the deconvolution process to obtain the charge density distribution along the radial direction.

1.3 Overview and issues of pulsed electroacoustic method

As one of the commonly used methods today for space charge measurement, the pulsed electroacoustic (PEA) method was developed in 1987 by Takada [23]. The principle is shown in Fig. 1-2. In this measurement method, a DC voltage and a pulse voltage with given characteristics are applied to the sample through an external circuit. The pulse voltage generates a corresponding pulse electric field in the sample, which vibrates the charge and generates a corresponding acoustic wave. The acoustic wave then reaches the piezoelectric transducer polyvinylidene fluoride (PVDF), which outputs an electrical signal proportional to the space charge in the sample. The PEA method has been widely used for the measurement of space charge in cable. The conventional typical PEA method has a spatial resolution of > 10 μm, and it is suitable for the measurement of film specimen > 50 μm. Using a deconvolution process facilitated one of the first implementations of the PEA method for a resolution as high as 2 μm [24].

For a sample free from space charge, the pressure wave generated by the PEA method is shown as Fig. 1-1 (a). The static Maxwell stress P_M generated at the electrodes under the DC high voltage can be presented as

$$P_M = \frac{1}{2}\varepsilon(\frac{V_{DC}}{d})^2 \quad (1\text{-}1)$$

Where ε is the conductivity (F/m) and d is the thickness (m) of the specimen. The pressure P_M acts in the direction of attraction between the electrodes. This pressure e caused by DC voltage will not be generated in a long time after the DC voltage application. When a pulse voltage is applied during the DC voltage application, the Maxwell stress $p(t)$ can be expressed as

$$p(t) = \frac{1}{2}\varepsilon\left(\frac{V_{DC}+v_p(t)}{d}\right)^2 = \frac{1}{2}\varepsilon(\frac{V_{DC}}{d})^2 + \varepsilon\frac{V_{DC}}{d}\frac{v_p(t)}{d} + \frac{1}{2}\varepsilon(\frac{v_p(t)}{d})^2 \quad (1\text{-}2)$$

For this Equation, the first component is the static Maxwell stress, and the second and the third components are dynamic Maxwell stress which change with time and generate pressure waves in pulse shape when the pulse voltage is applied.

The specimen with space charge is shown in Fig. 1-2(b). For simplicity of presentation, a specimen with space charge distributed inside, density $\rho(z)$ (C/m3) and thickness Δz (m) is used as an example. When a pulsed voltage $V_p(t)$ is applied, a pressure wave is generated and propagates in two directions. The space charge induced at positions $z = 0$ and $z = d$ can be expressed by the following equations,

$$\sigma(0) = -\varepsilon\left(\frac{V_{DC}}{d}\right) - \frac{d-z}{d}\rho(z)\Delta\text{z} \quad (1\text{-}3)$$

$$\sigma(d) = +\varepsilon\left(\frac{V_{DC}}{d}\right) - \frac{z}{d}\rho(z)\Delta\text{z} \quad (1\text{-}4)$$

The equations show that the dynamic Maxwell stress acts on $\sigma(0)$, $\sigma(d)$ and $\rho(z)\Delta z$, and generates a pressure wave at each part inside the sample under the pulse voltage $V_p(t)$.

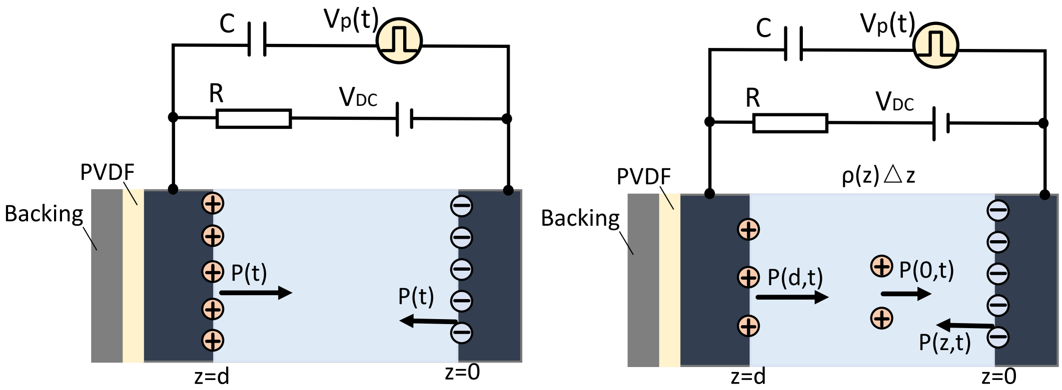

(a) (b)

Fig. 1-2 Conceptual illustration of PEA method.

A piezoelectric (PVDF) transducer attached to the specimen receives the pressure wave generated by the interaction of a pulsed electric field and a space charge and converts it into an electrical signal. The PVDF used in the measurement is a transducer that generates a potential difference at both ends generated by an external pressure in the thickness direction, by which the potential difference caused by the space charge can be obtained. However, the signal obtained directly from the PEA method does not correctly represent the space charge distribution because it contains distortions due to the applied pulse voltage, as well as distortions caused by the acoustic and electric characteristics of the PVDF and the measurement system, and therefore a calibration process is required to recover the signal.

In the calibration, deconvolution is seen to be an important part for signal processing, it is to calculate the output waveform by the system transfer function of the measurement system. This processing is shown below.

Representing the input signal as $x(t)$, the output signal as $y(t)$ and the system impulse response as $g(t)$. In the condition that the system is a linear time invariant type, the equation bellows is established,

$$y(t) = \int_{-\infty}^{+\infty} g(t-\tau)\, x(t) dt \qquad (1\text{-}5)$$

After the Fourier transformation, equation (1-5) can be represented as

$$Y(\omega) = G(\omega)X(\omega) \qquad (1\text{-}6)$$

Where $Y(\omega)$, $G(\omega)$ and $X(\omega)$ correspond to $y(t)$, $g(t)$ and $x(t)$, in addition, the $G(\omega)$ stands for the transfer function of the system. Besides, the applied pulse voltage is considered as $v(t)$, the space charge accumulates inside the insulation material as $\rho(t)$, both can be observed at oscilloscope. So, the equation below can be established.

$$y(t) = g(t)\rho(t) \qquad (1\text{-}7)$$

After the Fourier transformation, the connection between input signal and output signal can be represented in the frequency domain, shown as

$$V(\omega) = G(\omega)\rho(\omega) \qquad (1\text{-}8)$$

According to Equation (1-8), the transfer function $G(\omega)$ can be acquired for the condition that space charge does not exist inside the insulation material. In this condition, the induced charge at the electrodes can be represented as σ_0, the pressure waves generated at electrodes can be obtained by the convolution results of σ_0 and the pulse voltage applied. So, the measured space charge at the electrodes ρ_r is shown as

$$\rho_r(t) = a\sigma_0 v_p(t) \qquad (1\text{-}9)$$

Where a is constant, and the values of integral of $\rho_r(t)$ and the σ_0 is the same. Therefore, the voltage signal obtained in condition that the insulation material is free from space charge is shown as

$$v_r(t) = g(t)\rho_r(t) \qquad (1\text{-}10)$$

The transfer function of the system $G(\omega)$ can be obtained in the frequency domain by Fourier transform as

$$G(\omega) = {}^{v_r(\omega)}\!/_{\rho_r(\omega)} = {}^{bv_r(\omega)}\!/_{v_p(\omega)} \qquad (1\text{-}11)$$

where $b = \frac{1}{a\sigma_0}$, $\rho(\omega)$ can be represented as

$$\rho(\omega) = v_p(\omega)({}^{a\sigma_0 v(\omega)}\!/_{v_r(\omega)}) \qquad (1\text{-}12)$$

By the inverse Fourier transform for $\rho(\omega)$, the space charge distribution in the time domain $\rho(t)$ can be calculated. Moreover, the spatial distribution of the space charge along the position axis can be calculated using the speed of sound of the insulation material.

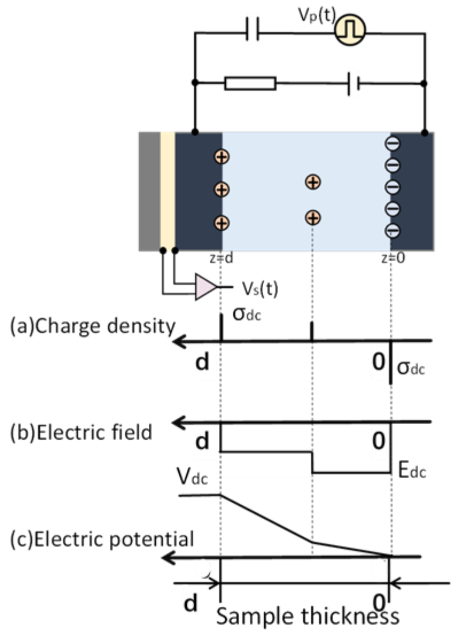

Fig. 1-3 Results of calibration process (conceptual graph).

By integrating the space charge signal in the direction of the specimen thickness, the electric field distribution inside the specimen can be obtained, and the potential distribution can be obtained by further integration, as shown in Fig. 1-3.[25]-[28]

1.4 Practical issues related to space charge measurement of thick insulating systems

As a commonly used method of space charge measurement, a basically complete system has been established in recent years for the measurement of space charge in film specimens with a thickness of less than 1 mm using the pulsed electroacoustic method (PEA). However, when measuring insulating materials with a thickness of more than 1 mm, the sensitivity decreases significantly. Therefore, during the development of high-voltage DC insulation systems, measurements are usually made on thin film specimens with a thickness of up to 1 mm in order to characterize the space charge distribution. However, since the proportionality law for insulation properties often does not hold, it is necessary to use full-size insulation specimens (typically >10 mm thick) to confirm the space charge distribution. Regarding the measurement of thick insulating materials, some pioneering researchers have attempted to increase the strength of the signal by increasing the intensity of the applied pulse voltage, for example. At the same time, some researchers have focused on the propagation characteristics of acoustic signals in insulating materials, and have investigated, in particular, the characteristics of attenuation and velocity dispersion that occur when acoustic waves propagate through them [29]. Specific examples will be given in Chapter II. However, experience with space charge measurements on full-size UHV DC insulation systems is still very limited, and measurements on the cables themselves have only recently reached a satisfactory level of accuracy. Therefore, it is unlikely that the problem of measuring insulation materials such as junction boxes, which are even thicker than the cable body, can be solved by extending existing measurement methods.

Measurement of insulation materials thicker than 10 mm requires an improvement of the measurement system itself to overcome the problem of reduced sensitivity.

The author is conducting research on the measurement of space charge in full-scale thick insulators, mainly ultra-high voltage power cables, and has obtained the following results.

(1) Methods to efficiently apply the pulse voltage necessary for measurement

(2) Increasing the sensitivity and miniaturization of the measurement system using polymer acoustic couplers

(3) Correction of the frequency response of the measurement system

In addition, application research is being conducted in cooperation with the Central Research Institute of Electric Power Industry and power cable manufacturers to test full-scale ultra-high-voltage cables.

On the other hand, the calibration method for accurately estimating charge distribution and electric field distribution in insulators has been based on the method used for film samples, and some electro statistically inconsistent results have been obtained. The work described in this PhD thesis was aimed at analyzing the problems of measurement and calibration in full-scale insulating systems and proposing a calibration method that is as accurate as possible without the need to prepare special samples for calibration.

1.5 The organization of the thesis

This thesis contains 6 chapters, as shown below.

Chapter I is an introduction to the background of the study, which briefly describes the practical significance of space charge measurements for power insulation systems, the history of the development of space charge measurements in terms of their generation and the impact they have brought about, and a brief description of the PEA method and the principle of deconvolution. At the same time, it is illuminated that in the measurement of practical insulation systems, the existing measurement system is not applicable to the thickness of insulation materials in practical scale.

Chapter II describes a proposed PEA measurement system using a non-metallic acoustic coupler for the measurement of space charge in thick insulating materials. Both hardware and software configurations of the system are described and experimental results are presented to demonstrate that the maximum thickness of the insulating material that can be measured has been increased to 88 mm.

Chapter III describes lock-in calibration, waveform correlative method and frequency-resolved analysis calibration. In this study, by considering the various measurement environments, the author provides multiple calibration methods. This chapter compares the three new calibration methods with the established conventional one and experimentally verifies the methods for practicality.

Chapter IV discusses methods to reduce the fluctuations in the offset and tilt of the baseline of the response signal caused by the spike noise generated by the application of a high-voltage pulse, using as an example the measurement results of a parallel-plate electrode insulation system.

Chapter V shows actual measurements of a cross-linked polyethylene cable with an insulation thickness of 10 mm using the method proposed in Chapter III, which decomposes the changes in bias voltage and response signals into a spectrum over a frequency range suitable for analysis and extracts a reference waveform based on the correlation. The measurements were performed at room temperature and at high temperature (conductor temperature 90°C).

Chapter VI provides some thoughts on the future direction of the research.

1.6 References

[1] G. Chen, M. Hao, Z. Xu, A. Vaughan, J. Cao and H. Wang, "Review of high voltage direct current cables," in CSEE Journal of Power and Energy Systems, vol. 1, no. 2, pp. 9-21, June 2015.

[2] K. N. Mathes, “A brief history of development in electrical insulation,” Proceedings of the 20th Electrical Electronics Insulation Conference, pp. 147-150, 1991.

[3] J. Zhao, P. Zhao, Z. Chen, B. Ouyang and Z. Xinlong. “Development of Insulation Material for HVDC Cables[J]”. High Voltage Engineering, 43(11), pp. 3490-3503, 2017.

[4] Y. Zhao, G. Liu, Y. Xie, J. Huang and N. Zhu “Space charge behaviour of retired high-voltage XLPE cables[J].” Electric Power Engineering Technology, 39(3), pp. 151-157, 2020.

[5] B. Ouyang, J. Zhao, H.Li and J. Li “Influence of crosslinking by-products on dielectric and mechanical properties of XLPE cable insulation[J]”. Insulating Materials, 48(5), pp. 31-34, 2015.

[6] M. Sampei. “Innovation on Energy Power Technology (8): First HVDC Transmission System in Japan”, IEEJ Trans. B, Vol. 128, No.7, pp. 908-911, 2008.
三瓶 雅俊.「電力技術のイノベーション（8）日本初の直流送電」. 電気学会論文誌B（電力・エネルギー部門誌） 128 (7), pp. 908-911, 2008.

[7] 齊藤 紀彦, 高島 弘, 布施 和夫.「紀伊水道直流送電プロジェクト」. 電気学会論文誌B（電力・エネルギー部門誌） 118 (9), pp. 927-930, 1998.

[8] 田島 俊雄. 光陰似箭「西電東送」と貴州省電力事情. 中国研究月報 Monthly journal of Chinese affairs. 62(9) (通号 727), pp. 49-51, 2008.

[9] L. Zhou, M. Wang and Y. Zhou. Deterioration condition evaluation of XLPE cable insulation by dielectric spectroscopy [J]. Insulating Materials, 2019, 52(1): 52-56.

[10] G. Li, S. Li, D. Min, N. Zhao and Y. Zhu, "Influence of trap depths on space charge formation and accumulation characteristics in low density polyethylene," 2013 IEEE International Conference on Solid Dielectrics (ICSD), Bologna, Italy, pp. 698-701, 2013.

[11] T. Takahashi, H. Miyata, T. Nakatuka and A. Yokoyama. “Some factors for the space charge formation in polyethylene”, IEEJ Trans. A, Vol. 115, No.5, pp. 430-436, 1995.
高橋 享, 宮田 裕之, 中司 徹, 横山 綾子.「ポリエチレンの空間電荷形成に及ぼす因子」. 電気学会論文誌. A 115 (5), 430-436, 1995.

[12] Y. Zhao, S. Zheng, D. Liu and X. Yan, "Study on Space charge Transport and accumulation characteristics of XLPE Cable during DC Operation," 2022 IEEE 5th International Electrical and Energy Conference (CIEEC), Nangjing, China, pp. 3514-3519, 2022.

[13] O. Gallot-Lavallee, G. Teyssedre, C. Laurent and S. Rowe, "Space charge and orientational polarization within epoxy as probed by the Pulsed Electro-Acoustic technique," 2003 Annual Report Conference on Electrical Insulation and Dielectric Phenomena, Albuquerque, NM, USA, pp. 249-252, 2003.

[14] M. S. Khalil, A. Cherifi, A. Toureille and J. -P. Reboul, "On effects of variation of polarizing temperature and additive content on space charge formation and electric field distribution in plain LDPE and LDPE doped with BaTiO/sub 3/ additive: evidence from measurements using the thermal step method," Proceedings of 1995 IEEE

5th International Conference on Conduction and Breakdown in Solid Dielectrics, Leicester, UK, pp. 288-292, 1995.

[15] H. Li, L. Xu, T. Liu and Z. Yang. “Summarization of space charge suppression methods in DC XLPE cable insulation.” Electric Power Engineering Technology, 40(5), pp. 54-62, 2021.

[16] W. Wang, S. Li. “Research status and development of insulation breakdown in engineering solid dielectrics[J].” Chinese Science Bulletin, 65(31), pp. 3461-3474, 2020.

[17] J. Lewiner, "Direct determination of space charge distributions in dielectrics: the pressure wave propagation method," IEEE 3rd Int’l. Conf. Conduction and Breakdown in Solid Dielectr., pp. 548-554, 1989.

[18] R. Liu, C. Törnkvist, and M. Jeroense, Space Charge Measurement Technologies and Their Potential Applications, Sens. Mater., Vol. 29, No. 8, p. 1089-1098, 2017.

[19] A. Imburgia, R. Miceli, E. R. Sanseverino, P. Romano and F. Viola, "Review of space charge measurement systems: acoustic, thermal and optical methods," in IEEE Transactions on Dielectrics and Electrical Insulation, vol. 23, no. 5, pp. 3126-3142 2016.

[20] P. Laurenceau, G. Dreyfus, and J. Lewiner, New Principle for the Determination of Potential Distributions in Dielectrics, Physical Review Letters, vol.38, issue.1, pp.46-49, 1977.

[21] G. Teyssedre, C. Villeneuve, P. Pons, K. Makasheva and B. Despax. “Challenges in probing space charge at sub-micrometer scale[C]”, 2012 Annual Report Conference on Electrical Insulation and Dielectric Phenomena. Montreal, Canada: IEEE, pp. 234-237, 2012.

[22] P. Notingher, S. Agnel and A. Toureille, “Thermal step method for space charge measurements under applied dc field,” in IEEE Transactions on Dielectrics and Electrical Insulation, vol. 8, no. 6, pp. 985-994, Dec. 2001.

[23] T. Takada, T. Maeno and H. Kushibe, "An Electric Stress-Pulse Technique for The Measurement of Charges in A Plastic Plate Irradiated by an Electron Beam," IEEE Trans. Electr. Insul., Vol. 22, No. 4, pp. 497-501, 1987.

[24] T. Maeno, K. Fukunaga. “High-resolution PEA charge distribution measurement system[J].” IEEE Transactions on Dielectrics and Electrical Insulation, 3(6), pp. 754-757, 1996.

[25] Y. Li: “Space charge measurement in lossy solid dielectric materials by pulsed electroacoustic method,” Ph. D thesis, Musashi Institute of Technology, 1994.
李 英.「パルス静電応力法による損失固体誘電体中の空間電荷分布測定に関する研究」: [D].武蔵工業大学, 1994.

[26] B. Vissouvanadin, T. T. N. Vu, L. Berquez, S. L. Roy, G. Teyssèdre and C. Laurent, "Deconvolution techniques for space charge recovery using pulsed electroacoustic method in coaxial geometry," in IEEE Transactions on Dielectrics and Electrical Insulation, vol. 21, no. 2, pp. 821-828, April 2014.

[27] Technical Committee for Investigation of Space Charge Distribution Measurement Methods and Standardization of Dielectric and Insulating Materials, “Space Charge Distribution Measurement Methods and Standardization for Dielectric and Insulating Materials”, IEEJ Technical Report, No. 834, 2001.
誘電・絶縁材料の空間電荷分布計測法と標準化調査専門委員会.「誘電・絶縁材料の空間電荷分布計測法と標準化」, 電気学会技術報告, 第 834 号, 2001.

[28] Technical Committee for Investigation of Space Charge Distribution Measurement Methods and Standardization of Dielectric and Insulating Materials, “Standardization of Calibration and Advanced Measurements of Space

Charge Distribution at High Temperature Using the Pulsed Electro-acoustic Method," IEEJ Technical Report, No. 1491, 2020.
誘電・絶縁材料の空間電荷分布計測法と標準化調査専門委員会.「高温下における PEA 法を用いた空間電荷分布測定の校正法標準化と PEA 法の応用測定技術」, 電気学会技術報告, 第 1491 号, 2020.

[29] J.O. Parra, C.L. Hackert, R. Ababou, M.J. Sablik, "Dispersion and attenuation of acoustic waves in randomly heterogeneous media", Journal of Applied Geophysics, Vol.42, Issue 2, pp. 99-115, 1999.

Chapter II

Measuring system for thick insulation systems

Space charges are usually formed inside the insulation when high DC voltage is applied [1]. The localized accumulation of space charges is considered to be one of the main reasons for the degradation of the insulating properties of materials [2]. As a countermeasure, the generation of space charges is usually suppressed by means such as the addition of nanofillers to the insulating material [3]. During the development of high-voltage DC insulation systems, thin-film specimens with a thickness of up to 1 mm are usually measured to characterize the space charge distribution. Since the law of similarity for insulating properties often does not hold so that the insulation properties change when it goes to thick specimen such as full-scaled cables, it is necessary to confirm the space charge distribution by using full-size insulating specimens with thicknesses typically greater than 10 mm [4]-[7]. In relation to measurements of thick insulating materials, Fukuma et al. measured a 27 mm thick insulating material using a 7 kV pulse voltage to increase signal strength [8]. Ozaki et al. analyzed acoustic propagation in insulating materials, suggesting the need to consider velocity dispersion in addition to attenuation [9]. However, the experience of space charge measurements on full-scale ultra-high-voltage DC insulation systems is limited, and satisfactory accuracy has only recently been achieved for the cable itself. Although there is hope for successful measurements on thicker cable junction boxes, it is unlikely that this can be solved by extending the measurement methods established so far.

The signal strength obtained by the pulsed electro-acoustic (PEA) method is roughly proportional to the DC field formed by the space charge and the probing pulsed electric field. As a result, the signal strength is inversely proportional to the square of the specimen thickness as the attenuation inside the thick specimen cannot be ignored. The thicker the specimen it is, the smaller the acoustic signal will be [10]-[12]. Therefore, some improvements to the measurement system are needed to overcome the problem of reduced sensitivity. As the signal intensity strongly relates to the pulse voltage, enhancing the pulse voltage maybe can be considered as a solution, however, the high pulse voltage application is difficult to achieve. On the other hand, high pulse voltage may cause strong noise which is hard to avoid.

In this chapter, a PEA space charge measurement system for thick insulating materials with a polymer acoustic coupler is presented. The PEA device presented in this chapter allows direct measurement on insulation materials larger than 10 mm, thus making insulation performance measurements possible for full-size insulation systems such as high-voltage DC cables and GIS. The new equipment utilizes non-metallic acoustic couplers (e.g., polystyrene) with acoustic impedance close to the specimen to improve acoustic matching and sensitivity. In this chapter, the improvements made to the sensitivity of the PEA unit are discussed, to allow stable data acquisition and analysis. The author will improve the sensitivity by several direction: (1) to increase the frequency of the applied pulse voltage; (2) to use polymer acoustic coupler with similar acoustic impedance as specimen; (3) to change backing material.

2.1 Hardware

2.1.1 Pulse generator

An improved pulse generator which can provide pulse voltages in high repetition rate was used in the measurement system for improving the signal accuracy, the circuit is illustrated in Fig. 2-1. By using an appropriate square wave to excite the circuit, a pulse with an amplitude of up to 1 kV can be generated, and the wave width can be changed within the range of 300 ns ~ 1 μs by adjusting the excitation circuit. The maximum pulse generation frequency is 5000 cycles per second. The improved pulse generator makes it possible to increase the averaging times for noise reduction.

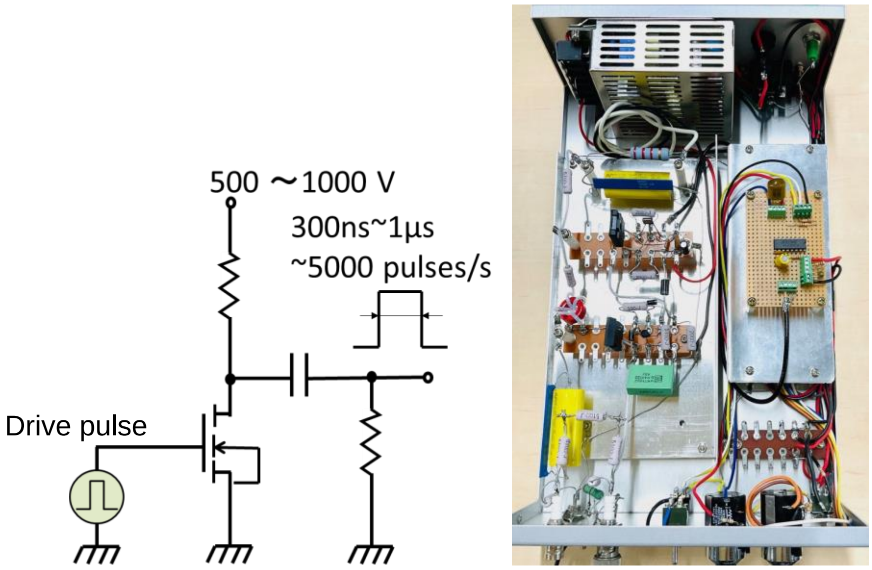

Fig. 2-1 Circuit of pulse generator.

2.1.2 Measuring cell

To maximize the measurement sensitivity of a PEA system, the acoustic matching within the system structure needs to be considered. However, there are other factors that may not always result in optimal acoustic conditions. For example, thick metal block electrodes are often used as acoustic couplers for electromagnetic shielding in order to escape strong spike noise. In many cases, the acoustic impedance of the polymer material being measured as a specimen is much smaller than that of the metal, so that most of the acoustic power generated inside the specimen will be reflected at the interface between the specimen and the metal electrodes, with only a very small portion reaching the transducer. In addition, when using polymer-based piezoelectric transducers, the interface between the transducer and the metal electrode produces negative reflections, which may further reduce the intensity of the acoustic power detected by the transducer.

The acoustic signal propagation of the newly proposed PEA cell structure is compared with the conventional structure in Fig. 2-2. The use of acoustically transparent polymers, such as polystyrene, as acoustic couplers improve the acoustic matching between the specimen and the transducer, resulting in high sensitivity. Although a thin metal electrode is required between the acoustic coupler and the specimen, it is negligible from an acoustic point of view because it is sufficiently thin compared to the shortest wavelength in the acoustic signal component. Therefore, an 11 μm thick aluminum foil was used as the electrode in this device. Also, when heavy metals such as brass or lead are used as backing materials, the acoustic signal that passes through the PVDF film will be directly reflected, thereby approximately doubling the sensitivity.

Assuming that the acoustic parameters are as shown in Fig. 2-2, a system using a non-metallic acoustic coupler produces 4 to 5 times the signal strength of a conventional system using a metallic coupler. The measurement system is illustrated in Fig. 2-3. Silicone oil was used for acoustic matching between each layer. The specimens were found to be internally charged at the time of manufacture. The hot end of the pulse generator was connected to the lower electrode, and the DC feed line was used as the coupling impedance for the pulse voltage. This connection has the advantage that the coupling capacitor can be omitted, but protection is necessary because if the specimen is breakdown, the effect will spread to the measurement system.

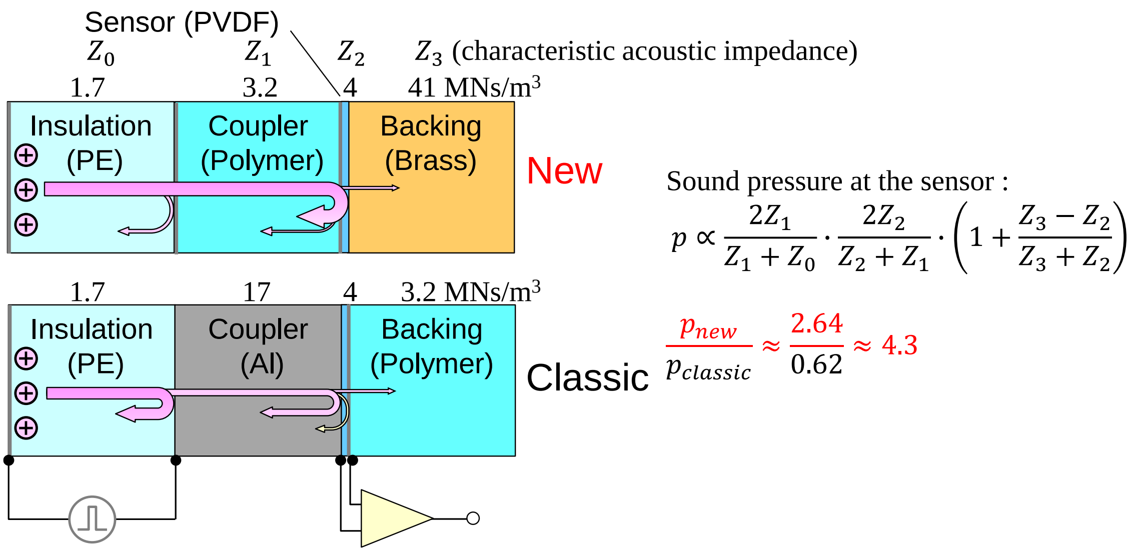

Fig. 2-2 Propagation of the acoustic signal power of the PEA method.

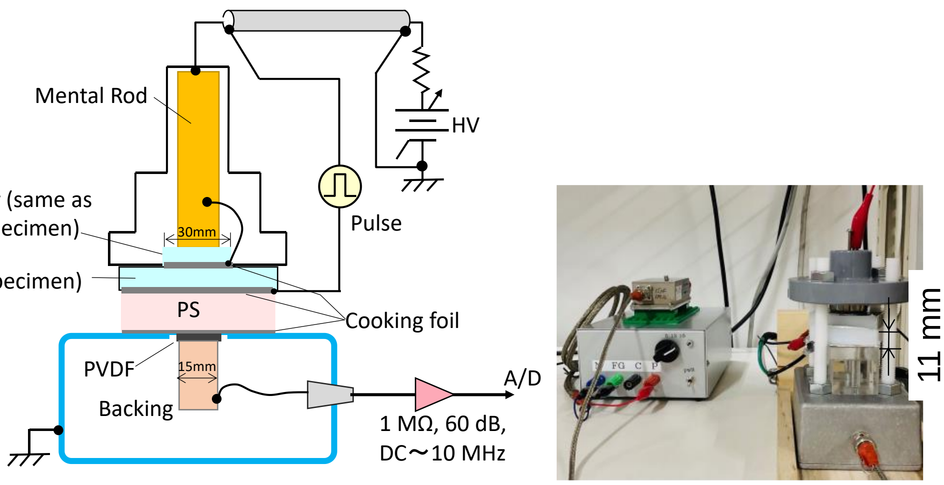

Fig. 2-3 Space charge measurement system for thick specimen

Figure 2-4 illustrates the modification based on the use of a polymer acoustic coupler in the previous section 2.1.2. The figure depicts the acoustic pressure signal detected when the thickness of the PVDF sensor is 100 μm and the acoustic pressure pulse is a square wave of 400 ns width. To simplify the calculations, only the propagation of the longitudinal wave (pressure wave) is considered. The characteristic acoustic impedance of the polymer coupler and the polymer backing material are the same, about 3.2 MNs/m^3, and the characteristic acoustic impedance of the PVDF transducer is assumed to be about 4 MNs/m^3, ignoring multiple reflections in the transducer. The acoustic impedances of aluminum and cast iron were assumed to be about 17 MNs/m^3 and 40 MNs/m^3, respectively.

The signal intensities obtained with conventional Al electrodes as acoustic couplers and those with acrylic material (PMMA) were compared. Figure 2-4 shows the results. The difference between the signals obtained by applying a DC voltage of 10 kV to the specimen and those obtained by DC short-circuiting the specimen is shown. The signal intensities are compared by considering the charge peak at the lower electrodes.

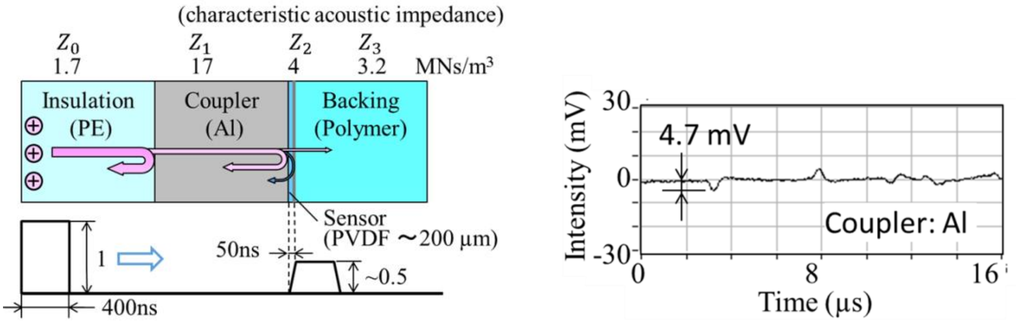

Type (a) Configuration with aluminum electrodes as acoustic couplers.

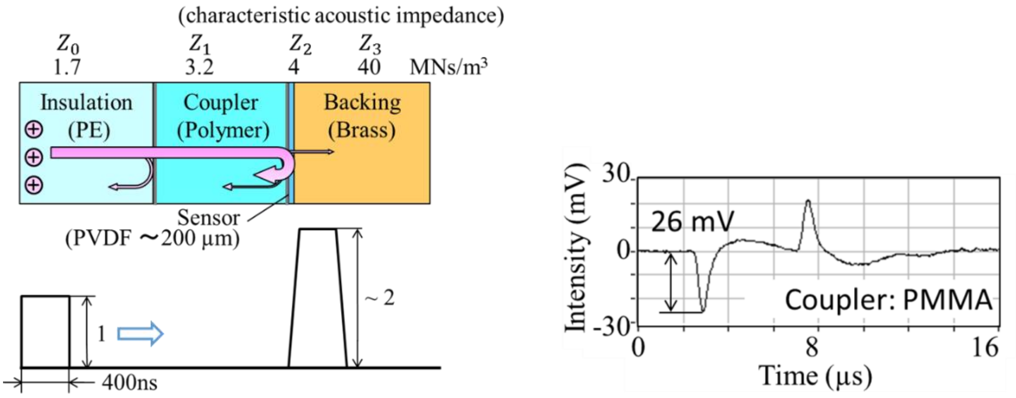

Type (b) Configuration using polymeric acoustic couplers.

Fig. 2-4 Increased sensitivity with polymeric acoustic couplers.

Type (a) is a conventional used structure. Since the acoustic impedance between the specimen and the PVDF transducer is large, most of the incoming sound waves are reflected at the interface between the specimen and the aluminum, and at the interface between the aluminum and the PDVF transducer, resulting in reduced sensitivity.

Type (b) was proposed by the author, and since the values of acoustic impedance from the sample to the polymer coupler and PVDF transducer are close, the reflection of the signal is suppressed and the intensity of the incoming signal is further enhanced by the positive reflection at the interface between the PVDF transducer and the metal backing material. As assumed, the sensitivity is improved by a factor of 4 to 5 compared to type (a). The measurement results fit the calculation at Fig. 2-2.

2.1.3 Backing material

In the proposed method, a metal backing material is placed behind the transducer to increase sensitivity, but as the specimen becomes thicker, signals reflected further behind the backing material are returned to the transducer and overlap with signals from inside the specimen. To avoid this, it is necessary to increase the thickness of the backing material. However, since the sound speed of metal is high, for example, when the insulation thickness of the specimen is 100 mm, the required thickness of the backing material exceeds 150 mm, resulting in a larger size of the system. Therefore, we proposed a method to obtain the same signal strength (voltage stroke) as when a metal backing material is used by placing a thin polymer plate and an air layer behind the transducer, and confirmed the effect by actual measurement.

For the measurement cell shown at section 2.1.2, the acoustic reflection from the back of the backing material returns. Since the round-trip sound pressure transmission from the metal backing material to the PVDF transducer is about 33%, sound pressure attenuation inside the backing material cannot be expected, and if the sample is thick, it will be superimposed on the signal related to space charge, causing errors, as Fig. 2-5 shows.

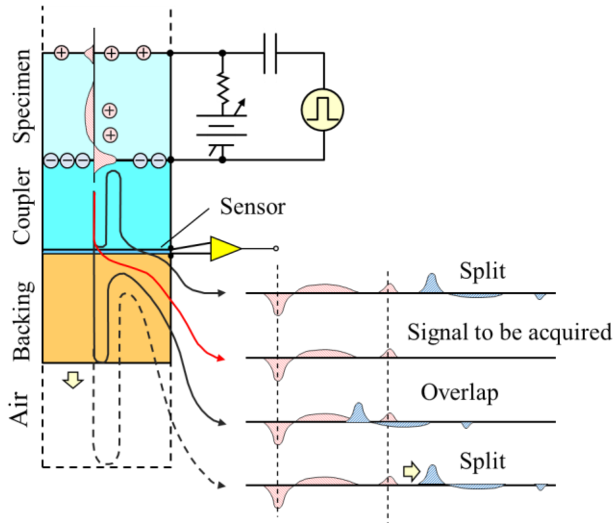

Fig. 2-5 Back-end reflection of metal backing.

Although it is possible to solve this problem by increasing the thickness of the backing material, the specimen thickness is expected to reach 120 mm or more for extremely thick insulation systems, such as cable joint. If the sound velocity of the rubber specimen is 1500 m/s and that of the metal backing material is 4500 m/s, it is necessary to increase the thickness of the backing material to 180 mm or more. Assuming the sound velocity in the polymer acoustic coupler is about 2500 m/s, the thickness required to avoid multiple reflections here is about 100 mm. Adding this to the thickness (length) of the entire measurement cell, it will reach to about 280 mm, making the measurement system larger.

Therefore, in this section, a method to eliminate multiple reflections in the backing material while minimizing the decrease in sensitivity was investigated. In ultrasonic engineering, a cone-shaped backing material is sometimes used to eliminate reflections from the back of the cell, but this design was excluded from this study because it is difficult to design a method that can handle all frequency components from the direct current component to the maximum frequency band, as in the PEA method.

Figure 2-6 illustrates the elimination of multiple reflections through an air backing. In type (c), the PVDF transducer is backed by a layer of air, and the incident acoustic wave is negatively reflected at the interface between PVDF and air backing. Since the signal does not propagate through the air layer, the effect of multiple reflections inside the backing material is eliminated. However, because the positive and negative signals cancel each other out, the final signal strength obtained is greatly reduced.

In contrast, type (d) has a polymer backing material placed behind the transducer with an acoustic thickness of about half the pulse width and an air layer was placed behind it. Because the acoustic impedance values of the PVDF, polymer coupler, and polymer backing material are close, most of the sound wave passes through the polymer backing material and reaches the air layer interface. Due to the time delay caused by the polymer backing material, the positive and negative reflected signals do not overlap, and two peak waveforms of almost the same intensity are obtained. The voltage stroke definition is expected to be almost the same as when metal backing material is used (shown at Fig. 2-4 type (b)).

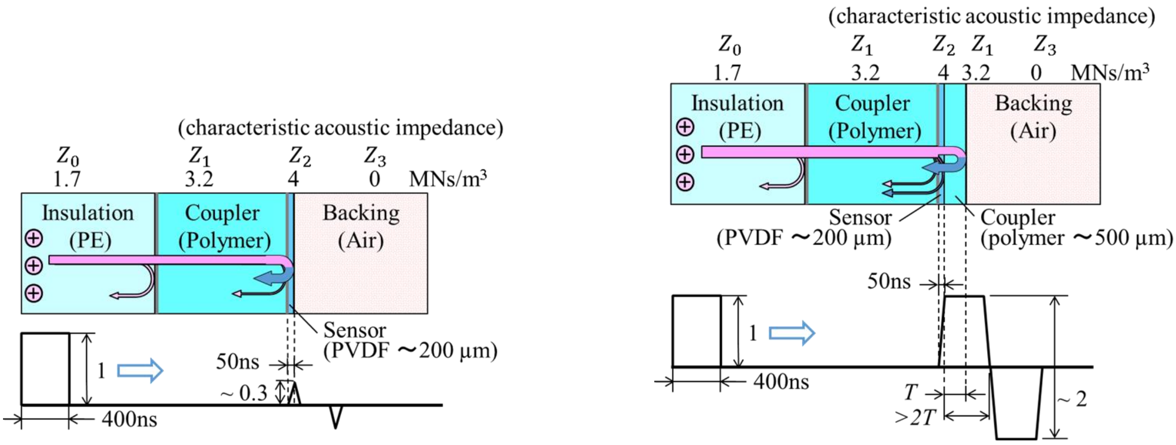

Type (c) Configuration with an air layer behind the transducer.

Type (d) Configuration in which a coupling layer is inserted between transducer and the air layer.

Fig 2-6 Removal of multiple reflections by air backing.

For the measurement cell using type (d) as the backing, the acoustic coupler between the specimen and the PVDF transducer was made of 40 mm thick acrylic resin (PMMA); the PVDF transducer was a stack of two 110 µm thick, 15 mm diameter polarized films; the coupling layer behind the PVDF transducer was a 500 µm thick sheet made of the same material as the acoustic coupling material, with an air layer behind it.

The installation is shown in Fig. 2-7. When an air layer is used in the substrate, the PVDF signal extraction electrode polymer sheet needs to be adhered to the backside of the polymer coupler via oil of the appropriate viscosity, and the backside of the polymer plate needs to be brought into direct contact with the air. Since some interfacial pressure is required to provide adhesion, a porous polymer material is used in this study rather than air layers. Some of these materials have limited apparent acoustic impedance, resulting in a slight reduction in receive sensitivity.

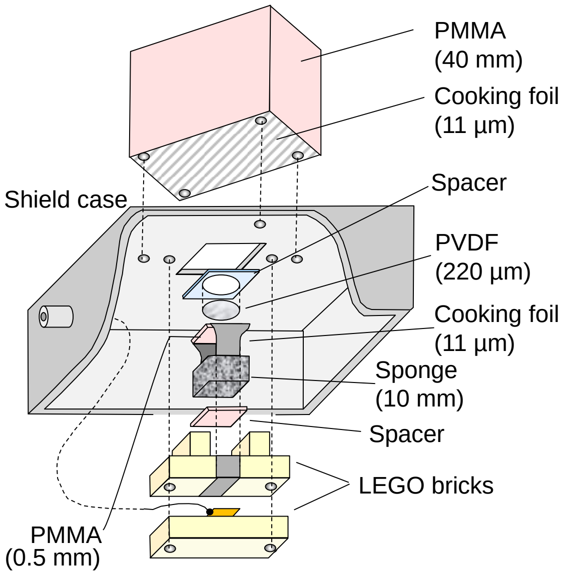

Fig. 2-7 Backing Layer Implementation.

The acoustic impedance was measured and was found that the use of commercially available sponge tape provided sufficient reflection. The measurement used a frequency band above 100 kHz, and it was assumed that the acoustic signal propagating inside the sponge tape would not reach the back of the tape due to its large attenuation, and thus no reflection signal would be detected from the back of the tape. When the thickness of the sponge tape was about 5 mm, no reflection from the back of the tape was detected, suggesting that the detection system from the PVDF detector to the air layer does not limit the thickness of the specimen.

For the signal sensitivity comparison, -10 kV DC voltage was applied and measured, then the voltage was removed, resistively short-circuited, and the measured waveform was subtracted to extract only the signal caused by the induced charge of the electrode. Fig. 2-8 shows the measurement results.

The signal comparison between type (a), which uses a metal acoustic coupler, and type (b), which uses a polymeric material has been reported at Section 2.1.2, showing that type (b) is approximately 4 to 5 times more sensitive than type (a). For type (c), in which the back of the PVDF transducer is in direct contact with air. The measurement was not performed because the direct and reflected signals cancel each other out.

In Fig. 2-8, a comparison is made between type (b), which uses metal backing, and types (d-1) and (d-2), which use different air layer materials. Comparing the signals from the electrode closer to the transducer, the (d-1) and (d-2) types show larger positive and negative swings than the (b) type, indicating that the negative reflection from behind the polymer plate enters the transducer with a time delay. Compared to (d-1), which uses low foamed polyvinyl chloride resin (PVC) as the air layer, (d-2), which uses a sponge, shows a larger voltage stroke and its value is almost the same as that of (b), which uses metal backing.

It was found that by using a polymer bonding layer and an air layer as backing materials, the signal intensity was equivalent to that using metal. Fig. 2-9 compares the spectral intensities of the two types (type (b) and (d-2)). Only the portion of the signal component obtained from the induced charge on one side electrode was cut out by an appropriate window function and Fourier transformed. The frequency components are shown as well. The low-frequency component is large for type (b), which uses brass backing material, while the DC component is very small and the low-frequency component is suppressed for type (d-2), which combines a polymer bonding layer and an air layer as the signal oscillates positively and negatively, but the high-frequency component is large. When the two signals were integrated separately, the areas obtained were found to be almost the same.

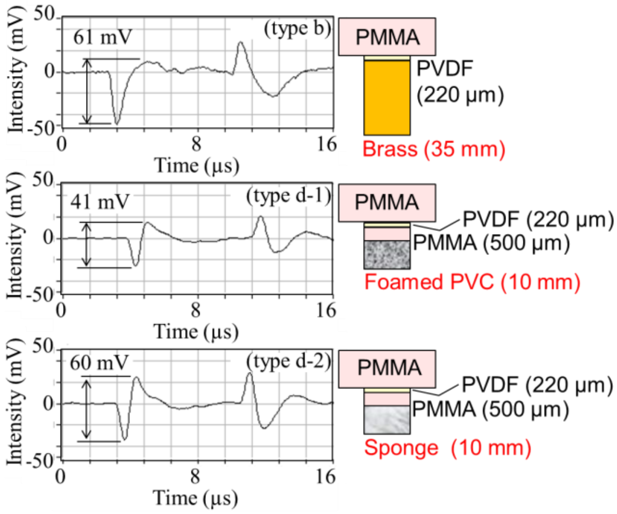

Fig. 2-8 Comparison of sensitivity based on actual measurements.

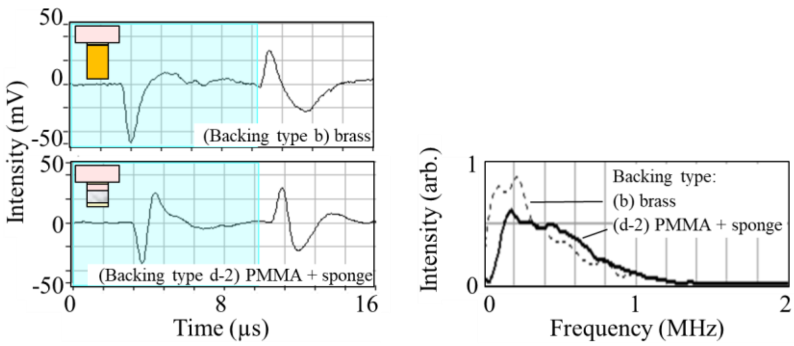

Fig. 2-9 Comparison of intensity spectrum.

In the measurement cell proposed in Section 2.1.2, metals such as copper and lead were used as backing materials, and a certain thickness of the metal backing material was necessary to avoid superposition of the reflected signal from the back of the backing material on the target signal caused by the electric charge in the specimen. If lead is used instead of brass, the thickness of the backing material can be reduced because of its slow sound velocity of about 2000 m/s. However, the use of large amounts of lead is not recommended because of its tendency to be avoided in technical fields. The apparatus using air as backing material proposed in this section can significantly reduce the size of the apparatus required for thick specimen. The proposed measurement system avoids multiple reflections from the backing material and, at the same time, provides a signal intensity equivalent to that of a metal backing.

2.1.4 Signal recording system

The amplifier was 1 MΩ in input impedance, 60 dB in voltage gain, and DC - 10 MHz in bandwidth. By an A/D converter with a sampling interval 16 - 50 ns and 15-bit resolution, 80,000 times maximum averaging was available in a few tens of seconds.

2.2 Software (signal processing)

The following description is given in the software (signal processing) by way of an example of space charge measurement on a thick polyethylene specimen. A specimen of 1 to 8 stacked low-density polyethylene plates of 11 mm thickness was prepared and space charge was measured by applying a DC voltage of 10 kV and a pulse voltage of 500 V or 1 kV with a width of 400 ns (Fig. 2-10), noted that the PE plate at top is used as a coupler attached to the metal rod electrode, and it was covered by aluminum film, so it is not counted in to specimen system. Cross-linked polystyrene (XLPS), which is considered acoustically transparent, was used as the acoustic coupler, cut to a thickness of about 55 mm; to avoid multiple reflections inside the backing material, lead, which has a slow sound velocity, was cut to 45 mm.

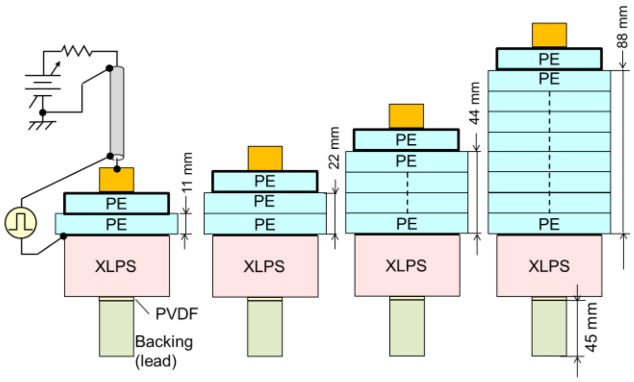

Fig. 2-10 Measurement of multi-layer polyethylene stacked specimen.

Figure. 2-11 illustrates the results of acquiring a reference signal for calculating the space charge using an 11 mm thick specimen.

As the polyethylene plate was expected to have already been internally charged during the manufacturing process, the signal was obtained when a DC voltage of 10 kV was applied, then the DC voltage was switched to -10 kV and the signal measured immediately after that was subtracted. This was used as the signal unaffected by space charge (reference signal A), and only the signal component caused by the electrode on one side was cut out using a window function to form reference signal B. When reference waveform A is deconvolved with reference waveform B, the signals from both electrodes appear as narrow peaks, but the acoustic signal propagating through the specimen is attenuated and the peak caused by the electrode farther from the piezoelectric sensor becomes smaller. This is recovered and the signal is proportional to the charge intensity. This was integrated to give the electric field, which was further integrated to give the applied voltage, and the proportionality constant was set to match the actual applied voltage.

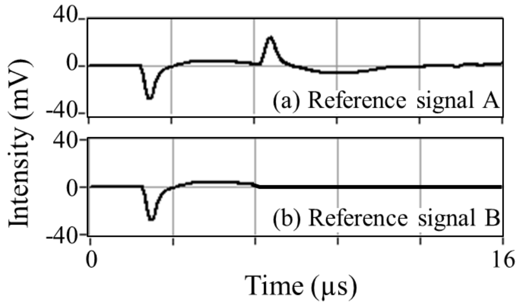

Fig. 2-11 Acquisition of reference waveform
(11 mm thick single layer specimen, equivalent 20 kV DC voltage application)

In Fig. 2-12 through 2-15, to get a stronger reference signal, the subtracted signal of 10 kV and -10 kV was acquired, which can be seen as the reference signal when an equivalent DC of 20 kV is applied, and is shown as a red line in (a). And the target signal which contains space charge component under 10 kV DC is represented as a thick black line, respectively. If the DC and pulse voltages remain the same, the signal from the electrode closer to the piezoelectric sensor is inversely proportional to the square of the thickness, so that the signal from an 88 mm-thick specimen is 1/64 of that from an 11 mm-thick specimen, but 1/32 because the pulse voltage is doubled for the 88 mm-thick measurement. Figures (a) to (b) in Fig. 2-12 to 2-15, respectively, display the signals when an equivalent DC of 20 kV is applied. The signals near the piezoelectric sensor from the two specimens are approximately 28 mV for a thickness of 11 mm and 1.1 mV for a thickness of 88 mm, which are generally consistent with the estimates. The signal on the far side from the piezoelectric sensor is almost the same as that near the piezoelectric sensor for the 11-mm-thick specimen, but for the 88-mm-thick specimen, the signal drops to about 0.1 mV due to acoustic attenuation. The space charge distribution, electric field, and potential distributions obtained after correcting for acoustic attenuation are shown in Fig. 2-12 to 2-15 (c) through (e), respectively.

From Fig. 2-12 (c), a positive charge is spread inside the single layer specimen, while a negative charge is formed on the surface side, keeping the specimen neutral. It is difficult to distinguish this negative charge from the charge on the electrode when measuring a single layer specimen, but when measuring a stacked specimen, a negative charge appears at the boundary between the layers, as shown in Figures 8-10 (c) and (d).

Since the space charge in a stacked specimen appears periodically in the thickness direction, the electric field intensity obtained by integrating it in the thickness direction also fluctuates periodically in the thickness direction. This pattern is displayed in (d) in Fig. 2-14 and Fig. 2-15. Since the charge density of each layer is almost the same, the fluctuation of the electric field intensity is almost the same regardless of the total thickness.

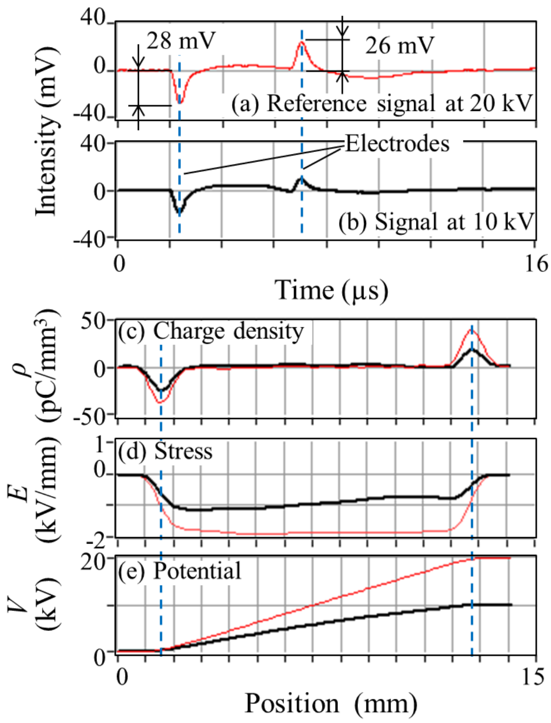

Fig. 2-12 Measurement Analysis Results.
(11 mm thick single layer specimen, 10 kV DC, 500 V pulsed)

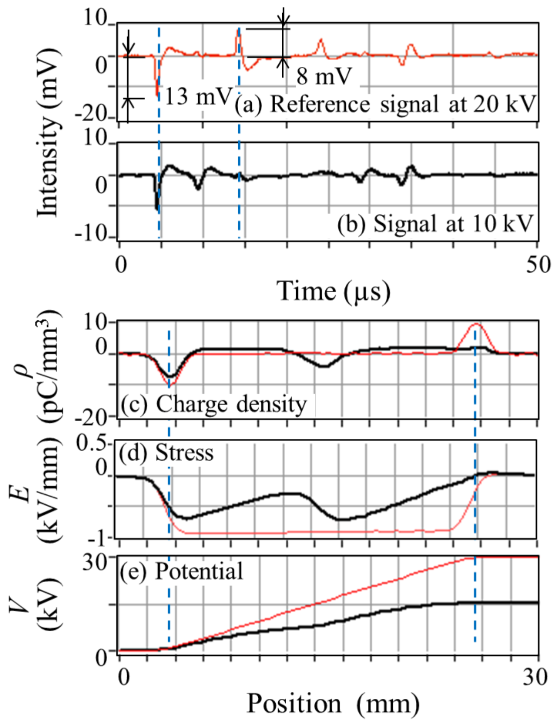

Fig. 2-13 Measurement Analysis Results.
(22 mm thick stacked specimens, DC 10 kV, pulsed 1 kV)

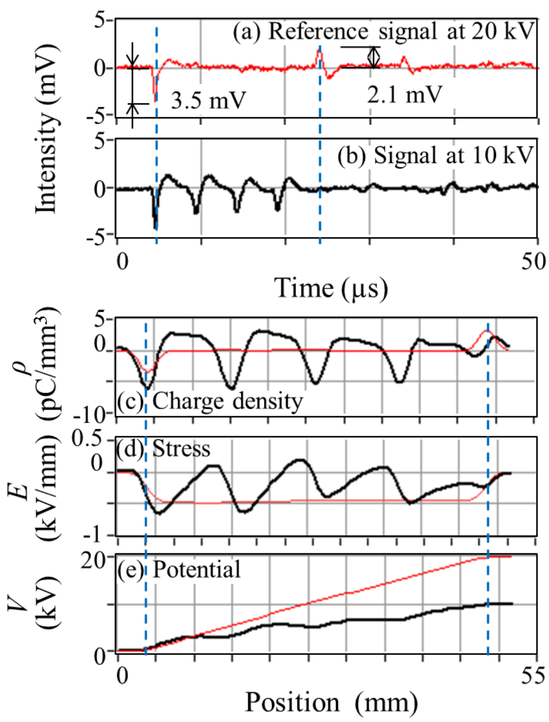

Fig. 2-14 Measurement Analysis Results.
(44 mm thick stacked specimens, DC 10 kV, pulsed 1 kV)

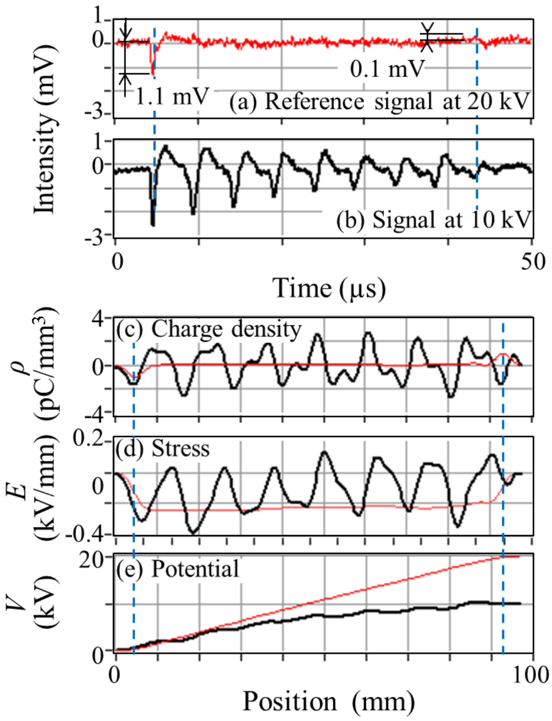

Fig. 2-15 Measurement Analysis Results.
(88 mm thick stacked specimens, DC 10 kV, pulsed 1 kV)

The electric field distribution when 10 kV DC was applied to each specimen is shown in Fig. 2-16, with the scales aligned. In this experiment, positive space charge spreads at a density of about 2 ~ 3 pC/mm^3 in the single layer state, and as a result, fluctuations of about 0.5 kV/mm in the electric field strength are observed.

On the other hand, since the average electric field strength exactly corresponds to the value obtained by dividing the applied DC voltage by the thickness, the average electric field strength is 0.91 kV/mm for the specimen with a thickness of 11 mm, and decreases as the thickness increases, reaching 0.11 kV/mm for the 88 mm specimen (12.5% of the value).

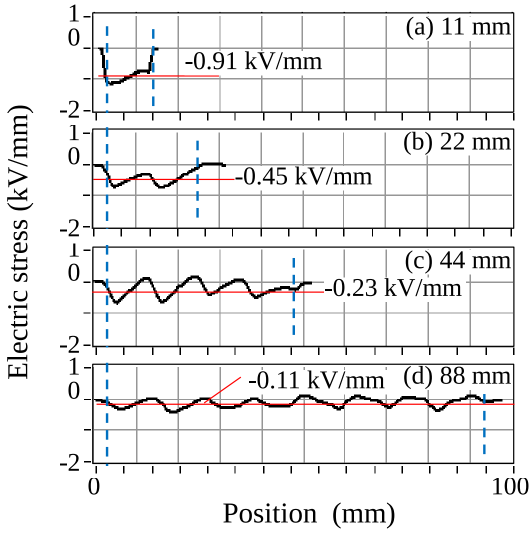

Fig. 2-16 Comparison of electric field distribution at 10 kV DC application.

Since the above results are consistent with electromagnetic findings, we believe that the space charge measurements are generally accurate over a wide thickness range of 11 mm to 88 mm.

To examine the effect of the modified backing material, the signals obtained through the modified device were analyzed and processed in this section as well.

Space charge, electric field, and potential distribution were calculated from signals measured with a DC voltage of -10 kV applied to a 22 mm thick laminated polyethylene specimen and a pulse voltage of 1 kV and 400 ns width. The results are shown in Fig. 2-17. The signals before and after the application of a DC voltage of 10 kV were acquired and the differentiated signal can be calculated, shown as signal (a), which can be considered as the signal without the influence of space charge. The component on one side electrode of signal (a) was extracted by the window function and used as a reference signal showing the impulse response of the system. For the deconvolution process, it has been found that when the low-frequency component is small, the deconvolution calculation in the frequency domain causes low-frequency spuriousness and disturbs the resultant baseline. In the case of the (d-2) type of Fig. 2-8, where the received signal oscillates positively and negatively, the low-frequency component is suppressed, so it is disadvantageous to perform deconvolution processing in the frequency domain. However, if an algorithm that includes deconvolution processing in the time domain is used, the entire waveform is referenced instead of decomposing it into frequency components, which suppresses low-frequency spuriousness and produces stable results [13].

The red lines in (c), (d) and (e) show the space charge, electric field and potential distribution when there is no space charge. The peak waveforms from both electrodes after correction were proportionally distributed to construct the transfer matrix [10].

The results obtained by signal processing the target signal (b) based on the above transfer matrix are shown in (c), (d), and (e) as black lines. Positive space charge is uniformly distributed inside the two stacked specimen, and the counter charge cancels out the electrode-induced charge due to the application of voltage, so that the charge at the left electrode is close to zero. This situation can be inferred from the fact that a negative charge is observed at the interface of the two polyethylene plates. Integration of the signal in (c) yields the electric field distribution in (d), which shows that the electric field distribution fluctuates periodically due to the internal charge. The above results are in general agreement with those obtained by using metal for backing [14].

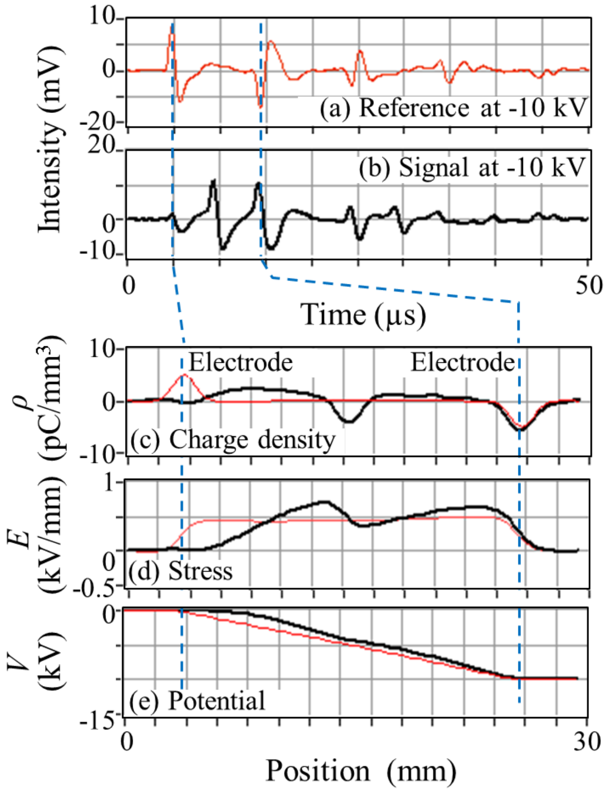

Fig. 2-17 Signal correction by reverse convolution process.
Specimen thickness 22 mm, DC -10 kV, pulse 1 kV 400 ns.

2.3 Summary

In this chapter, space charge measurements were investigated using the pulsed electroacoustic method with a very thick flat insulation material as the specimen. By using a polymer as the acoustic coupler, the sensitivity was about 5 times higher than that of a conventional system in which an aluminum electrode was used as the acoustic coupler. By reducing the noise by performing an additive averaging of up to 100,000 times with a pulse generation frequency of up to 5,000 times/second, it was shown that the space charge inside a laminated polyethylene specimen from 11 mm to a maximum thickness of 88 mm can be measured under the measurement conditions of 10 kV DC voltage and 0.5 to 1 kV pulse voltage.

This chapter also discussed the solution to the problem that the thickness of the backing material required to be placed behind the detector increases with the thickness of the specimen to be measured when using the pulsed electroacoustic method for space charge measurements on thick insulating materials.

Section 2.1.3 of this chapter proposed a backing structure that combines a thin polymer binder and an air layer instead of using a metal or polymer material as the usual backing material. In this way, even if a very thin backing material is used, it will not be affected by multiple internal reflections, independent of the thickness of the specimen thickness.

When using a PVDF transducer as a detector, it is appropriate to use a material with a characteristic acoustic impedance close to the transducer as the backing polymer coupler layer and to make its acoustic thickness more than half of the pulse voltage variation width.

For installation, a structure was designed to replace the air layer with a thin sponge tape to create a surface thickness between the detector and the acoustic coupler. And the practical measurements showed that voltage stroke signals comparable to those obtained when using metal as the substrate material could be obtained.

2.4 References

[1] N. Hozumi, T. Okamoto and T. Imajo, “Space Charge Accumulation and Decay at The Interface Between Polyethylene and Ethylene - Vinylacetate Copolymer,” 8th International Symposium on High Voltage Engineering, Yokohama, Japan, pp. 115 - 118, 1993.

[2] Y. Li, T. Takada, “Space Charge Distribution in Multi-Ply LDPE,” Proc. IEEE Conf. Electr. Insul. Diel. Phenom, pp. 397 - 402, 1992.

[3] N. Zhao, S. Li, X. Wang and G. Li, “Effects of LDPE/Nanofilled LDPE Interface on Space Charge Formation,” 2013 IEEE International Conference on Solid Dielectrics, Bologna, Italy, pp. 944 - 947.

[4] N. Hozumi, T. Kawashima and T. Imajo, “Space Charge Distribution Measurement in A Long Size XLPE Cable Using the Pulsed Electroacoustic Method,” Proc. IEEE Int. Symp. Electr. Insul. pp.294 – 297. 1992.

[5] T. Maeno, H. Kushibe, T. Takada and C. M. Cook, “pulsed Electro-Acoustic Method for The Measurement of Volume Charge in the e-Beam Irradiated PMMA,” Proc. IEEE Conf. Electr. Insul. Diel. Phenom. pp.389 – 397, 1985.

[6] Y. Li, T. Takada, “Progress in Space Charge Measurement of Solid Insulating Materials in Japan, IEEE Electrical Insulation Magazine,” Vol. 10, No.5, pp. 16 – 28, 1994.

[7] 電気規格調査会, “パルス静電応力法による空間電荷分布測定の校正法, JEC-TR-61004-2012, ”電気学会, 2012.

[8] M. Fukuma, H. Tomita and T. Maeno, “Space Charge Measurement for 27mm Thick XLPE Sample in PEA,” Conference Proceedings of ISEIM2014.

[9] R. Ozaki, K. Kadowaki, “Analysis of Attenuation and Dispersion of Acoustic Waves in Low-Density Polyethylene,” IEEE Transactions on Dielectrics and Electrical Insulation, vol. 27, No.6, pp.2007 2013- 397, 2020.

[10] Y. Li. "Space Charge Measurement in Lossy Solid Dielectric Materials by Pulsed Electroacoustic Method", Ph. D thesis, Musashi Institute of Technology, 1994.

[11] H. Matsumura, Y. Murakami, Y. Muramoto, N. Hozumi and M. Nagao. "Carrier Mobility in Acetophenone-Soaked Polyethylene Estimated by Transient Space Charge", Trans. IEE Japan, Vol. A-121, No. 8, pp.778 – 783, 2001.

[12] N. Hozumi, T.Takeda, H. Suzuki and T. Okamoto, "space charge behavior in XLPE cable Insulation under 0.2-1.2MV/cm dc fields", IEEE transactions on Dielectrics and Electrical insulation, Vol. 5, No.1, pp.82 -90, 1998.

[13] N. Hozumi, E. B. Prastika, S. Zahra, T. Kawashima and Y. Murakami, "Dual-domain Deconvolution Process Applied to Time-resolved Quantitative Dielectric Measurement," 2020 IEEE 3rd International Conference on Dielectrics (ICD), pp. 347-350, 2020.

[14] 李　暁欣, Shafira Zahra, 歌川　真生, 川島　朋裕, 村上　義信, 穂積　直裕.「厚い絶縁材料のための空間電荷測定システム」. 電気学会, pp. 72-78, 2021.

Chapter III

Method of reference signal acquisition for calibration

Space charge in high voltage insulation alters the internal electric field, which should be as homogeneous as possible, leading to a degradation of the dielectric properties. Therefore, space charge measurements to evaluate the dielectric properties have been considered as one of the important steps to improve the performance of insulation materials. For example, cross-linked polyethylene, commonly used in extra-high voltage transmission cables, generates a large amount of internal space charge when exposed to high DC voltages. At this point, space charge measurements are required to verify the stability of the internal electric field [1][2].

For space charge distribution measurement, by using pulse electro-acoustic method (PEA method), to determine the distribution of space charge in an insulation system by applying a pulse voltage and detecting the acoustic response with using piezoelectric device and signal amplifier [3].

It estimates the location and magnitude of charges from time-domain signals. For quantitative analysis, a bias voltage is applied to a specimen with no space charge, and the acoustic signal generated from the electrodes only is used as a reference waveform for calibration. However, for some specimen, such as a full-scale, extra-high voltage insulation system often already contains space charges in it. In this situation, the conventional methods for reference signal acquisition will be impractical, especially when the possibility of the space charge distribution changing in that process is counted into consideration.

Therefore, methods of acquiring a reference signal under such conditions are studied in this chapter. The acquisition has been applied in practical experiments when space charge is pre-existing, or when the space charge distribution changes due to the varying bias voltage.

For the space charge pre-exist specimen, the author considered to use the lock-in calibration to avoid the space charge effect, but it seems difficult to apply stable bias voltages at different values in practical measurement for real insulating system. For this, the waveform correlative method is proposed, which can be applied during the bias voltage variation. And to take the situation that space charge may vary along with the bias voltage variation into account, the author proposed the frequency-resolved analysis calibration to response to the case. These three methods are explained in this chapter, and the analyzed results are shown as well.

3.1 Conventional method

In common situation of PEA method, calibration signal is obtained by applying pulse and DC voltages on the specimen which is supposed to be completely without space charge.

For this reason, the acquisition of the reference signal is commonly performed by applying a low voltage prior to the evolution of space charge. Then the reference signal will be extracted by means of an appropriate window function.

Up to now, when the measurement is performed, it was necessary to measure the specimen that is absolutely without space charge prior to the measurement of the target. This can be done by two different ways; one is to bring a different material that can hardly generate space charge [4], and the second is to acquire the reference signal in the target itself by applying a low voltage prior to the evolution of space charge.

The former is time consuming and may lead to a measurement error because of using two different specimens. The latter is often employed when the specimen unique like a full-size cable, but it often happens that the specimen already has space charge inside, under which the reference signal can hardly be acquired.

3.2 Lock-in calibration

3.2.1 Introduction

Space charge in high voltage insulation modifies the internal electric field that is supposed to be as uniform as possible, and may reduce dielectric strength. For this reason, space charge measurement has been widely performed in many scenes of evaluation of dielectric performance. For instance, the cross-linked polyethylene that is commonly used as extra high voltage transmission cables may generate a significant space charge, when it is exposed to a high DC voltage. Space charge measurement is thus necessary to validate the stability of the internal electric field [1][2].

For space charge distribution measurement, by using pulse electro-acoustic method (PEA method), in a position to get some sound pulse with using piezoelectric device and signal amplifier from which the signal of the space charge distribution can be obtained by analyzing [3]. In this section, measurement has been done on XLPE based specimens, and the signal acquired by the piezoelectric device can be interpreted to the signal describing the distribution of space charge.

In this section, a solution by applying two different levels of DC voltages on the identical specimen is proposed. The reference signal that derives from only induced charges at the electrodes will be extracted by subtracting the responses. The lock-in measurement by giving a periodical change in applied voltage will be proposed in order to obtain the difference of waveforms while stably maintaining the space charge distribution.

3.2.2 Methodology

The concept of the proposed methodology is illustrated in Fig. 3-1. As shown in the diagram (a), charge distribution with space charge can be represented as:

$$\rho^{H}(x) = \rho_{ind}^{H}(x) + \rho_{SC}(x) \qquad (3\text{-}1)$$

$$\rho^{L}(x) = \rho_{ind}^{L}(x) + \rho_{SC}(x) \qquad (3\text{-}2)$$

where *H* and *L* stand for high and low voltages, *ind* and *SC* stand for induction and space charges, respectively. Although the equations are composed of volume densities (ρ) in the diagram, the induction charge is sheet charge and space charge is volume charge. However the equations include no contradiction if a finite spatial resolution is assumed. If the space charge can be assumed as stable, the calibration signal composed of only induced charges can be found as:

$$\rho^{CAL}(x) = \rho^{H}(x) - \rho^{L}(x) = \rho_{ind}^{H-L}(x) \qquad (3\text{-}3)$$

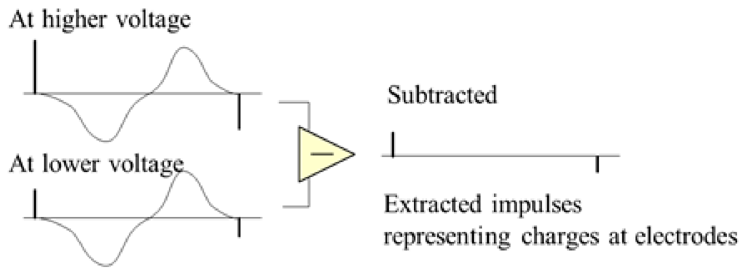

Fig. 3-1 The concept of the proposed methodology.

The calibration signal can be acquired in a same manner even in the case of dealing with practical signal that is given as a convolution of the charge distribution and system function.

If the space charge is unstable, the period at lower voltage (represented by TL in Fig. 3-2) needs to be reduced, however it may lead to a reduction in S/N ratio, as only a limited number of averaging may be available. In such a case, the disturbance with a short time may be given periodically in order to avoid the change in space charge distribution, as illustrated in Fig. 3-2.

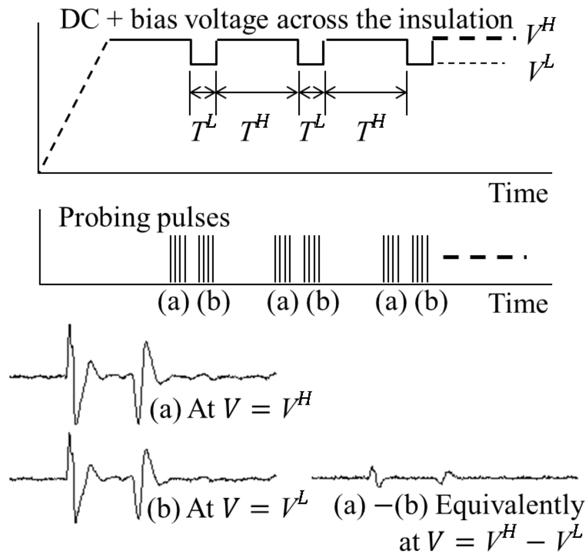

Fig. 3-2 Conceptual illustration of the lock-in acquisition.

3.2.3 Specimen

In the experiment, an XLPE film with a thickness of 500 μm was employed as the specimen. The XLPE film was cut into an appropriate size to match the shape of electrode of the measurement system. In order to compare the conditions in terms of space charge distribution the XLPE film was soaked with acetophenone for 48 hours.

3.2.4 Measurement condition

The proposed method assumes that the space charge remains stable throughout the term of disturbance T^L. As

$$v_d = \mu E \qquad (3\text{-}4)$$

where v_d is velocity of carrier, μ is carrier mobility and E is applied field, displacement of space charge under the same condition must be less than

$$d = v_d T^L \qquad (3\text{-}5)$$

Therefore, the required condition for taking the reference signal by means of lock-in measurement must be

$$T^L \ll \Delta x / v_d = \Delta x / \mu E \qquad (3\text{-}6)$$

where Δx is spatial resolution of the measurement.

In this report DC voltages applied to 500 μm-thick specimens in experiment were -4 kV and -3 kV, corresponding to 8kV/mm and 6kV/mm, respectively. The spatial resolution of the space charge measurement was as fine as 20 μm. Assuming that the carrier mobility of a polymer is as less as 10^{-13} m^2/Vs [5], term of disturbance should be short enough compared with 25 s.

In the experiment the disturbance was set at 1 s. It might lead to less than 1.6 μm in displacement of the space charge. However as space charge is indicated as the net charge of all the carriers, displacement of the space charge distribution might be much less significant than the order of carrier mobility. In order to upgrade the S/N ratio, 32 times of data acquisitions were performed to average the waveforms. Furthermore this disturbance of 1 s was given periodically with an interval of 1 + 10 s ($T^L + T^H$ in Fig. 3-2), the acquisitions being locked in the periodical disturbance. It was realized by applying a modulation bias voltage superposed onto the DC poling voltage. In this particular study as many as 10 times of periodical acquisition were performed. After finding that the space charge was stable the term of disturbance in some cases was set as long as 5 s.

3.2.5 Results and discussion

A. Waveform Acquisition

The measurement devices were connected as the schematic diagram shown in Fig. 3-3. After placing a drop of silicone oil on the surface of specimen and electrode, it was made sure that there was no air bubble between the contact surface of specimen and electrode. The as-received XLPE was subjected to the experiment at first, applying voltages as periodically -4 kV for 10 seconds and -3 kV for 1 second assuming that carrier mobility was lower than 10^{-13} m^2/Vs.

In this section, an XLPE film which has been treated with acetophenone was employed as specimen as well. Acetophenone is a kind of chemical oily liquid with easy volatility. In XLPE cable insulation, it is naturally included as a byproduct after cross-linking. In many cases it has an effect of modifying the characteristic of space charge accumulation [6]. For instance, it will make the specimen easier to be evolved with hetero space charges, and once it has been evolved it can hardly be reduced [7].

The signal acquisitions were done with subtraction procedure as shown in Fig. 3-4, the signal after 32 times of averaging contains much noise which should be avoided. It is obvious that by increasing the times of averaging, the obtained signal had become smooth and with less noise, as shown in signals (b) through (d) in Fig. 3-4, which are indicated in the same scale. The reference signal for deconvolution was finally extracted by applying an appropriate cosine tapered window function.

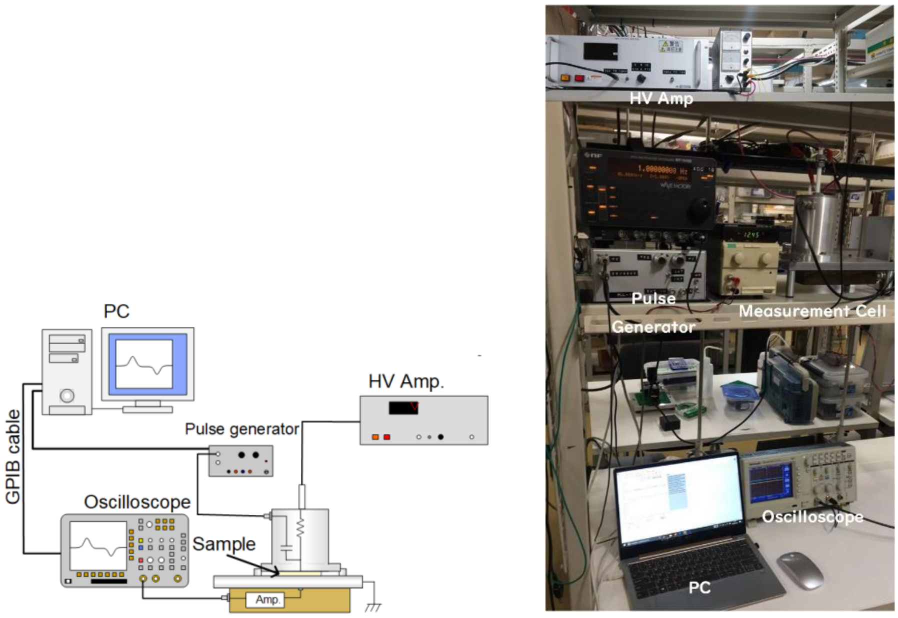

Fig. 3-3 Schematic diagram of the measurement system.

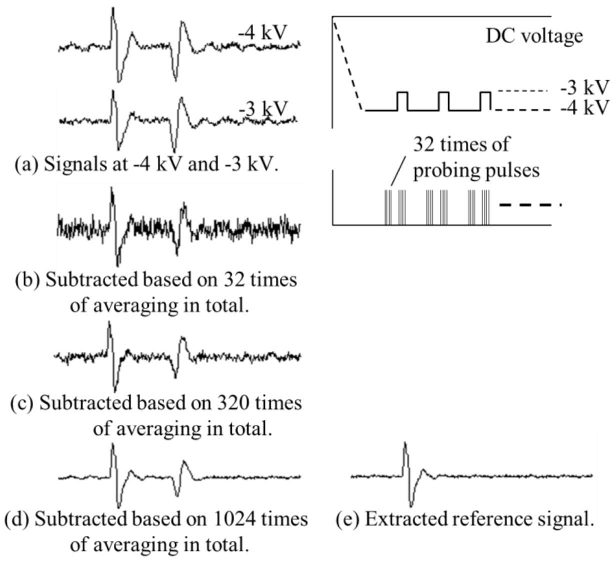

Fig. 3-4 Subtracted signals under various averaging conditions.

B. Deconvolution

The deconvolution process is illustrated in Fig. 3-5. In the experiment, waveform at two different voltages were obtained, both of them already might contain signal component of space charge. After extracting the reference signal, both the target and reference signals were Fourier transformed, and each frequency component of the target signal was divided by the corresponding frequency component of the reference signal. The result was subjected to the Gaussian filter before performing the inverse Fourier transform. The process was partially helped by the dual-domain deconvolution [8] in order to retain the straightness of the baseline. The result of the deconvolution performed on the XLPE specimen is shown in Fig. 3-6. In this particular case no significant space charge is seen.

The result of field analysis is shown in Fig. 3-7. As it had been expected, the XLPE as received had only a small intensity of space charge, making field distribution flat and potential distribution strait. On the other hand, strong hetero charges were observed, strongly distorting the field and potential distribution.

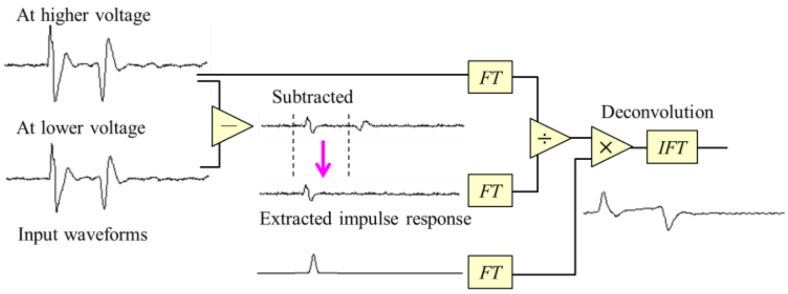

Fig. 3-5 Deconvolution process.

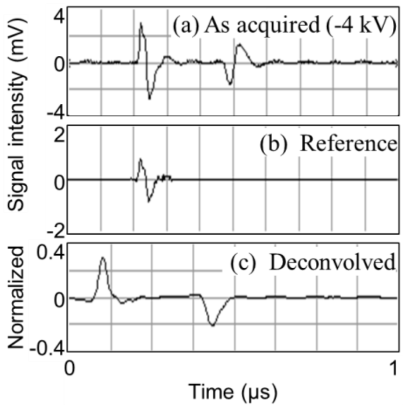

Fig. 3-6 Deconvolution on the XLPE specimen.

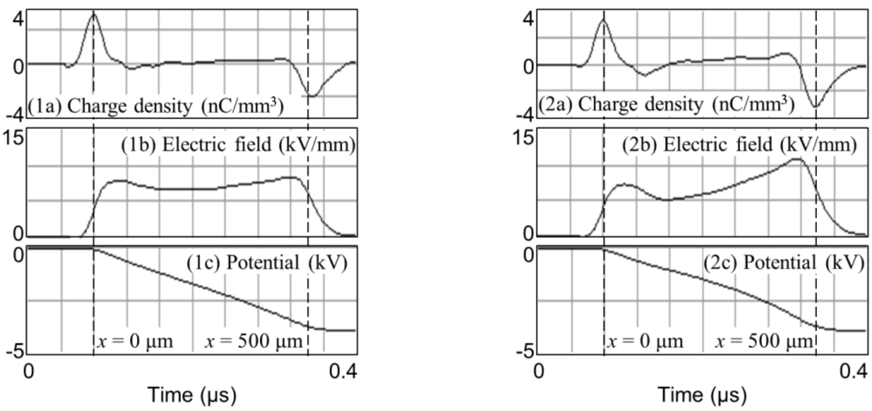

(a) XLPE as received. (b) XLPE soaked with acetophenone.

Fig. 3-7 Deconvolution on the XLPE specimen.

C. Discussion

In addition to its practical importance, it is of interest to the researchers in insulating materials to examine the specific condition of the space charge, like the accumulation in terms of intensity and location inside insulation. Although the XLPE specimen as received had almost no space charge in it under voltages up to 4 kV, the specimen soaked with acetophenone had a significant space charge as expected. As the space charge had been build up in a short time it was not easy to acquire the reference signal shortly after the application of the step voltage. In addition, acquisition under a very low voltage prior to space charge build up ended with a noisy signal that leads to a poor result in signal processing.

Using a different specimen like PMMA film that can hardly build up space charge is widely employed for acquiring the reference signal; however, different specimen may change the impedance at the end of the feeder line of the pulse source and may change the spectrum of the applied pulse voltage, which may lead to a different measurement conditions for the target and reference signals. The proposed method has no such a problem as it can be performed with the identical specimen.

Furthermore, if the specimen is something like full-size cable, an adequate specimen like PMMA block that can be applied with extra high voltage can hardly be found. The proposed methodology can be applied even in such a case.

3.2.6 Conclusion

In this section, a measurement method was proposed, with which the calibration as well as target signal can be obtained at the same time without changing the specimen in the whole process.

A modulation bias voltage was superimposed onto the DC poling voltage. Probing pulse voltages were applied synchronized to the modulation bias voltage. After differentiating between signals with high and low levels of bias voltage, the signal without the influence of space charge was acquired.

In this process, a reference signal can be obtained by using a window function, which was applied to the subtracted signal. Then the distribution of space charge can be calculated accurately.

This process can be performed even when space charges have been built up, by using the identical specimen at the same time when the target signal with space charges is being acquired.

3.3 Waveform correlative method

3.3.1 Introduction

To obtain quantitative estimation, a bias voltage is applied when there is no space charge, and acoustic signals produced by electrode's surface charge are used as reference for calibration [9]-[10]. However, in measurement of extra-high voltage cables and other real-scale insulation systems, there are many cases when space charge was already produced through charging history and thermal history; thus, reference signals must be acquired in that state. In Section 3.2, we acquired differential waveforms of acoustic signals when two different bias voltages were applied, thus canceling the influence of existing space charge, and considered use of these waveforms as reference signals. In addition, voltage application and measurement take much time in testing of real-scale extra-high voltage insulation systems; particularly, there is concern that space charge conditions may change during tests in high temperature environments. In this context, we considered correlating transient changes in bias voltage and acoustic signals as a method for fast acquisition of reference signals.

This section proposes on results of this consideration as well as of measurement using an 11-mm thick polyethylene specimen.

3.3.2 Calibration using differential waveforms

Measurement of space charge by the pulsed electroacoustic method [11]-[13] is illustrated in Fig. 3-8. A specimen put between parallel plate electrodes has uniform permittivity; space charge that occurs in the middle induces charge in the electrodes. With zero bias voltage, the total charge is zero. On the other hand, the charge induced in the electrodes changes when bias voltage is applied. Pulsed voltage is applied to measure space charge, and acoustic signals produced through interaction with the charge are detected with a piezoelectric sensor. A coupler including acoustic matching and a backing are used to improve sensitivity. Signal intensity and delay correspond to charge density and location, respectively. Detected signals are affected by pulsed voltage waveform, acoustic propagation route, and frequency characteristics of piezo element and amplifier.

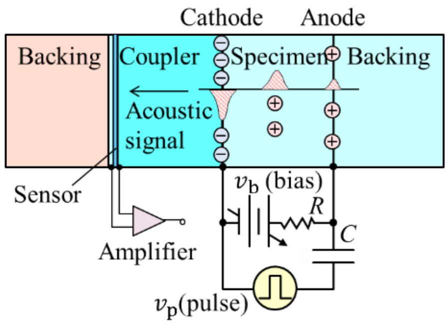

Fig. 3-8 Schematic diagram of the measurement.

Induced charge is a surface charge, and acoustic signals produced by this charge can be interpreted as impulse response of the measuring system. Signals from the electrode closest to the sensor are extracted using an appropriate window function. Using these signals as a reference, space charge distribution can be estimated by deconvolution of acoustic signals from the specimen. In Fig. 3-9, bias voltage v_b and pulsed voltage v_p are applied between the electrodes. When there is no space charge, stress applied between the electrodes is as follows.

$$\frac{\varepsilon}{2}E^2(t) = \frac{\varepsilon}{2d^2}\{v_b + v_p(t)\}^2 = \frac{\varepsilon}{d^2}\left[\frac{1}{2}v_b^2 + v_b v_p(t) + \frac{1}{2}v_p^2(t)\right] \quad (3\text{-}7)$$

where E is instantaneous electric field, ε is permittivity, and d is specimen thickness. Bias voltage in Equation (3-7) can be considered as a constant, and the 1st term does not generate any acoustic signals. The 2nd term can be considered as Coulomb force produced by interaction between the charge induced on electrode surface due to the bias voltage and pulsed electric field. The 3rd term is Maxwell stress due to the pulsed electric field. Assuming that $v_b \gg v_p$, only $\varepsilon v_b v_p / d$ remains. According to reports by IEE Japan, this is proportional to surface charge density on the electrode, and therefore, used as a reference signal [14]-[16]. When a difference of waveforms is taken under application of positive and negative pulses with same waveforms, signals produced by Maxwell stress can be extracted; signal components due to Coulomb force can be obtained by subtracting these from target waveforms [17].

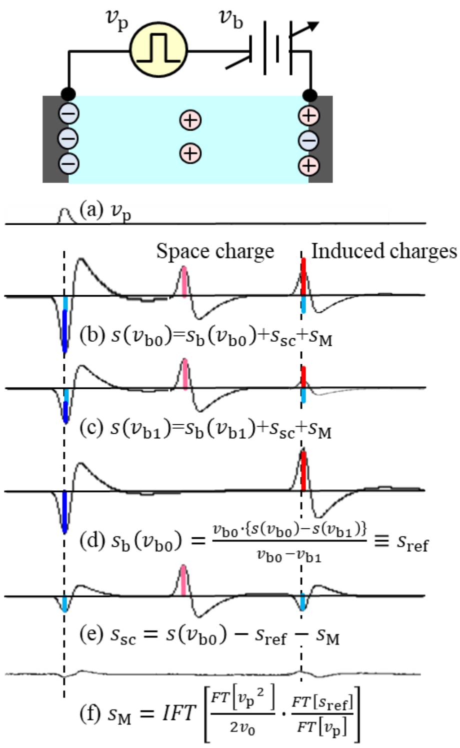

Fig. 3-9 Extraction of signal corresponding to space charge. (a) Pulse voltage, (b)(c) response at different bias voltages, (c) differential waveform, (d) signal component corresponding to space charge. (e) signal component due to the Maxwell stress.

If space charge exists, it is difficult to separate a signal generated by the space charge from the reference signal used for calibration; however, when difference between two different bias voltages v_{b0} and v_{b1} is taken, the following is obtained because the signal component due to space charge does not depend on bias voltage.

$$\frac{\varepsilon}{d^2}(v_{b0} - v_{b1})v_p(t) \qquad (3\text{-}8)$$

This signal is proportional to the pulsed voltage. Thus, the influence of Maxwell stress in the 3rd term of Equation (3-7) can be eliminated in Equation (3-8). Here the differential waveform in response to the bias voltages v_{b0} and v_{b1} is multiplied by $v_{b0}/(v_{b0} - v_{b1})$ to determine reference signal $s_{ref}(t)$ under reference voltage v_{b0}. Signal components due to Maxwell stress overlap with target signals in space charge measurement, and therefore, must be removed for accurate measurement as explained below. Reference signal $s_{ref}(t)$ is a convolution of the product $v_{b0} \cdot v_p(t)$ of bias voltage and pulse voltage with impulse response $h(t)$ of the system including specimen.

$$s_{ref}(t) = v_{b0} \cdot v_p(t) * h(t) \qquad (3\text{-}9)$$

where the symbol $*$ denotes convolution. The 3rd term in Equation (3-7) is proportional to squared pulsed voltage, irrespective of bias voltage and space charge; therefore, $h(t)$ is found from Equation (3-9) by deconvolution, then convoluted with $v_p^2(t)$ and multiplied by ½ to obtain signal component $s_M(t)$ due to Maxwell stress.

$$s_M(t) = \frac{1}{2}v_p^2(t) * h(t) = \frac{1}{2}IFT\left[FT\left[v_p^2(t)\right] \cdot \frac{S_{ref}(\omega)}{v_{b0}\cdot V_p(\omega)}\right] \qquad (3\text{-}10)$$

where FT and IFT denote Fourier transform and inverse Fourier transform; $V_{\mathrm{p}}(\omega)$ and $S_{\mathrm{ref}}(\omega)$ are Fourier transforms of $v_{\mathrm{p}}(t)$ and $s_{\mathrm{ref}}(t)$, respectively. Thus, signal components due to Maxwell stress can be calculated from pulsed waveforms, and then subtracted from target waveforms.

3.3.3 Calibration to correlate bias voltage and signals

Time of several minutes is required for voltage to settle after a change in DC source used in testing of extra-high voltage insulation systems; in addition, more averaging iterations are needed to compensate for decline in sensitivity in measurement of thick insulators, which adds several minutes to time taken by acquisition of reference signals for calibration. In the meantime, calibration accuracy declines if space charge conditions have changed [18]. There were attempts at resolving this issue synchronizing bias voltage changed periodically within a short time, and lock-in detecting differential response waveforms [19]-[20]; in so doing, however, a new control system must be introduced, which is difficult in testing of extra-high voltage insulation systems. Thus, we considered a method to acquire reference signals through fast measurement by applying transient changes to bias voltage, and correlating them with transient changes in response signals.

Figure 3-9 illustrates how reference signals are extracted by correlating bias voltage with signals. Positive space charge exists in the middle of a specimen and acoustic signal (II) varies in response to bias voltage (I). For example, considering instantaneous signal components at sampling points (a)–(c), different variations occur in each point as shown by (III). Point (a) corresponds to the cathode, and signal component swings negative as bias voltage swings positive. As can be seen from the diagram (IV) showing correlation between voltage bias (I) and acoustic signal component (III), the gradient α_1 at point (a) is negative. Because of charge induced by space charge, negative signal component is obtained when bias voltage is zero; therefore, the offset α_2 (y-intercept in the diagram) is negative. Similarly, considering signals at the sampling point (b) and (c), the former is signal component due to positive space charge in the middle of a specimen, thus being unrelated to bias voltage variation. Thus, in the correlation diagram, the gradient α_1 is close to zero, and the offset α_2 is positive. Point (c) corresponds to the anode, and signal component swings positive as bias voltage swings positive. In the correlation diagram, the gradient α_1 becomes positive. Because of charge induced by space charge, negative signal component is obtained when bias voltage is zero, and the offset α_2 is negative.

Response component unaffected by space charge when bias voltage v_{b0} is applied can be extracted through linking α_1 when sampling time t_j is changed, and multiplying by v_{b0}. Component related to one of the electrodes is clipped with an appropriate window function, and used as a calibration signal for conversion to electric space charge distribution or electric field distribution. Similarly, signal component under zero bias voltage is obtained by linking α_2; therefore, component due to space charge is extracted by removing component due to Maxwell stress in Equation (3-10).

This is explained below in mathematical terms. Let $v_{\mathrm{b}}(t_i)$ denote instantaneous value of bias voltage. Here t_i is the time of signal waveform acquisition, being of the millisecond or second order. Let $s(t_i, t_j)$ denote acoustic signal. Here t_j is waveform sampling time, being of the nanosecond order. Let $s_{\mathrm{b0}}(t_j) \equiv s_{\mathrm{ref}}(t_j)$ denote reference signal that should be obtained as a signal under bias voltage v_{b0}; then response signal $s(t_i, t_j)$ for arbitrary bias voltage $v_{\mathrm{b}}(t_i)$ is as follows.

$$s(t_i,t_j) = s_{\mathrm{b}}(t_i,t_j) + s_{\mathrm{sc}}(t_j) + s_{\mathrm{M}}(t_j) + n(t_i,t_j) = \frac{v_{\mathrm{b}}(t_i)}{v_{\mathrm{bo}}} s_{\mathrm{b0}}(t_j) + s_{\mathrm{sc}}(t_j) + s_{\mathrm{M}}(t_j) + n(t_i,t_j) \quad \text{(3-11)}$$

where $s_b(t_i,t_j)$ is signal component due to bias voltage $v_{\mathrm{b}}(t_i)$, and $s_{\mathrm{sc}}(t_j) + s_{\mathrm{M}}(t_j)$ is signal component due to space charge and Maxwell stress (not depending on bias voltage); besides, $n(t_i,t_j)$ is noise component. The following is obtained by fixing sampling time t_j and applying linear regression to relationship between acquired signal $s(t_i,t_j)$ and bias voltage $v_{\mathrm{b}}(t_i)$.

$$s(t_i,t_j) = \alpha_1(t_j) v_{\mathrm{b}}(t_i) + \alpha_2(t_j) + n_i(t_i,t_j) \quad \text{(3-12)}$$

where $\alpha_1 = s_{\mathrm{b0}}(t_j)/v_{\mathrm{b0}}$, $\alpha_2 = s_{\mathrm{sc}}(t_j) + s_{\mathrm{M}}(t_j)$. Now, $s_{\mathrm{M}}(t_j)$ can be estimated from Equation (3-10) and subtracted from target signal.

α_1 and α_2 can be estimated by least squares method.

$$\begin{pmatrix} s(t_1,t_j) \\ \vdots \\ s(t_m,t_j) \end{pmatrix} = \begin{pmatrix} v_b(t_1,t_j) & 1 \\ \vdots & \vdots \\ v_b(t_m,t_j) & 1 \end{pmatrix} \begin{pmatrix} \alpha_1 \\ \alpha_2 \end{pmatrix} + \begin{pmatrix} n(t_1,t_j) \\ \vdots \\ n(t_m,t_j) \end{pmatrix} \quad \text{(3-13)}$$

The above can be written in the following way.

$$\mathbf{s} = \mathbf{v}\boldsymbol{\alpha} + \mathbf{n} \quad \text{(3-14)}$$

Then $\boldsymbol{\alpha}$ to minimize the square sum of $n(t_1,t_j) \cdots n(t_m\,,t_j)$ can be expressed as follows. Here T denotes transposition.

$$\widehat{\boldsymbol{\alpha}} = (\mathbf{v}\mathbf{v}^{\mathrm{T}})^{-1}\mathbf{v}^{\mathrm{T}}\mathbf{s} \quad \text{(3-15)}$$

3.3.4 Results of measurement

Figure 3-10 shows experimental system for measuring an 11-mm thick low-density polyethylene plate. The system includes an acoustic coupler with acoustic impedance close to that of specimen, and a backing [21]-[22] The upper limit of bias voltage was +10 kV, and pulsed voltage of 0.9 kV, 400 ns was applied to the specimen; polarity of applied voltage was defined as positive at the upper electrode. Bias voltage was applied via a common 50 Ω coaxial cable; open-circuit stub was used for pulsed voltage, but the line was short as compared to propagation length about 80 m corresponding to the pulse width, and worked as a coupling capacitor about 300 pF. The pulsed power line had impedance of 75 Ω including output impedance of pulse generator.

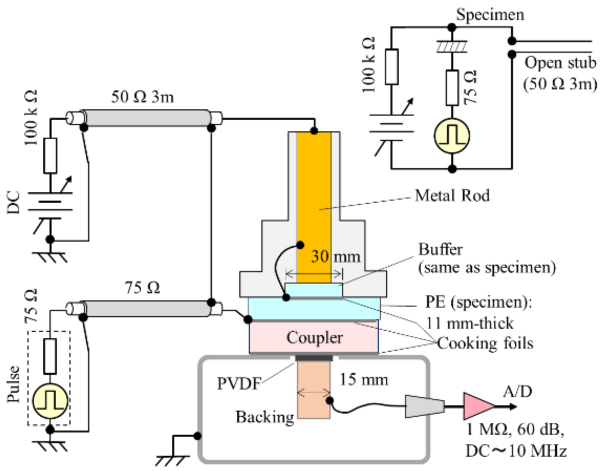

Fig. 3-10 Measurement equipment and equivalent electric circuit. PS: polystyrene, PE: polyethylene, PVDF: polyvinylidene fluoride.

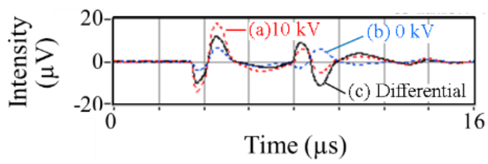

Fig. 3-11 Differential waveform of response when different bias voltages are applied.

Figure 3-11 shows response waveforms (amp input referred) at bias voltage of 10 and 0 kV as well as the differential waveform. When acquired quickly, this waveform can be used as reference signal. When bias voltage control takes time, the correlation-based method considered in Section 3.3.3 may be useful.

Figure 3-12 shows an overlay of response signal (II) at varied bias voltage (I); actually, about 200 waveforms are recorded. Acoustic signals were sampled at 1000 points; the waveforms (III) are result of tracking time variation of signal components at (a)–(c) in Fig. 3-9. Point (a) corresponds to the cathode, and the signal swings negative when bias voltage grows. Negative offset is observed here due to charged induced by space charge. At point (b), wave tail of response due to cathode charge overlaps with signal due to positive space charge. Point (c) corresponds to the anode, and the signal swings positive when bias voltage grows; besides, because of the induced charge, negative offset is observed. Figure 3-13 shows correlation between bias voltage and response signal at certain sampling time. Here correlation is obtained at all sampling point; thus, Fig. 3-14(a) presents a waveform obtained by linear regression at gradient α1; this agrees completely with the differential waveform in Fig. 3-11(c), and therefore, can be used as reference signal. The waveform (c) corresponding to space charge distribution in uniform electric field is obtained when the waveform (b) due to one electrode is clipped, the entire waveform is deconvoluted, and frequency-dependent acoustic attenuation of the specimen is compensated [23]-[24].

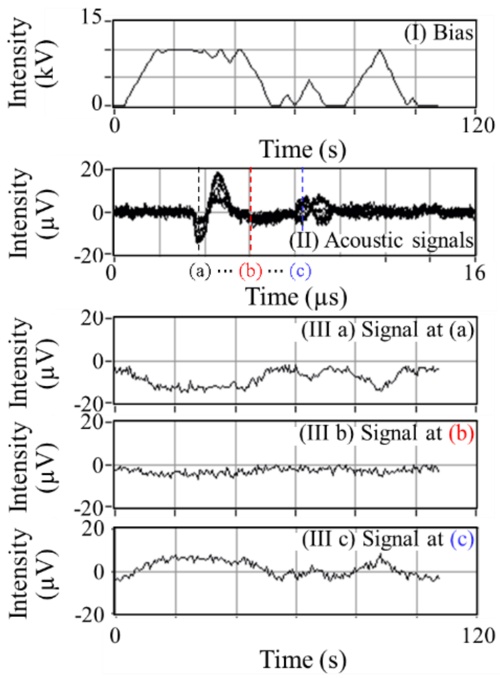

Fig. 3-12 Change in time of the bias voltage and corresponding response signals.

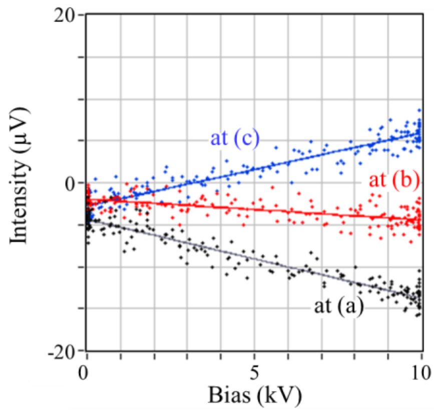

Fig. 3-13 Correlation between bias voltage and response signal at different.

Figure 3-15(a) shows signal obtained under bias voltage of 10 kV; the signal contains components due to internal space charge and Maxwell stress. The waveform (d) is obtained by using Equation (3-10) to calculate Maxwell stress-related component from the reference signal (b) and pulsed voltage waveform (c). The bias voltage is 10 kV, and pulsed voltage is 0.9 kV; thus, assuming square pulses, $v_{\mathrm{p}}(t)$ and $v_{\mathrm{p}}^2(t)$ have the same shape, and according to Equation (3-7), signal strength due to Maxwell stress is 4.5% of that due to Coulomb force. In this measurement, the ratio is about 4.2%, which is a good agreement. The diagram (e) shows the waveform (a) less the component due to Maxwell stress, but both waveforms are almost same because the pulsed voltage is low. However, removal of Maxwell stress-related signal component is necessary to improve accuracy in some cases, for example, when evaluating extremely small space charges. The diagram (f) shows the waveform (e) less waveform (b), that is, signal component due to space charge only.

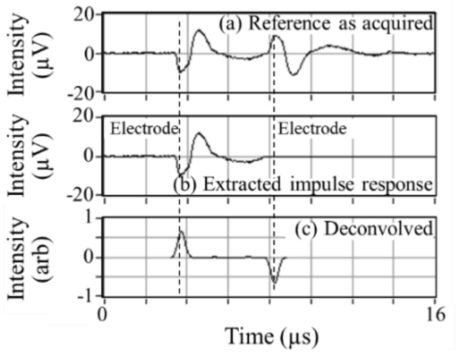

Fig. 3-14 Extraction of the impulse response. Voltage is output equivalent at the sensor.

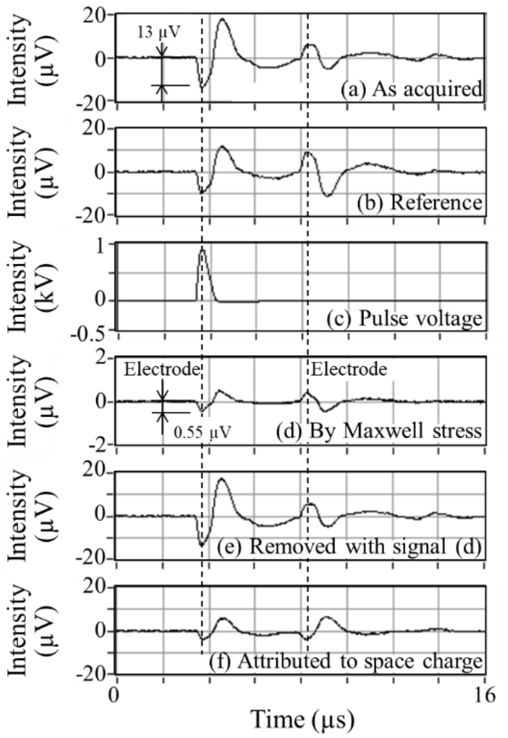

Fig. 3-15 Extraction of signal corresponding to space charge from practically acquired signal.

Figure 3-16 presents distributions of (I) charge density, (II) electric field, and (III) potential; these distributions were calculated by deconvolution with reference to waveform of the left electrode obtained from the reference signal (b) in Fig. 3-15. The dotted lines pertain to deconvoluted waveforms expressing uniform electric field. Here positive space charge expands in the dielectric regardless of bias voltage. This charge induces negative charge in both electrodes; this induced charge is smaller or bigger in the anode when positive or negative bias voltage is applied. As a result of expansion of positive space charge, electric field swings negative on the left and positive on the right.

Distortion of electric field due to space charge reaches about 0.4 kV/mm against the uniform field. Electric field under zero bias voltage (II-(b)) swings positive and negative around the center, while potential (III-(b)) has a symmetric shape, its value at the center being about 1.5 kV.

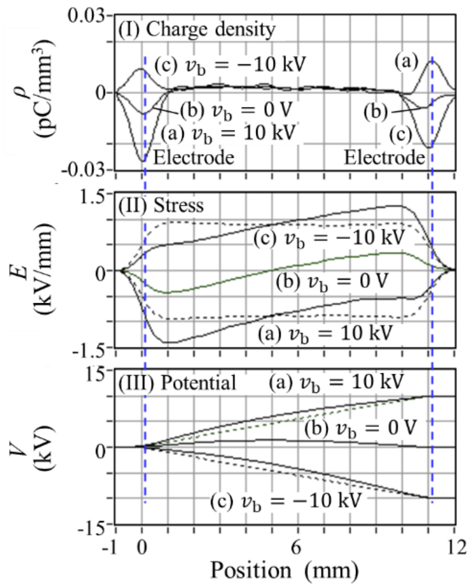

Fig. 3-16 Distributions of (a) charge density, (b) Electric stress and (c) potential at 10 kV of bias voltage. Dashed lines represent distributions assuming uniform electric field.

3.3.5 Discussion

When different bias voltages are applied to obtain a differential waveform, a reference waveform can be extracted even in presence of space charge; however, in testing of extra high voltage insulation systems, this method requires voltage control and certain time for measurement; moreover, reference waveforms may be affected by space charge variation. Lock-in detection techniques address this problem be repeatedly extracting signals synchronously to periodic variation of bias, but his requires a separate control system, which is unsuitable for extra-high voltage power sources. In correlation method that uses correlation between bias voltage and response signal, data can be collected asynchronously with respect to irregular variation of bias voltage. In both differential and correlation methods, influence of space charge and Maxwell stress can be eliminated in calibration.

As shown in Fig. 3-16, electric field distortion about 0.4 kV/mm caused by original space charge in specimen (11-mm thick polyethylene plate) was measured. This corresponds to accuracy of 2% assuming operating field of 20 kV/mm in extra-high voltage DC cables.

In case of high bias voltage, space charge may change during measurement; therefore, one has to assign an appropriate weight to bias voltage in analysis, or to take some measures to suppress bias voltage variation and/or to speed up measurement. Dealing with substantial variation of space charge is somewhat complicated issue to be considered separately.

3.3.6 Conclusion

1. As regards space charge measurement using pulsed electroacoustic method, a technique was proposed to extract reference signals (expressing impulse response) required for calibration by changing bias voltage, and correlating it with acoustic signal variation.

2. Distributions of electric charge, field, and potential can be calibrated by acquiring reference signals after eliminating influence of space charge and Maxwell stress.

3. No additional functions are needed for data sampling even if an extra-high voltage source is used for bias.

4. Calibration signals can be acquired under unchanged conditions of a specimen and measuring system even if temperature distribution varies or a charging history exists.

3.4 Frequency-resolved analysis calibration

3.4.1 Introduction

In Section 3.3, the author proposed the correlating calibration method, providing a way to record the acoustic signal as well as the calibration voltage simultaneously [25]. The signal without any effect of space charge can then be used as a reference signal, is obtained by determining the slope for all the sampling points, which represents the intensity of the free charge induced at the electrode depending on the bias voltage, when space charge in the specimen stays still. For this method, the premise is that the space charge distribution in the specimen does not change when the bias voltage is varied during the measurement.

However, in an actual measurement, it is difficult to guarantee that the space charge distribution remains static if the bias voltage applied to the insulating material is in a constantly changing and unpredictable state [26].

To solve this problem, the author now introduce frequency - resolved analysis to the calibration measurement, determining the dielectric response spectrum and observing the change of the imaginary component in the frequency domain after performing a Fourier transform. The dielectric relaxation spectrum is used to estimate the optimal frequency to acquire the reference signal.

For simulation and experimental validation, EVA (ethylene-vinylacetate copolymer) film was used as a test specimen, and the acoustic signal during the bias voltage application was analyzed. The author exploited the fact that the electrode charge responds immediately to a change in bias voltage, whereas the space charge distribution changes with a time delay due to a change in bias voltage. The space charge formation acquired from both the high frequency domain, where the imaginary part is close to zero, and the low frequency domain, which is still affected by the moving space charge, are compared by a practical measurement.

3.4.2 Methodology

Figure 3-17 illustrates a space charge measurement by the PEA method [27]-[29]. The dielectric constant (permittivity) of a specimen sandwiched between parallel plate electrodes is uniform across the specimen thickness, with a space charge in the center and its induced charges on both electrodes. The sum of the charges is always zero because of the Gaussian law. In this figure, it is assumed that when the bias voltage is applied, the induced charge on the electrodes changes, whereas the space charge and its induced charges stay stable. However, it is considered that the space charge may vary along with the bias voltage especially when high DC voltage is applied or the conductor is at high temperature. And the waveform correlative method mentioned at former section has a necessary condition, which is that the space charge stays still during the measurement and makes it not fit this situation.

In order to measure the charge distribution, a pulse voltage is applied. The acoustic signal generated by the interaction with the charge is detected by a piezoelectric sensor. The linearity of the piezoelectric sensor and amplifier is assumed to be ensured. The intensity and time lag of the signal correspond to the charge density and position, respectively. The detected signal is affected by the pulse voltage waveform, the acoustic propagation path, and the frequency response of the piezoelectric element and amplifier. To reconstruct the true charge distribution, a deconvolution process is required, using an appropriate reference signal.

The induced charge on the electrode is a surface charge, and the signal component obtained from this source of acoustic signal (sound source) can be regarded as the impulse response of the measurement system including all the factors mentioned above. In case of a parallel electrode system, the signal from the electrode closer to the sensor is normally used as the impulse response. An appropriate window function is applied to remove the signal component originated from the other electrode. To obtain a reference signal, it is necessary to eliminate the effect of space charge. Referring to the signal obtained in this way, the signal from all the sound sources in the specimen can be processed by deconvolution to obtain a signal proportional to the charge distribution.

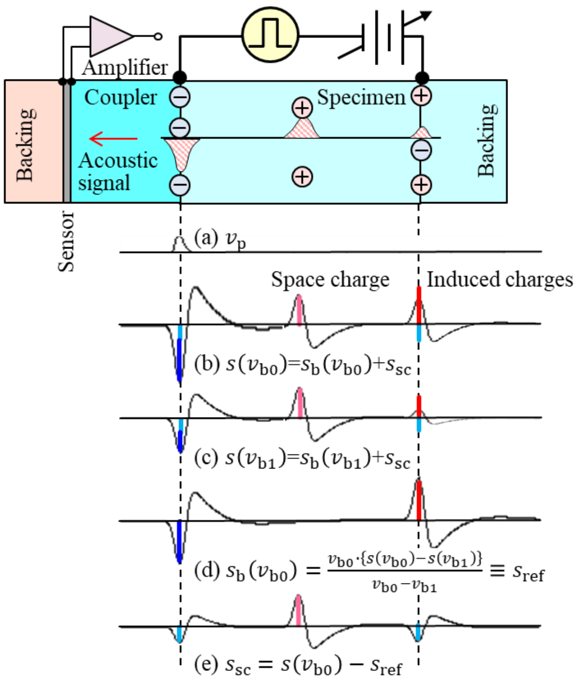

Fig. 3-17 Extraction of signal corresponding to space charge. (a) Pulse voltage, (b)(c) response at different bias voltages, (c) differential waveform, (d) signal component corresponding to space charge. (e) signal component due to the Maxwell stress.

Figure 3-17 also illustrates basic idea of the extraction of the reference signal and the signal corresponding to space charge. Under the application of bias voltage v_b and pulse voltage v_p, the Maxwell force between the electrodes in the absence of space charge can be represented as:

$$\frac{\varepsilon}{2}E^2(t) = \frac{\varepsilon}{2d^2}\{v_b + v_p(t)\}^2 = \frac{\varepsilon}{d^2}\left[\frac{1}{2}v_b^2 + v_b v_p(t) + \frac{1}{2}v_p^2(t)\right] \quad (3\text{-}16)$$

where E is the instantaneous electric field, ε is the dielectric constant and d is the thickness of the specimen, respectively. The first term is caused by the bias voltage which can be considered as a constant, so this component does not generate any acoustic signal. The second term comes from the interaction between the pulsed electric field and the induced charge at the electrodes caused by the bias voltage (as space charge is not assumed). The third component represents the Maxwell force caused only by the pulsed electric field. In most cases, the bias and pulse voltages conform to the condition $|v_{\mathrm{b}}| \gg |v_{\mathrm{p}}|/2$, so this term can be ignored.

When the specimen contains space charge, the process to extract the reference signal is to apply two different levels of DC voltage to the specimen, v_{b0} and v_{b1}. Two signals, $s(v_{\mathrm{b0}})$ and $s(v_{\mathrm{b1}})$, in diagrams (b) and (c), are thus obtained. Both of them contain three components, induced charge generated by the bias voltage, the space charge and induced charge generated by the space charge. As the signal components due to space charge are independent of the bias voltage, they cancel out after taking the difference between the two signals as:

$$\frac{\varepsilon}{d^2}(v_{\mathrm{b0}} - v_{\mathrm{b1}})v_{\mathrm{p}}(t) \quad (3\text{-}17)$$

The resulting signal is proportional to the pulse voltage. The signal without the effect of space charge at $v_{\mathrm{b}} = v_{\mathrm{b0}}$ can be assumed as shown in the diagram (d) as:

$$s_{\mathrm{b}}(v_{\mathrm{b0}}) = \frac{v_{\mathrm{b0}} \cdot \{s(v_{\mathrm{b0}}) - s(v_{\mathrm{b1}})\}}{v_{\mathrm{b0}} - v_{\mathrm{b1}}} \equiv s_{\mathrm{ref}} \quad (3\text{-}18)$$

In addition, the signal containing only the component associated with space charge can be obtained as:

$$s_{\mathrm{sc}} = s(v_{\mathrm{b0}}) - s_{\mathrm{ref}} \quad (3\text{-}19)$$

as indicated in diagram (e).

The above methods assume that the space charge does not fluctuate over time. However, there is a concern that the space charge may fluctuate in the process of acquiring the calibration signals, especially when measuring at high temperatures or when the voltage change takes time. For this reason, it is necessary to acquire the signals for calibration at intervals of as short time as possible before and after the voltage fluctuation, but the condition for this is not clear. This section describes the signal processing when the space charge changes with a certain relaxation time (delay) following the change in the bias voltage.

Figure 3-18 illustrates the reference signal extraction by means of frequency domain analysis. The extraction is explained in detail below. The instantaneous value of the fluctuating bias voltage $v_{\mathrm{b}}(t_i)$ and corresponding acoustic signal $s(t_i, t_j)$ are simultaneously recorded, t_j represents time correlated to the specimen location of each signal acquisition, and t_j represents j-th sampling point of each acquired waveform. In general, t_i is of the order of seconds or milliseconds, and t_j is of the order of nanoseconds or microseconds.

Let $s_{\mathrm{b0}}(t_j) \equiv s_{\mathrm{ref}}(t_j)$ be the reference signal that is obtained with the bias voltage v_{b0}. Then, the response signal $s(t_i, t_j)$ for any bias voltage $v_{\mathrm{b}}(t_i)$ is:

$$s(t_i, t_j) = s_{\mathrm{b}}(t_i, t_j) + s_{\mathrm{sc}}(t_i, t_j) + n(t_i, t_j) = \frac{v_{\mathrm{b}}(t_i)}{v_{\mathrm{b0}}} s_{\mathrm{b0}}(t_i, t_j) + s_{\mathrm{sc}}(t_i, t_j) + n(t_i, t_j) \quad (3\text{-}20)$$

where $s_{\mathrm{b}}(t_i, t_j)$ is the component due to the induced charge on the electrodes caused by the instantaneous bias voltage $v_{\mathrm{b}}(t_i)$, $s_{\mathrm{sc}}(t_i, t_j)$ is the component due to space charge and the resulting induced charge on the electrodes, and $n(t_i, t_j)$ is the noise component. Equation (3-20) represents the relationship between the bias voltage $v_{\mathrm{b}}(t_i)$

and the response signal component $s(t_i, t_j)$ assuming the sampling point t_j is fixed. The Fourier transform of each signal component at t_j gives:

$$S(\omega_i, t_j) = S_{\mathrm{b}}(\omega_i, t_j) + S_{\mathrm{sc}}(\omega_i, t_j) + N(\omega_i, t_j) = \frac{V_{\mathrm{b}}(\omega_i)}{v_{\mathrm{bo}}} S_{\mathrm{b0}}(\omega_i, t_j) + S_{\mathrm{sc}}(\omega_i, t_j) + N(\omega_i, t_j) \quad (3\text{-}21)$$

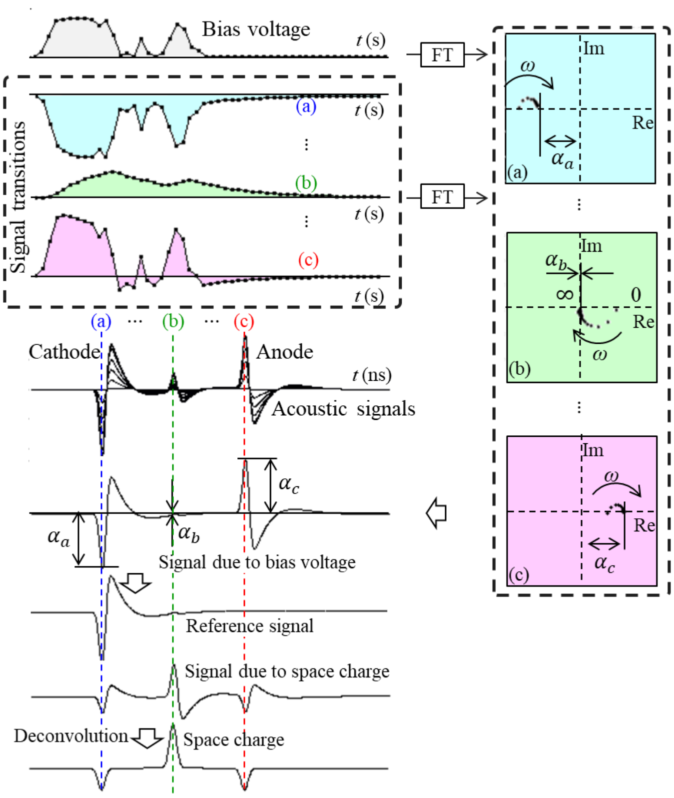

Fig. 3-18 Extraction of the reference signal using frequency domain analysis.

If the space charge does not fluctuate, the signal component $s_{\mathrm{sc}}(t_i, t_j)$ will be constant, so the spectrum $S_{\mathrm{sc}}(\omega_i, t_j)$ will have only a DC component at any sampling point, which is independent of the fluctuation component of the bias voltage. $n(t_i, t_j)$ has no correlation with the bias voltage variation. If the noise is small, $S(\omega_i, t_j)$ is proportional to the frequency component of the bias voltage, $V_{\mathrm{b}}(\omega_i)$, for all $\omega_i \neq 0$. The estimate of $S_{\mathrm{b0}}(t_j)$, which can be considered as the reference signal under the bias voltage v_{b0} is obtained by using $W_i(\omega_i)$ as a weight function:

$$\widehat{S_{\mathrm{b0}}}(t_j) = \sum_i \frac{W_i(\omega_i) v_{\mathrm{bo}} S(\omega_i, t_j)}{V_{\mathrm{b}}(\omega_i)} \Big/ \sum_i W_i(\omega_i) \quad (3\text{-}22)$$

$$\omega_i \neq 0$$

If the signal component $s_{\mathrm{sc}}(t_i, t_j)$ due to the space charge varies with the signal acquisition time t_i, then $S_{\mathrm{sc}}(\omega_i, t_j)$ will have frequency components other than the DC component. However, in such a case there must be a delay in the response and an imaginary component must appear in the spectrum. Therefore, analysis in such a frequency range should be avoided or the weight in such a frequency range should be significantly reduced.

The space charge, whose transition follows the bias change with a certain delay, dominates the signal component at (b) in Fig. 3-18. The signal components at (a) and (c) are influenced by induced charges due to the space charge as well as induced charges strictly proportional to the bias voltage. The transition in each component is normalized in the frequency domain by the transition of the bias voltage by drawing a trajectory. Each trajectory shows a semicircle as the frequency changes from zero (DC) to high frequency, its imaginary component indicates that there is a component that follows the bias voltage with a certain delay time. The results analyzed for signals from the electrode surface have the same meaning as the dielectric relaxation spectrum as seen from the external circuit. The real component at high frequency represents the signal component that is linearly proportional to the change in bias without delay. Therefore this component can be attributed to the signal without the influence of the space charge.

Extracting this number (α) along the sampling time like α_a, α_b, and α_c in Fig. 3-18, a waveform without any influence of space charge can be extracted. The first component of the waveform that represents the impulse response of the measurement system is subsequently extracted, and used for deconvolving the signal that may include the space charge component.

3.4.3 Numerical simulation

A numerical simulation was carried out to illustrate the calibration methods described in Section 3.4.2.

The response signal was calculated by hypothetically varying the bias voltage, assuming that there is a space charge in the center of the specimen with a relaxation time τ = 27 s, where the relaxation time is defined as:

$$q = q_0(1 - \exp\left(-\frac{t}{\tau}\right)) \qquad (3\text{-}23)$$

In Fig. 3-19, the bias voltage is indicated as diagram (I), and transition of the response signal (II) corresponding to the sampling point (b) in Fig. 3-18. The imaginary component shows a peak at low frequency (8 mHz) and subsequently decreases gradually. The value of the imaginary component is almost 0 in the high frequency region (approximately above 105 mHz), which indicates that space charge no longer moves along with the bias voltage variation in this frequency region.

Figure 3-20 illustrates the comparison between signals extracted as the reference signals at different frequency points (8 mHz and 105 mHz). Signal extracted at 8 mHz shows a component suspected to be caused by space charge, indicating that it is not available to be used in the calibration process. On the other hand, the signal extracted at 105 mHz does not show such a component, suggesting that it can be considered as free from the effect of space charge.

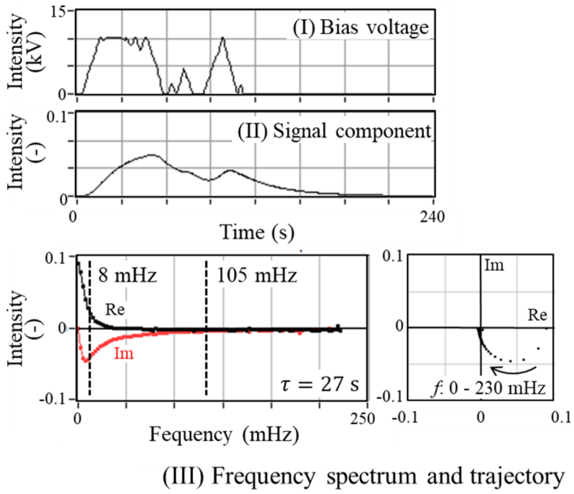

Fig. 3-19 Change in time of the bias voltage and corresponding response signals.

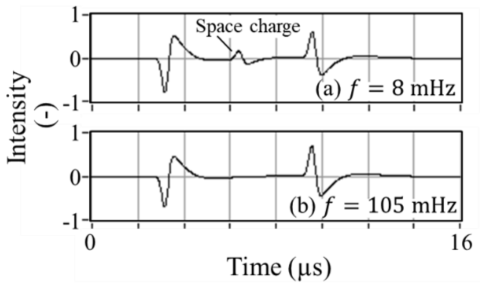

Fig. 3-20 Reference signals extracted by correlating the frequency component of bias voltage and that of response signal. (a) signal obtained at 8 mHz; (b) signal obtained at 105 mHz. Note that signal (a) is not suitable as a reference signal for practical calibration as it contains space charge component.

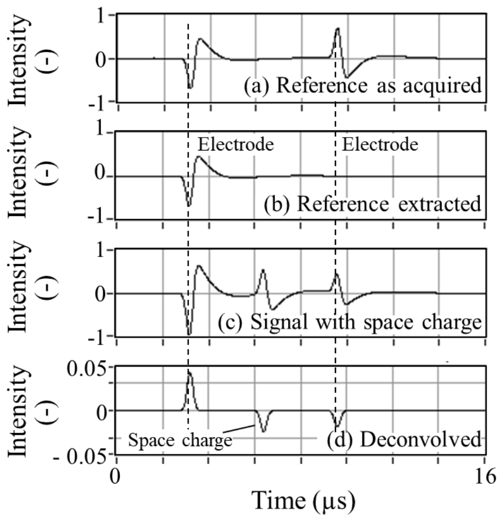

Fig. 3-21 Extraction of the impulse response. Voltage is output equivalent at the sensor ($\tau = 27$ s, f = 210 mHz).

The reference signal shown in Fig. 3-21(a) is extracted from the frequency component at 210 mHz, which is well above 105 mHz. In this frequency region, the imaginary component of the spectrum is almost zero. The signal (c), which is affected by space charge, is subsequently deconvolved referring to the signal component (b). As a result, the space charge component is reproduced at the center of the specimen.

3.4.4 Practical measurement and discussion

A. With Mobile Space Charge

To demonstrate the accuracy of the proposed methodology, we measured a 150 μm-thick EVA (ethylene-vinylacetate copolymer) film specimen, and analyzed the dielectric relaxation spectrum at different sampling points. Fig. 3-22 shows the result by applying a bias voltage changing from zero to -8 kV, its transition is indicated in diagram (I). The diagram (II) indicates the transition of the PEA signal intensity at sampling points (a) and (b), their sampling points are indicated in the diagram (III) with several PEA waveforms. Note that only a selection of the waveforms is shown for easier visibility.

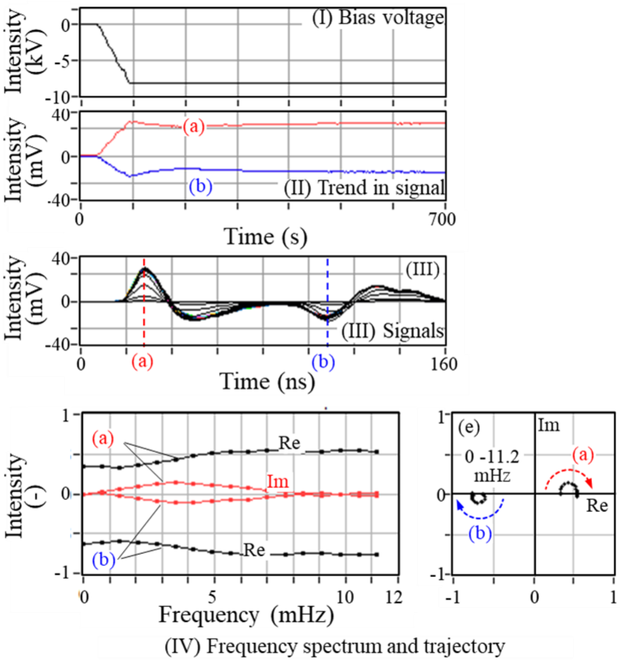

Fig. 3-22 Measurement results of mobile space charge.

Through the Fourier analysis, both transitions ((a) and (b) in diagram (II)) were normalized in the frequency domain to draw spectrum curves and trajectory as shown in the diagram (IV). The real part represents the component caused by the charge which is strictly proportional to the bias voltage. The imaginary component is due to the induced charge at the electrodes caused by space charge inside the specimen that changes its intensity following the bias voltage variation with a certain delay.

As the frequency changes from zero (the DC component) to higher frequency, each trajectory shows as a half circle. The peak in the imaginary part for each electrode signal appears at almost identical frequency, although the polarity of the peak depends on the sampling point. At higher frequencies the value of the imaginary component gradually decreases to zero. The reference signal should be extracted at a frequency range where the space charge component no longer follows the bias voltage variation, i.e. the value of the imaginary component should be close to zero.

Figure 3-23 compares reference signals by the frequency analysis, taken from different frequencies. The solid black curve (a) indicates the signal acquired at 9.1 mHz, and the red dashed curve (c) indicates the signal at 1.4 mHz.

For control, the signal acquired by differentiating two signals, namely the signals before applying -8 kV bias voltage and 2 s later is indicated as (b) with a black dashed curve. As curves (a) and (b) are quite identical, it seems that 2 s of interval with 8 kV stroke of bias voltage is not enough for space charge to change its distribution in the specimen. So both these curves can be employed as the reference signal. However, if only the differential signal (b) is obtained, there is no way to check whether it is appropriate as a reference signal. Frequency analysis is considered to be an effective method for checking this. In addition, in this measurement example, the rise time of the bias voltage was set to approximately 60 s, indicating that even if a steeply rising step voltage cannot be obtained, the reference signal can be extracted if it has sufficient frequency components for analysis. On the other hand, the signal (c) extracted at 1.4 mHz is supposed to be still influenced by the space charge component.

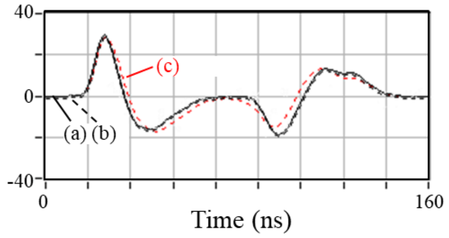

Fig. 3-23 Extracted calibration signals. (a): signal acquired at 9.1 mHz; (b): signal acquired by differentiating two signals in 2 s intervals; (c): signal acquired at 1.4 mHz.

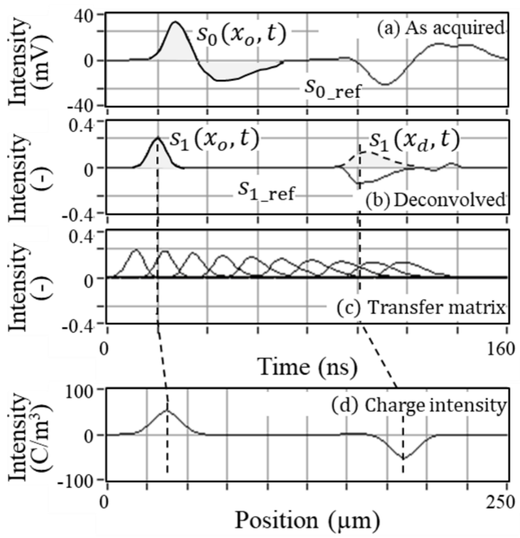

Fig. 3-24 Compensation of acoustic signal propagation in the measurement and specimen systems.

Figure 3-24 shows the deconvolution process taking into account the transfer function through both the measurement system and specimen system. The diagram (a) indicates the reference signal taken from 9.1 mHz (s_{0_ref}). A signal component corresponding to the left side electrode (closer to the acoustic sensor) was extracted as $s_0(x_0,t)$ using an appropriate window function. This can be recognized as the impulse response of the measurement system. The whole signal s_{0_ref} was deconvolved referring to $s_0(x_0,t)$. The result is shown as the solid curve in Fig. 3-24(b) as s_{1_ref}.

The component corresponding to the right-side electrode, $s_1(x_d,t)$, was normalized in frequency domain by one corresponding to the left side electrode $s_1(x_0,t)$. Note that $s_1(x_d,t)$ was rearranged to the polarity was identical to $s_1(x_0,t)$. The transfer function from any point in the specimen to the left side electrode was calculated as:

$$s_1(x,t) = IFT\left[\frac{x}{x_d-x_0}\frac{S_1(x_d,\omega)}{S_1(x_0,\omega)}\right] \quad \text{(3-24)}$$

where S represents the Fourier transform of s, x is a position, x_0 and x_d are the positions of two electrodes. Diagram (c) represents these transfer functions in discreet and thinned out form. After creating a transfer matrix using these transfer functions, the signal s_{1_ref} can be deconvolved again to show the waveform corresponding to charge intensity.

Figure 3-25 shows the process to calculate the charge intensity distribution after acquiring the target signal s_{0_tgt}. The signal as acquired was deconvolved referring to $s_0(x_0, t)$ in Fig. 3-24, and deconvolved again referring to the transfer matrix indicated in Fig. 3-24(c). The signal s_{1_ref} in Fig. 3-24 corresponds to the charge produced by applying a bias voltage v_{b0}.

$$q_0 = \varepsilon_0 \varepsilon_r \frac{v_{b0}}{x_d - x_0} \quad (3\text{-}25)$$

q_0 has the dimension of surface charge density. Therefore, the signal in Fig. 3-25(b) multiplied by q_0 represents the charge density distribution (c).

Electric stress and potential distributions are:

$$E(x) = -\varepsilon_0 \varepsilon_r \int_{-\infty}^{x} \rho(x) dx \qquad (3\text{-}26)$$

$$\Phi(x) = \int_{-\infty}^{x} E(x) dx \quad (3\text{-}27)$$

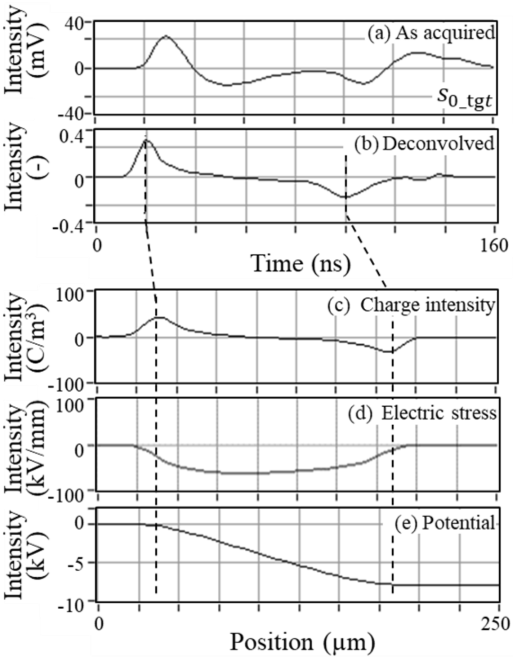

Fig. 3-25 Calculated charge distribution, electric field distribution and potential distribution when -8 kV is applied to 150 µm-thick EVA.

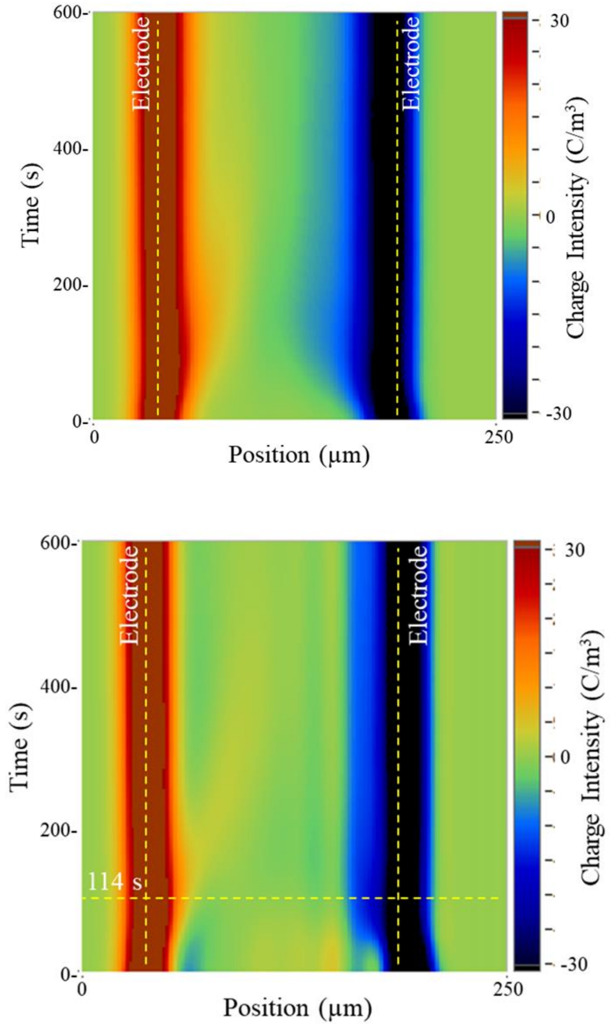

Fig. 3-26 Charge distribution at time variation. The bias voltage is considered to reach to its final value (- 8 kV) at 0 s.

To analyze the formation of space charge during continuous bias voltage application, the processes above were applied to all the target signals. Fig. 3-26 (a) and (b) represent the results using the reference signals taken at 9.1 mHz and 1.4 mHz, respectively. Fig. 3-26 (b) shows a slight residual space charge at the time of applying the bias voltage, the induced charge formed on the electrode immediately after applying the voltage, and the space charge formation process in the vicinity of the electrode.

In the profile (a), almost no space charge is seen shortly after the bias voltage reached to -8 kV. The space charge inside the specimen started to increase from the electrode and spread inside the specimen. As time increases, the number of space charges of positive and negative polarities within the specimen tends to be similar, so that a region of charge density close to zero due to the cancellation of positive and negative charges occurs in the latter part of the time axis. This result is consistent with previous experiments using EVA as a specimen [29].

On the other hand, as can be seen in profile (b), when the reference signal is taken at 1.4 mHz, both positive and negative space charges seem to be pre-existent near the electrodes, and decrease to zero as with time. This is because the signal not affected by the space charge has been deconvolved by the reference signal affected by the space charge. This suggests that the signal extracted using the low-frequency component is not suitable as a reference signal.

B. With stable space charge

Figure 3-27 shows the result of a space charge measurement and calibration using an 11 mm-thick low-density polyethylene sample which was assumed to have a stable pre-existing space charge. The bias voltage was changed as in diagram (I), and the signal at sampling point (a) of the acoustic waveform was extracted, as shown in diagram (II). The signal at sampling point (a) is affected by induced charge due to the bias voltage, as well as the counter charge caused by space charge that exists inside the specimen. So the signal at sampling point (a) has two components, namely, dynamic induced charge which is proportional to the bias voltage, and a stable induced charge caused by the pre-existing space charge. As shown in diagram (IV), the imaginary component is very low through the analyzed frequency. In addition, the trajectory was limited to a single point on the Re-axis, except for one plot at 0 mHz. For plot at 14 mHz, where the bias voltage transition spectrum seems to be near to 0, so the frequency spectrum shows a fluctuation, which leading a high value during the normalization. These features suggest that the space charge inside the specimen is stable even when the bias voltage is varying.

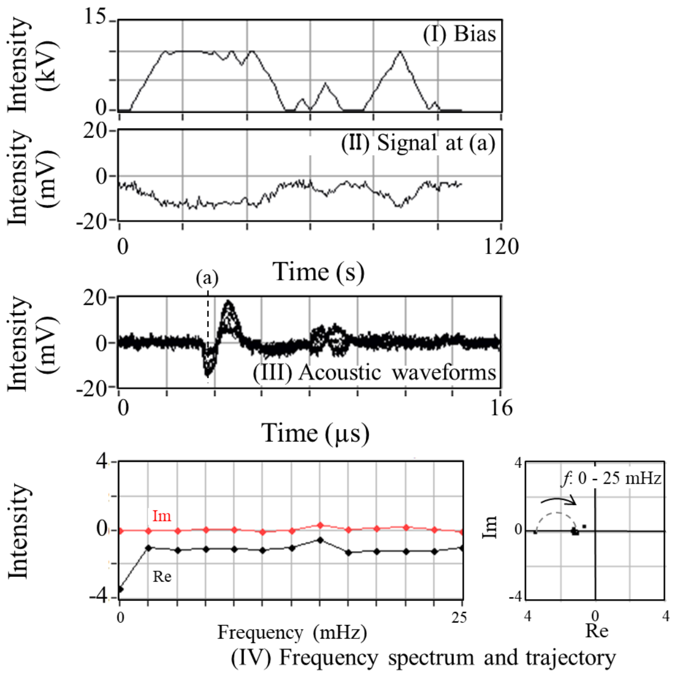

Fig. 3-27 Measurement results of stable space charge.

The same process as in Fig. 3-25 was performed to extract the reference signal as shown in Fig. 3-28 (b), and compared with the signal (a) under the DC bias voltage of 10 kV. The result of deconvolution was compensated considering acoustic attenuation depending on the depth along the specimen thickness and interpreted into charge density distribution (c). It is seen that the specimen was positively charged along a wide range through the thickness. As a result, the electric stress distribution (d) was not flat, and the potential distribution (e) was not straight.

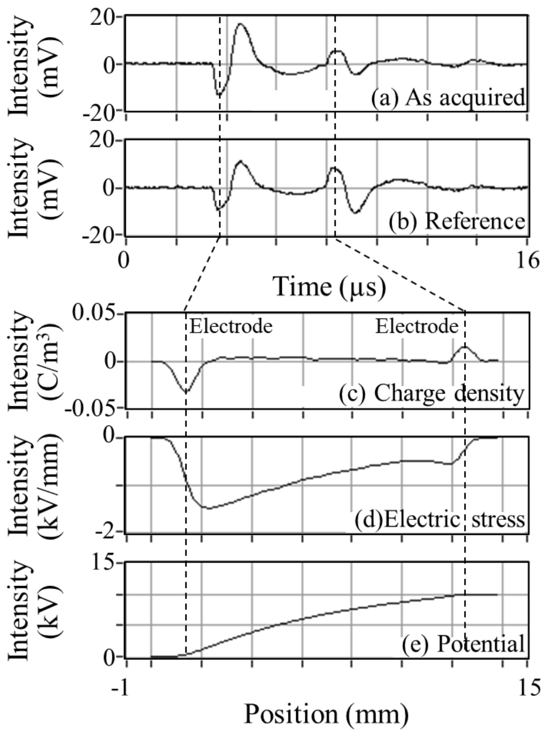

Fig. 3-28 Calculated charge distribution, electric field distribution and potential distribution when -8 kV is applied to 11 mm-thick low-density polyethylene.

C. The space charge response to bias voltage

The space charge buildup time is represented in Equation (3-24) by the relaxation time τ. In thick insulating systems such as power cables, the space charge buildup time is expected to be longer than the order of seconds (and it is in many cases). When the bias voltage changes, the orientation polarization with a low response frequency follows. However, as ε in Equaition (3-16) is the dielectric constant for the high frequency region of the pulsed electric field, it is not affected by the occurrence of uniform orientation polarization with a much lower response frequency. Therefore such polarization is not detected by the PEA method.

If the time variation of the space charge follows the time variation of the bias voltage, it becomes difficult to separate the signal due to the space charge from the signal due to the free charge on the electrode. However, if the change in bias voltage has a broad frequency spectrum and only the appropriate frequency components are extracted from it and correlated with the response signal, the signal components caused by the space charge can be removed and the signal caused by the free charge on the electrode can be extracted as a reference signal.

Figure. 3-22 (I) shows a voltage variation that can be manually applied in a high voltage laboratory and has a frequency component up to about 100 mHz. In the figure, the characteristic frequency due to relaxation of the dielectric response due to space charge is assumed to be 6 mHz (corresponding to 27 seconds in relaxation time), which is sufficiently lower than 100 mHz. If the frequency at which the bias voltage is correlated with the response signal is set to 100 mHz, a correct reference signal can be extracted because the space charge cannot follow the change in bias voltage. However, when this is set to 8 mHz, the space charge follows the change in bias voltage, indicating that the correct reference signal cannot be extracted.

This relaxation time varies significantly with temperature, even for the same material. Under conditions where the space charge relaxation time is short, for the reference signal acquisition, the bias voltage must change faster, i.e., have a higher frequency component.

Polarity reversal or short-circuiting the sample produces a steep time variation in the bias voltage that may be suitable for obtaining a reference signal. However, since this can damage the sample and interfere with subsequent testing, it is practical to manipulate the output of the high voltage power supply to vary the bias voltage. Since it takes several tens of seconds for the voltage to stabilize in an extra-high-voltage DC power supply, experiments were conducted to show that a reference signal can be retrieved even when assuming a rise time of that magnitude.

3.4.5 Conclusion

A method for acquiring the reference signal necessary for calibrating the space charge distribution of a specimen whose space charge is prone to movement was studied. And the proposed frequency - resolved analysis is proved to be feasible in a space charge moving circumstance based on both simulation and practical experiment

(1) The relationship between the bias voltage and the change in time of the response signal is analyzed with the aid of the Fourier transform to obtain a spectrum of the response.

(2) In the low-frequency region where the space charge follows the change in bias voltage, an imaginary component appears in the spectrum because of the delay in the response.

(3) In the high-frequency region, where the spectrum has only a real component, only the induced charge on the electrode follows the bias voltage without delay, so this component is extracted and used as a reference signal that is not affected by the space charge.

(4) Using this reference signal, deconvolution of the target signal yields a profile representing the charge distribution.

(5) The methodology was explained with the aid of simulations. Experiments were conducted using thin EVA film, in which space charge is easily changed, and a thick LDPE slab, in which space charge is stable. The distribution of charge density, electric field, and potential were analyzed and the feasibility of the proposed methodology was demonstrated.

3.5 References

[1] M. Abou Dakka, A. T. Bulinski and S. S. Bamji, "An improved technique for space charge distribution measurements in solid dielectrics," *Conference Digest Conference on Precision Electromagnetic Measurements*, Canada, pp. 12-13, 2002.

[2] Z. Xu, J. Zhao and G. Chen, "An improved pulsed electroacoustic system for space charge measurement under AC conditions," *2010 10th IEEE International Conference on Solid Dielectrics*, Potsdam, pp. 1-4, 2010.

[3] Y.L. Chong, H. Miyake, Y. Tanaka, T. Takada, H. Nakama and G. Chen, “Space Charge in Polyethylene under AC Electric Stress using the Pulsed Electroacoustic Method,” *Annual Report Conference on Electrical Insulation and Dielectric Phenomena*, pp.77-80, 2004.

[4] T. Mori, H. Miyake, Y. Tanaka and T. Takada, "Simultaneous measurements of space charge distribution and external current," P*roceedings of 2011 International Symposium on Electrical Insulating Materials, Kyoto*, pp. 370-373, 2011.

[5] N. Hozumi, Y. Muramoto and M. Nagao, "Carrier Mobility in Ethylene- Vinylacetate Copolymer Estimated by Transient Space Charge," *IEEE Transactions on Dielectrics and Electrical Insulation*, vol. 8, No.5, pp.849-853, October, 2001.

[6] C. Li, B. Han, H. Zhang, H. Zhao and C. Zhang, "Effect of acetophenone on the breakdown strength of polyethylene," *2015 IEEE 11th International Conference on the Properties and Applications of Dielectric Materials (ICPADM)*, Sydney, pp. 492-495 , 2015.

[7] N. HUSSIN, G. CHEN, "Modification of Space Charge Pattern and Charge Mobility of Low Density Polyethylene (LDPE) in the presence of Crosslinking Byproducts," *Proceedings of the 9th International Conference on Properties and Applications of Dielectric Materials*, Harbin, China, pp.950-953, July 2009.

[8] N. Hozumi, E. B. Prastika, S. Zahra, T. Kawashima and Y. Murakami, "Dual-domain Deconvolution Process Applied to Time-resolved Quantitative Dielectric Measurement," 2020 IEEE 3rd International Conference on Dielectrics (ICD), Valencia, Spain, pp. 347-350, 2020.

[9] Technical Committee for Investigation of Space Charge Distribution Measurement Methods and Standardization of Dielectric and Insulating Materials, "Space Charge Distribution Measurement Methods and Standardization for Dielectric and Insulating Materials", IEEJ Technical Report, No. 834, 2001.
誘電・絶縁材料の空間電荷分布計測法と標準化調査専門委員会.「誘電・絶縁材料の空間電荷分布計測法と標準化」, 電気学会技術報告, 第 834 号, 2001.

[10] Technical Committee for Investigation of Space Charge Distribution Measurement Methods and Standardization of Dielectric and Insulating Materials, "Standardization of Calibration and Advanced Measurements of Space Charge Distribution at High Temperature Using the Pulsed Electro-acoustic Method," IEEJ Technical Report, No. 1491, 2020.
誘電・絶縁材料の空間電荷分布計測法と標準化調査専門委員会.「高温下における PEA 法を用いた空間電荷分布測定の校正法標準化と PEA 法の応用測定技術」, 電気学会技術報告, 第 1491 号, 2020.

[11] N. Hozumi, T.Takeda, H. Suzuki and T. Okamoto: "space charge behavior in XLPE cable Insulation under 0.2-1.2MV/cm dc fields," IEEE transactions on Dielectrics and Electrical insulation, vol. 5, No.1, pp.82 – 90, 1998.

[12] T. Maeno, K. Fukunaga, Y. Tanaka, and T. Takada: "Signal Processing of the High Resolution PEA Charge Measurement System," IEEJ Trans. A, Vol.115, No.5, pp.405 – 410, 1995.
前野恭, 福永香, 田中康寛, 高田達雄.「高分解能 PEA 空間電荷測定装置における信号処理」. 電学論 A, 115 巻 5 号, 平成 7 年 . pp.405 - 410.

[13] M. Fukuma, H. Tomita and T. Maeno: "Space Charge Measurement for 27mm Thick XLPE Sample in PEA," Conference Proceedings of ISEIM, pp.405 – 410, 2014.

[14] R. Ozaki, K. Kadowaki: "Analysis of Attenuation and Dispersion of Acoustic Waves in Low-Density Polyethylene," IEEE Transactions on Dielectrics and Electrical Insulation, vol. 27, No.6, pp.2007 2013 – 397, 2020.

[15] E. B. Prastika, S. Zahra, X. Li, Y. Murakami, T. Kawashima, N. Hozumi and Yoonhyoung Kim: “The Application of Signal Processing Using Dual Domain Deconvolution for New Space Charge Measurement Method in HVDC Full-Size Cables,” 2020 International Symposium on Electrical Insulating Materials (ISEIM), pp. 277-280, 2020.

[16] N. Hozumi, E. B. Prastika, S. Zahra, T. Kawashima and Y. Murakami: “Dual-domain Deconvolution Process Applied to Time-resolved Quantitative Dielectric Measurement,” 2020 IEEE 3rd International Conference on Dielectrics (ICD), pp. 347-350, 2020.

[17] K. Matsui, Y. Tanaka, T. Takada, T. Fukao and T. Maeno: “High Sensitivity PEA System with Dual Polarity Pulse Generator,” IEEJ Trans A, Vol. 126, No. 3, pp.178-184, 2006.
松井康平, 田中康寛, 高田達雄, 深尾正, 前野恭.「正負パルス電圧を用いた高感度 PEA 装置」電学論 A, Vol. 126, No. 3, pp.178 -184, 2006.

[18] S. Morita, N. Fuse, T. Takahashi, T. Takahashi, S. Zahra and N. Hozumi, "Space Charge Measurement of 23-mm-Thick XLPE Cable at Ambient and High Temperatures," in IEEE Transactions on Dielectrics and Electrical Insulation, vol. 29, no. 4, pp. 1491-1497, Aug. 2022.

[19] X. Li, S. Zahra, T. Kawashima, Y. Murakami and N. Hozumi, “Lock-in Calibration for Space Charge Measurement,” 2020 IEEE 3rd International Conference on Dielectrics (ICD), pp. 391-394, 2020.

[20] M. Utagawa, X. Li, S. Zahra, E. B. Prastika, T. Kawashima and Y. Murakami, N. Hozumi: “Study on Lock-in Calibration for Space Charge Measurement,” Technical Meeting on Electric Wire and Power Cable, IEE Japan, pp. 39-43, 2020.

[21] X. Li, M. Utagawa, Yeong-Guk AN, T. Kawashima, Y. Murakami and N. Hozumi: “Study on Acoustic Propagation Paths for Space Charge Measurement in Thick Insulating Materials,” Joint Technical Meeting on "Dielectrics and Electrical Insulation" and "Electric Wire and Power Cable", IEE Japan, pp. 41- 46, 2021.

[22] S. Zahra, T. Kawashima, Y. Murakami and N. Hozumi, “Small-size Space Charge Measurement Device for Power Cables by Using Electrically Insulated Acoustic Coupler,” 2020 IEEE 3rd International Conference on Dielectrics (ICD), pp. 359-362, 2020.

[23] S. Zahra, S. Morita, M. Utagawa, T. Kawashima, Y. Murakami, N. Hozumi, Peter Morshuis, Cho Young-il and Kim Yoon-hyoung:"Space Charge Measurement Equipment for Full-scale HVDC Cables Using Electrically Insulating Polymeric Acoustic Coupler," in IEEE Transactions on Dielectrics and Electrical Insulation, doi: 10.1109/TDEI.2022.3169106.

[24] Y. Li: “Space charge measurement in lossy solid dielectric materials by pulsed electroacoustic method,” Ph. D thesis, Musashi Institute of Technology, 1994.
李 英.「パルス静電応力法による損失固体誘電体中の空間電荷分布測定に関する研究」: [D].武蔵工業大学, 1994.

[25] X. Li, T. Kawashima, Y. Murakami and N. Hozumi "Basic study on calibration using waveform variation in space charge measurement by pulsed electroacoustic method" [J]. Electrical Engineering in Japan, 2023, 216(2): e23436.

[26] N. Hozumi, T.Takeda, H. Suzuki and T. Okamoto, “space charge behavior in XLPE cable Insulation under 0.2-1.2MV/cm dc fields,” *IEEE Trans. Dielectr. Electr. Insul.*, vol. 5, No.1, pp.82 - 90, 1998.

[27] M. Fukuma, R. Funo, Y. Murakami, M. Nagao and N. Hozumi, "Measurement of acoustic property for signal recovery in PEA method," Proceedings of 2011 International Symposium on Electrical Insulating Materials(ISEIM), pp. 69-72, Kyoto, Japan, 2011.

[28] Mazzanti, J. Castellon, G. Chen, J.C. Fothergill, M. Fu, N. Hozumi, J. H. Lee, J. Li, M. Marzinotto, F. Mauseth, P. Morshuis, C. Reed, I. Troia, A. Tzimas and K. Wu: “The Insulation of HVDC Extruded Cable System Joints. Part 1: Review of Materials, Design and Testing Procedures”, IEEE Trans. Dielectr. Electr. Insul., Vol. 26, No. 3, pp. 964-972, 2019.

[29] N. Hozumi, Y. Muramoto, M. Nagao and Yewen Zhang, “Carrier Mobility in Ethylene- Vinylacetate Copolymer Estimated by Transient Space Charge,” *IEEE Transactions on Dielectrics and Electrical Insulation*, vol. 8, No.5, pp.849-853, October, 2001.

Chapter IV

Reduction of the calculation error due to noise fluctuation

During measurements of UHV DC insulation systems (e.g., full-size DC cables) by pulsed electroacoustics (PEA) method and the calibration methods in chapter III, the spike noise generated by the applied high-voltage pulses leads to fluctuations in the offset and tilt of the response signal baseline, which can lead to errors in the measurement and analysis results. For the measurement of thick specimens, it is difficult to eliminate this effect due to the small response signal. In this chapter, method to minimize such errors will be discussed using measurement results from a parallel plate electrode insulation system as an example.

4.1 Experiment and analysis

In solid insulating systems, mainly polymer insulation, the space charge generated in insulation materials under a high DC electric field is one of the factors that determine the insulating performance [1]-[3]. Space charge measurement is becoming indispensable as an evaluation method for insulating materials, and recently it has become practical to measure space charge in full-scale extra-high voltage insulating systems such as extra-high voltage DC cables [4].

The PEA method, which is often used as a measurement method, applies a pulse voltage to an insulation system and detects acoustic signals generated by the interaction of space charge and electric field using a piezoelectric sensor. For quantitative measurement, a bias voltage is applied in the absence of space charge, and calibration is performed with reference to the acoustic signals generated from the surface charges on the electrodes. The calibration method for 1D measurements described in IEEJ Technical Report [8]-[9] is considered correct under limited conditions, i.e., (1) signals generated from both electrodes and free from space charge are available and (2) the dielectric constant is known and uniform. Regarding (1), there was a problem that a reference signal for calibration could not be obtained for practical specimens such as cables that were internally charged at the time of acceptance due to charging history, but this problem was generally solved by changing the bias voltage and correlating it with the response signal [10]. When the space charge follows the change in bias voltage, we proposed a method to analyze the relationship between the bias voltage and the response signal by frequency analysis, and to take out and correlate only the high-frequency components to the extent that the spectrum of the normalized response signal has no imaginary components [11]. The dielectric constant in (2) is the dielectric constant in the high frequency band of the pulse voltage waveform, and it is assumed that the frequency characteristics are flat, which is usually true for most polymer insulating materials.

Electromagnetically, the distribution of space charge, electric field, and potential in a specimen obtained as a result of calibration are described by the Poisson equation, and if one of them is known, the other two can be calculated. However, when the measurement results are calibrated and analyzed according to the method described in the IEEJ technical report, discrepancies may occur between the above three parameters even after making corrections for acoustic attenuation and acoustic matching. Specifically, for example, results in which the electric field appears to leak from a specimen sandwiched between parallel-plate electrodes. Although this does not seem to be a major problem when investigating the basic properties of materials, the use of inaccurate measurement results should be avoided as much as possible when using them as basic data for measurement and insulation design. In this chapter, this problem is illustrated and a method is proposed to avoid it in the calibration process. For simplicity of discussion, the measurement was considered to be applied at an acoustically uniform insulator sandwiched between parallel plate electrodes.

Figure 4-1 illustrates the calibration of space charge using the widely practiced PEA method. When the acoustic signal (b) generated from the left electrode is taken as the reference signal when bias and pulse voltages are applied in the absence of space charge, and the target signal (c) is processed by deconvolution, a response signal proportional to the space charge distribution is obtained. The previous report (10) as well as Chapter 3 shows the details of this calculation. The reference signal is the surface charge density of $V_{\mathrm{b\_ref}}/\varepsilon d$ as the source. $V_{\mathrm{b\_ref}}$ is the bias voltage at which the reference signal is acquired, ε is the dielectric constant of the specimen, and d is the distance between the electrodes. Converting time to position using sound velocity c to produce a waveform representing the charge density distribution in the specimen (in Fig. 4-1, the charge density distribution without bias voltage). Hereafter, the reference signal is identified by "ref" and the target signal to be calibrated by "tgt" as necessary.

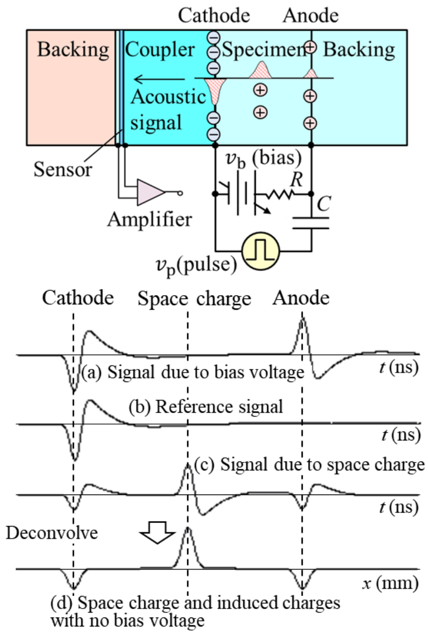

Fig. 4-1 Schematic diagram of the measurement and extraction of signal corresponding to space charge.

When acoustic attenuation is not negligible, the detection sensitivity changes depending on the location of the sound source charge, so the acoustic propagation parameters are obtained and corrected by comparing the signals generated by the electrodes on both sides in the reference signal to obtain the spatial charge distribution $\rho(x)$ in the specimen. x is the position in the thickness direction, $x = ct$, t is time. The charge distribution obtained is integrated in the thickness direction to obtain the electric field distribution, which is further integrated to obtain the electric potential distribution in the specimen.

$$E(x) = \frac{1}{\varepsilon}\int_{-\infty}^{x} \rho(x)dx \qquad (4\text{-}1)$$

$$V(x) = -\int_{-\infty}^{x} E(x)dx \qquad (4\text{-}2)$$

These are described in detail in the IEEJ Technical Report [8]-[9]. Since the specimen is sandwiched between electrodes and there are no lines of electric force entering or leaving the sample system, the electric field outside the electrodes should be zero and the potential difference between the electrodes should match the applied bias voltage, but this condition is not met in some previous published papers, for example, a finite electric field seems to be generated outside the electrodes. In the following, the experimental results for explanation and discussion of possible solutions are shown.

4.2 Measurement cell

Figure 4-2 shows the measurement system for a low-density polyethylene plate 11 mm thick. An acoustic coupling material with an acoustic impedance close to that of the specimen and a metallic backing material are used [10]. The pulse voltage applied to the sample was about 1 kV with a width of 400 ns, and the polarity of the applied voltage was defined on the upper electrode side.

The bias voltage feed line is a 50 Ω coaxial cable, which is open stub for the pulse voltage, but functions as a coupling capacitor of approximately 300 pF because of its short propagation distance of approximately 80 m, which corresponds to the pulse width. The pulse feed line was 75 Ω to match the output impedance of the pulse generator. The electrode on the side away from the piezoelectric sensor (110 μm-thick polyvinylidene fluoride (PVDF)) was made of the same polyethylene plate as the specimen with a thin electrode attached to it to ensure acoustic matching, so no acoustic signal reflection occurs in this area.

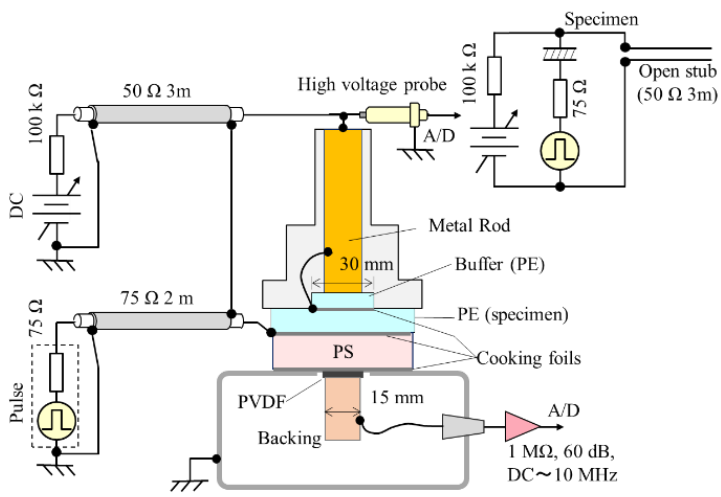

Fig. 4-2 Measurement system and equivalent electric circuit.
PS: polystyrene, PE: polyethylene, PVDF: polyvinylidene fluoride.

4.3 Analysis overview and calculation error due to baseline fluctuation

Figure 4-3(a) shows a reference waveform obtained by varying the bias voltage for a short time and correlating it with the variation component of the response waveform, which equivalently shows the response waveform when there is no space charge. The method of acquiring this waveform is described in detail in a previous report [10]. Hereafter, the intensity of the directly measured signal is indicated in μV as the value converted to the piezoelectric sensor output. From this waveform, the signal whose source is the left electrode (the lower electrode in Fig. 4-2) is extracted as the reference waveform $s_0(x_{e0}, t)$, which represents the transfer function of the measurement system, and the target signal is deconvolved. This process is defined as the first type of deconvolution processing in the PEA method for convenience, and the obtained signal is denoted as $s_1(t_k)$.

$$s_{1\_\mathrm{ref}}(t_k) = IFT\frac{FT(s_{0\_\mathrm{ref}}(t_k))}{FT(s_0(x_0,t_k))} \quad (4\text{-}3)$$

FT and IFT represent Fourier transforms and inverse transforms, respectively. However, for obtaining stable results, the numerical Laplace deconvolution was applied in this process [12]. From the obtained waveforms, the signals whose sources are the electrodes on both sides were extracted, and the acoustic propagation characteristics $\gamma(\omega) = \alpha(\omega) + j\omega/c(\omega)$ are calculated.

$$S_1(x_{e1}, \omega_k) \equiv e^{-\gamma(\omega_k)} = \frac{FT\{s_1(x_{e1},t_k)\}}{FT\{s_1(x_{e0},t_k)\}} \quad (4\text{-}4)$$

x_{e0} and x_{e1} are the left and right electrode positions, and ω is the angular frequency. The transfer function from each point x_j to the left electrode (thinned out in Fig. 4-3(c)) is

$$h_{jk}(x_j, t_k) = IFT\left[e^{-\gamma(\omega_k)}(x_j - x_{\mathrm{e0}})/(x_{e1} - x_{\mathrm{e0}})\right] \quad (4\text{-}5)$$

The deconvolution process using this transfer matrix is defined as the second type of deconvolution process for convenience, and the resulting signal is denoted as $s_2(x_j)$.

$$\begin{pmatrix} s_1(t_1) \\ \vdots \\ s_1(t_n) \end{pmatrix} \equiv \mathbf{S_1} = \begin{pmatrix} h_{11} & \cdots & h_{m1} \\ \vdots & \ddots & \vdots \\ h_{n1} & \cdots & h_{\mathrm{mn}} \end{pmatrix} \begin{pmatrix} s_2(x_1) \\ \vdots \\ s_2(x_m) \end{pmatrix} \equiv \mathbf{HS_2} \quad (4\text{-}6)$$

The estimate of $s_2(x_j)$ by the least squares method is

$$\mathbf{S_2} = (\mathbf{H}^{\mathrm{T}}\mathbf{H})^{-1}\mathbf{H}^{\mathrm{T}}\mathbf{S_1}^{\mathrm{T}} \quad (4\text{-}7)$$

Figure 4-3(d) shows the result of these deconvolution processes on the waveform s_{0_ref} when there is no space charge, and the charges of the electrodes on both sides are displayed with the same magnitude.

Figure 4-4 shows the converting result of the signal (a), which includes the effect of space charge, into the distribution of charge density, electric field, and electric potential by deconvolution processing using the transfer function of the measurement system and the transfer matrix of the specimen system obtained in Fig. 4-3. In Fig. 4-4(c), a positive space charge, which seems to have been generated at the time of specimen preparation, is observed spread over the entire area. This charge was found to be stable for more than three years. The charge on the electrode is a surface charge, but the measurement results have a certain spread because high-frequency components are usually removed by a Gaussian filter or the like. However, the problem in this chapter refers to the electric field component (arrowed area in Fig. 4-4(d)) that appears to be generated further outside of the surface charge. The integrated potential distribution (e) appears as if a potential distribution is generated within the electrode.

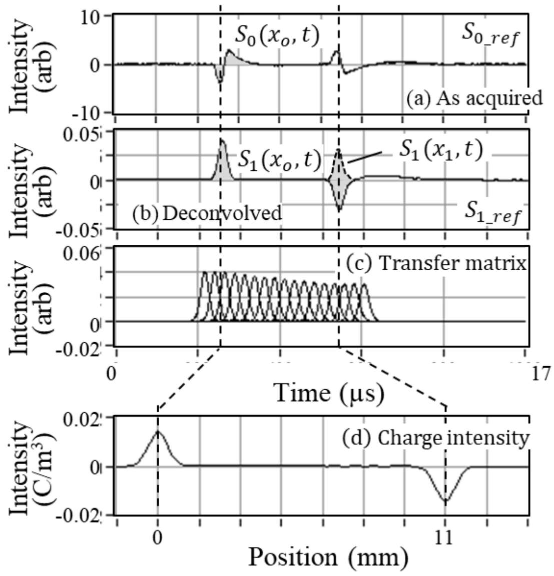

Fig. 4-3 Deconvolution process. $V_{\text{b\_ref}} = -7.5$ kV.

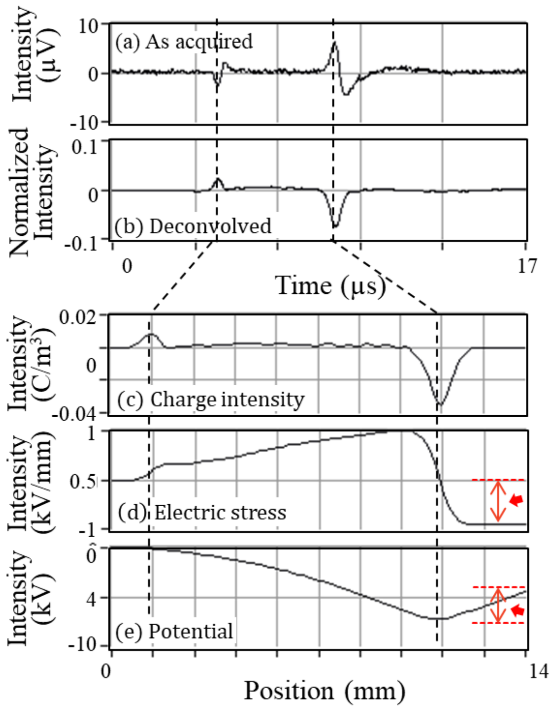

Fig. 4-4 Illustration of the disagreement among charge density, electric stress and potential. $V_{\text{b\_tgt}} = -7.5$ kV. Intensity in μV is input equivalent of the amplifier (piezo-sensor output).

Among the possible noise factors, high-frequency noise is considered to be mainly due to electromagnetic noise received from the outside and thermal noise of the amplifier, and since it is uncorrelated with the response signal, it can be reduced by averaging the waveforms. On the other hand, baseline offset and tilt are mainly due to spike noise caused by high-voltage pulses, and continue until the saturated amplifier output recovers due to overvoltage input, affecting the measurement results as the offset and tilt of the response signal. Since this noise has a strong correlation with the response signal, it cannot be reduced by additive averaging of waveforms. This effect remains as the same offset and slope after the deconvolution process. Figure 4-5 defines the offset and tilt within the time window of the signal measurement. x_L and x_R are the positions corresponding to the two ends of the time window of the analysis, converted from time based on sound velocity, and $\widehat{s_2(x)}$ is the signal representing the true charge density distribution. When the specimen is thick, the response signal is small and over a wide time domain, so the offset and tilt effects are relatively large. When calculating the electric field and potential, the integration of Equations (4-1) and (4-2) is performed along the time axis, so the error propagates backward and becomes apparent.

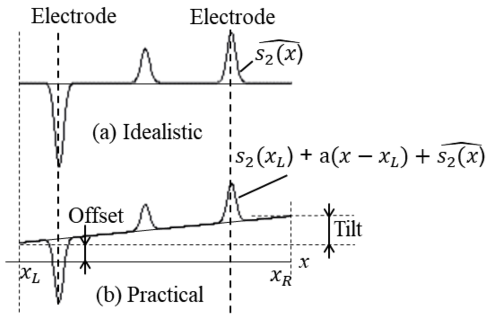

Fig. 4-5 Definition of (a) offset and (b) tilt of the baseline.

4.4 Measurement of the baseline fluctuation

Figure 4-6(a) shows the noise of the system measured prior to the space charge measurement. For this measurement, a small gap as thin as less 1 mm has been voluntarily set between the specimen and the acoustic coupler, to prevent any signal from the specimen.. Therefore, all the signals in this case could be recognized as noises. During signal acquisition, the acoustic signal is superimposed on this baseline. In (b), the offset and tilt are calculated from this waveform, and their time trends are displayed every 20 seconds. The tilt is converted to the difference between the values on both sides (t_L and t_R) of the time window of analysis and displayed. In this measurement example, the offset fluctuates about 1% and the tile fluctuates up to about 2% with respect to the signal intensity (sensor output equivalent of about 5 μV) during the space charge measurement described below. (d) is the spectrum of the slope variation, which shows that long-period variations reaching several mHz are included.

This degree of baseline and its variation does not introduce a large error in the charge distribution, but it does introduce a non-negligible error as it is integrated along the time axis in the process of calculating the electric field and potential. The reference signal also has a baseline offset and tilt, but this effect can be cancelled if the reference waveform is obtained by correlating the change in response when the bias voltage is varied. The baseline of the target signal is considered to vary during the measurement.

Figure 4-7 shows the results of 10 measurement analyzes under the same conditions as in Fig. 4-4, calculated from waveforms continuously acquired every 20 seconds. The charge density distribution is relatively uniform, but the electric field and potential distributions vary widely.

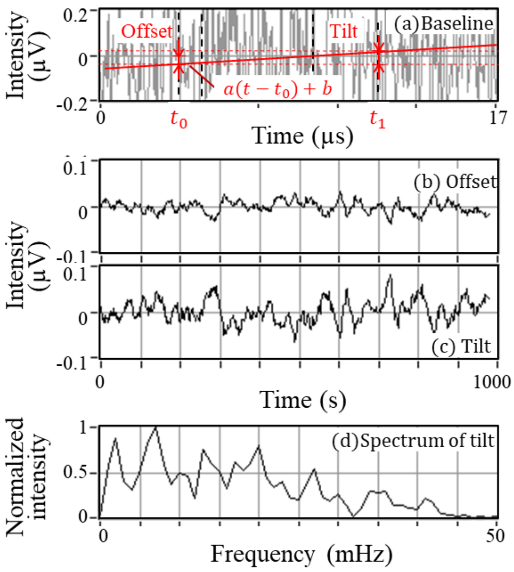

Fig. 4-6 Fluctuation in offset and tilt.

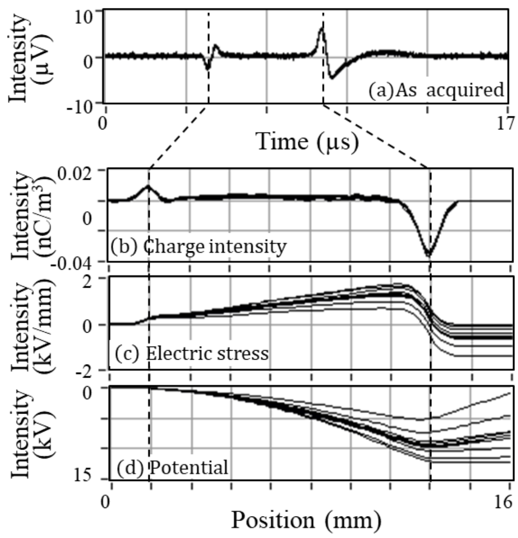

Fig. 4-7 Distributions of (b) charge density, (c)electric stress and (d) potential.

$V_{\mathrm{b\_tgt}} = -7.5$ kV. Without compensation.

4.5 Recovery

The waveform $s_2(x_j)$, obtained as a signal representing the charge distribution after the first and second type deconvolution process, and is done by Taylor Expansion around the leftmost x_1 (x_L in the continuous system display) as,

$$s_2(x_j) = s_2(x_1) + ax + \widehat{s_2(x_j)} \qquad (4\text{-}8)$$

The leftmost value $s_2(x_1)$ is the offset. a is the tilt of the baseline. $\widehat{s_2(x_j)}$ is the correction value excluding the effect of the baseline and is proportional to the charge density, so integrating from the leftmost x_1 to the rightmost x_m will be zero at the right end according to Gaussian law. And based on

$$\sum_{j=1}^{m} \widehat{s_2(x_j)} = \sum_{j=1}^{m}\{s_2(x_j) - s_2(x_1) - ax_j\} = 0 \quad (4\text{-}9)$$

$$\frac{1}{2}a(x_m - x_1)^2 = \sum_{j=1}^{m}\{s_2(x_j) - s_2(x_1)\} \quad (4\text{-}10)$$

a and $\widehat{s_2(x_j)}$ are obtained. Expressing the charge density as $\rho(x) = K\widehat{s_2(x)}$ (shown in a continuous system for consistency with Equations (4-1) and (4-2)),

$$E(x) = K\frac{1}{\varepsilon}\int_{x_L}^{x} \widehat{s_2(x)}dx \quad (4\text{-}11)$$

$$V(x_R) = -\int_{x_L}^{x_R} E(x)dx = V_\mathrm{b} \quad (4\text{-}12)$$

where V_b is the bias voltage at waveform acquisition. Numerically integrating $\widehat{s_2(x)}$ to obtain K yields the charge density $K\widehat{s_2(x)}$, which is integrated to obtain the electric field distribution $E(x)$ and potential distribution $V(x)$.

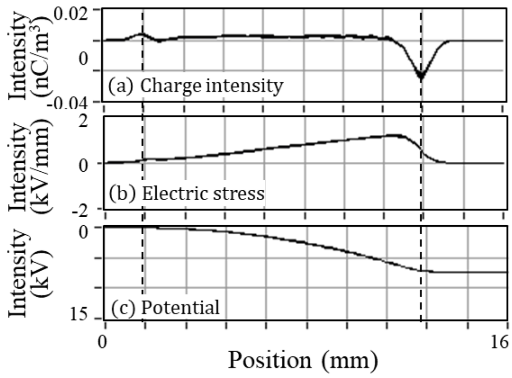

Fig. 4-8 Distributions of (b) charge density, (c)electric stress and (d) potential.

$V_\mathrm{b\_tgt} = -7.5$ kV. With compensation.

The results of the above recovery are shown in Fig. 4-8. The waveforms used in the analysis are the same as those in Fig. 4-5, but there is almost no variation in the charge density, electric field, and potential distribution. The fact that the electric field is zero and the electric potential is equal to the applied voltage at the right end is a natural result of such recovery, but there is no variation in the distribution within the specimen, indicating that the analysis is stable.

However, this method is less accurate when the bias voltage is low, and when $V_\mathrm{b} = 0$, the condition is indeterminate and K is not determined. Therefore, from $s_{2\_\mathrm{ref}}(x) + s_{2\_\mathrm{tgt}}(x)$, which is the sum of $s_{2\_\mathrm{ref}}(x)$ and $s_{2\_\mathrm{tgt}}(x)$, the result of deconvolution of the reference and target signals, we obtain $\widehat{s_{2\_\mathrm{ref}}(x) + s_{2\_\mathrm{tgt}}(x)}$ after recovery for offset and tilt, which represents the charge distribution when the bias voltage $V_\mathrm{b\_ref} + V_\mathrm{b\_tgt}$ is superimposed. According to

$$E(x) = K\frac{1}{\varepsilon}\int_{x_L}^{x}\{\widehat{s_{2\_\mathrm{ref}}(x) + s_{2\_\mathrm{tgt}}(x)}\}dx \quad (4\text{-}13)$$

$$V(x_R) = -\int_{x_L}^{x_R} E(x)dx = V_\mathrm{b\_ref} + V_\mathrm{b\_tgt} \quad (4\text{-}14)$$

the coefficient K can be obtained. By subtracting the charge distribution corresponding to the reference waveform (charge only on the electrode) from the obtained charge distribution, the charge distribution can be obtained when the bias voltage V_{b_tgt} is applied. The electric field and potential distribution also follow this procedure. When the voltage polarity of the reference waveform and the target waveform are different, the polarity of either reference signal and the bias voltage is reversed, and the sum of the both voltages is considered as the actual applied voltage and is brought into analysis.

Figure 4-9 illustrates the analyzing process. The bias voltages at the reference and target waveform acquisition are -7.5 kV and 0 kV, respectively. The electric field distribution obtained by applying baseline recovery to (a-3), which is the result of adding (a-1) and (a-2), which are the result of inverse superimposition of the first and second types of each waveform, is shown in (b-1). Since it represents the distribution when a bias voltage of -7.5 kV is applied to the specimen, the electric field distribution due to space charge when the bias voltage is 0 kV is obtained by subtracting the electric field distribution (b-2) acquired from the reference waveform. Space charge density distribution and electric potential distribution can also be calculated in a similar way.

Figure 10 shows an analysis of the results of 5 measurements made every 20 seconds with the bias voltage set to zero, followed by 5 similar measurements made with the bias voltage set to -7.5 kV, which shows stable results for space charge density, electric field, and potential.

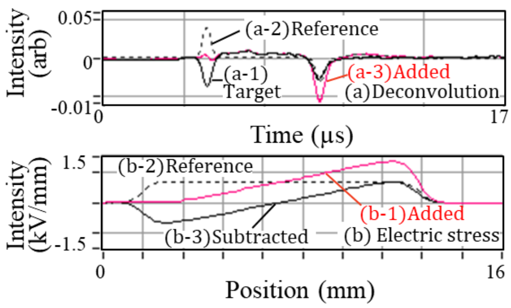

Fig. 4-9 Process for a signal acquired without bias voltage.

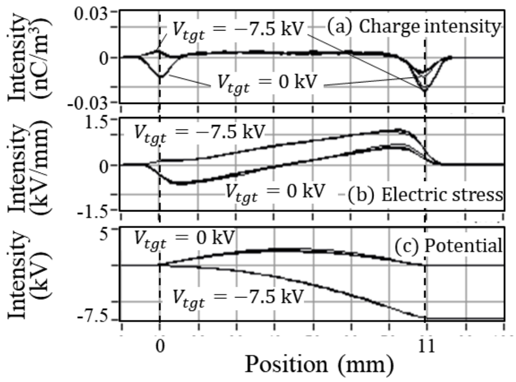

Fig. 4-10 Distributions of (a) charge density, (b)electric stress and (c) potential at 0 and -7.5 kV of bias voltages.

4.6 Investigation

As the author's goal is to accurately measure space charge in thick insulation systems such as ultra high-voltage cables and joints, and especially to evaluate the maximum electric field, which is problematic in insulation design. It is assumed that baseline fluctuations due to spike noise, which are treated in this chapter, especially affect the electric field distribution and have been an obstacle to accurate electric field calculations even in measurements of thin-leaf specimens where sufficient S/N ratio can be obtained. As a result, there are cases where the electric field leaks outside the right electrode in this paper (i.e., the electric field does not converge to zero away from the electrode interface) even after recovery for acoustic propagation. This violates Gaussian Law and is expected to cause errors in the calculation of the internal electric field as well.

As the specimen becomes thicker, the pulsed electric field tends to decrease, resulting in a lower S/N ratio, and the effect of baseline fluctuations becomes more significant. Fluctuations of 1-2% of the signal intensity measured in this chapter do not significantly affect the results of charge distribution calculations, but will introduce large errors in the field and potential distributions with thickness integration. According to Gaussian Law and the known applied voltage, it is considered to be available to do the analysis without the influence of baseline fluctuations based on the recovery. The previously reported reference signal acquisition method, in which a disturbance is applied to the bias voltage to obtain a correlation with the response signal, provides the shape of the impulse response (transfer function) of the measurement system at an arbitrary time during the measurement. The calibration method proposed in this chapter also takes into account the baseline information of the target signal, and in combination with the reference waveform acquisition method described above, it should be possible to deal with fluctuations in the measurement system, including the impulse response.

In this chapter, it was assumed that a perfectly acoustically matched system at the electrode interface on the far side from the piezoelectric sensor. In an ultra-high voltage power cable, there is no need to compensate for acoustic mismatch at this interface because there is a semiconducting layer inside the insulating layer that is almost acoustically identical to the insulating layer. However, if there is a metal electrode, which has different coefficients converted from charge density to acoustic signals at the top and bottom electrodes shown in Fig. 4-2, the recovery is necessary. Several methods have been proposed to compensate for known acoustic properties [13], but the quality of the analysis results is not sufficient, so the investigation for a method to extract acoustic property values directly from the reference signal has been made in this chapter. For temperature distribution in the insulation, it is possible to perform the compensation by referring to previous reports such as Morita et al.'s report on full-scale power cables [14].

4.7 Summary

In space charge measurements using the pulsed electroacoustic method on full-scale ultra high-voltage insulating systems, a method to display as accurately as possible the distribution of charge density, electric field, and electric potential was investigated. Although the thicker the specimen, the higher sensitive the measurement is necessary, it is shown by an actual example that non-negligible time fluctuations occur in the offset and tilt of the baseline of the acquired waveforms. In response to this, a method of correcting the signal to the extent that a contradiction with electromagnetism can be avoided was proposed, and its validity has been demonstrated through experiments. Combined with the reference waveform acquisition method described in the previous chapter, a relatively stable analysis was achieved, and the effectiveness of this method will be confirmed by applying it to measurements of full-scale ultra-high-voltage cables.

4.8 References

[1] K. Matsui, Y. Tanaka, T. Takada, T. Fukao, K. Fukunaga, T. Maeno and J.M. Alison: "Space charge behavior in low density polyethylene at pre-breakdown," in IEEE Transactions on Dielectrics and Electrical Insulation, vol. 12, no. 3, pp. 406-415, 2005.

[2] N. Hozumi, T. Okamoto and T. Imajo: “Space Charge Accumulation and Decay at The Interface Between Polyethylene and Ethylene - Vinylacetate Copolymer,” 8th International Symposium on High Voltage Engineering, Yokohama, Japan, pp.115 - 118 1993.

[3] A. Bradwell, R. Cooper and B. Varlow, "Conduction in Polyethylene with Strong Electric Field and the Effect of Prestressing on the Electric Strength", Proc. IEE, vol. 118, pp. 247-254, 1971.

[4] Mazzanti, J. Castellon, G. Chen, J.C. Fothergill, M. Fu, N. Hozumi, J. H. Lee, J. Li, M. Marzinotto, F. Mauseth, P. Morshuis, C. Reed, I. Troia, A. Tzimas and K. Wu. "The insulation of HVDC extruded cable system joints. Part 2: Proposal of a new AC voltage PD measurement protocol for quality control during routine tests," in IEEE Transactions on Dielectrics and Electrical Insulation, vol. 26, no. 3, pp. 973-980, 2019.

[5] K. Nagashima, Xiaokui Qin, Y. Tanaka and T. Takada, "Calibration of accumulated space charge in power cable using PEA measurement," ICSD'98. Proceedings of the 1998 IEEE 6th International Conference on Conduction and Breakdown in Solid Dielectrics (Cat. No.98CH36132), pp. 60-63, 1998.

[6] Y. Li, T. Takada: “Space Charge Distribution in Multi-Ply LDPE,” Proc. IEEE Conf. Electr. Insul. Diel. Phenom., pp. 397 – 402, 1992.

[7] Y. Li, T. Takada: “Progress in Space Charge Measurement of Solid Insulating Materials in Japan, IEEE Electrical Insulation Magazine,” Vol. 10, No.5, pp. 16 - 28 ,1994.

[8] 誘電・絶縁材料の空間電荷分布計測法と標準化調査専門委員会.「誘電・絶縁材料の空間電荷分布計測法と標準化」, 電気学会技術報告, 第 1367 号(2001).

[9] 誘電・絶縁材料の空間電荷分布計測法と標準化調査専門委員会.「高温下における PEA 法を用いた空間電荷分布測定の校正法標準化と PEA 法の応用測定技術」, 電気学会技術報告, 第 1491 号(2020).

[10] 李 暁欣, 川島 朋裕, 村上 義信, 穂積 直裕.「パルス静電応力法による空間電荷測定における波形変動を利用した較正手法の基礎検討」. 電学論 A，143 巻 4 号， pp.136 - 141, 2023.

[11] N. Hozumi, X. Li, T. Kawashima and Y. Murakami, "Fundamental Study on Calibration of Space Charge Distribution by Frequency-resolved Analysis," 2022 9th International Conference on Condition Monitoring and Diagnosis (CMD), Kitakyushu, Japan, pp. 142-145, 2022.

[12] Yeongguk An, X. Li, T. Kawashima, Y. Murakami and N. Hozumi: “Signal Processing for Space Charge Measurement Using Laplace Deconvolution”, Proc. CMD 2022 Kitakyushu, Japan, pp. 811-814.

[13] 賀新鈞, 川島朋裕, 穂積直裕, 村上義信.「パルス静電応力における電極系の音響特性を考慮した空間電荷分布補正」. 誘電・絶縁材料/電線・ケーブル合同研究会, pp. 31 – 34, 2023.

[14] 森田 翔亮, 川島 朋裕, 村上 義信, 穂積 直裕.「超高圧直流ケーブル用空間電荷計測における温度勾配下での信号歪みの補正方法の検討」. 電学論 B，140 巻 4 号, pp.271-276, 2020.

Chapter V

Demonstration measurement using 66 kV-class cable

In quantitative analyses using PEA method, a bias voltage is applied to a specimen without space charge and the signal generated by the electrodes only is considered as a reference waveform for calibration [1]. However, many full-size UHV insulation systems already contain space charge [2]. Therefore, in previous published paper (as well as in chapter 3), a way has been proposed to correlate the bias voltage with the response signal fluctuations to obtain a signal equivalent to the space-charge-free state [3].

For deconvolution, the signal generated by the electrodes when a bias voltage is applied to the specimen with no space charge. When there is a pre-existing space charge, the differential waveform of the response of different bias voltages can be used as an alternative reference signal. However, under high-temperature conditions, changes in space charge may appear within a few minutes after the bias voltage is applied, whereas voltage sources for ultra-high-voltage testing may take several minutes to change the voltage, and there is concern that the space charge may change during this time and the correct reference signal may not be obtained.

Therefore, the variations of bias voltage and response signal were decomposed into spectra and extracted reference waveforms based on the correlation, in a frequency range suitable for analysis [4]. This chapter presents the results of analyses of actual measurements using cross-linked polyethylene cables with an insulation thickness of 10 mm. The measurements were carried out at room temperature and at high temperature (conductor temperature 90°C).

5.1 Calibration method schematic

The upper portion of Figure 1 shows a space charge measurement on a parallel plate electrode system. For a specimen with a voltage imprinted history or thermal history, the space charge may be present prior to the application of a bias voltage. When a pulsed voltage is superimposed, the interaction between the charge and the pulsed electric field produces an acoustic pressure that is measured by a piezoelectric sensor. The acoustic pressure indicates the charge density and the propagation delay time indicates the charge position. The charge induced on the electrodes is a surface charge, and the signal from the electrodes close to the piezoelectric sensor represents the transfer function (impulse response) of the measurement system, so that deconvolution can be performed with reference to this signal to recover the charge distribution. Here, the signal obtained from the single side electrode as the source when there is no space charge is defined as the reference signal and the extraction method is discussed. For details, see references [3]-[4].

When the bias voltage varies, the acoustic signal fluctuates accordingly. For example, the main components of the signal at sampling points (a) and (c) in Fig. 5-1 correspond to the induced charge on the electrodes caused by the bias voltage and the space charge inside the specimen. The bias voltage fluctuates on the order of milliseconds to seconds, and the acoustic signal is sampled at intervals on the order of nanoseconds to microseconds. If the space charge is stable, this signal component is proportional to the change in bias voltage (with a constant offset), but if the space charge fluctuates with the bias voltage, the signal component due to the induced charge lags behind the change in bias voltage. The signal at sampling point (b) comes mainly from the space charge. If the space charge fluctuates with the change in bias voltage, this signal component will also be delayed with the change in bias voltage. When the variation of the acoustic signal in the frequency domain is normalized by the variation of the bias voltage, the trajectory of the signal component associated with the space charge takes on a shape close to a semicircle in the complex plane. No imaginary component appears on the high-frequency side of the trajectory, which indicates that signal component from this region follows the bias voltage without any time delay, and therefore it can be considered as unaffected by the space charge. Extraction of this component yields a reference signal.

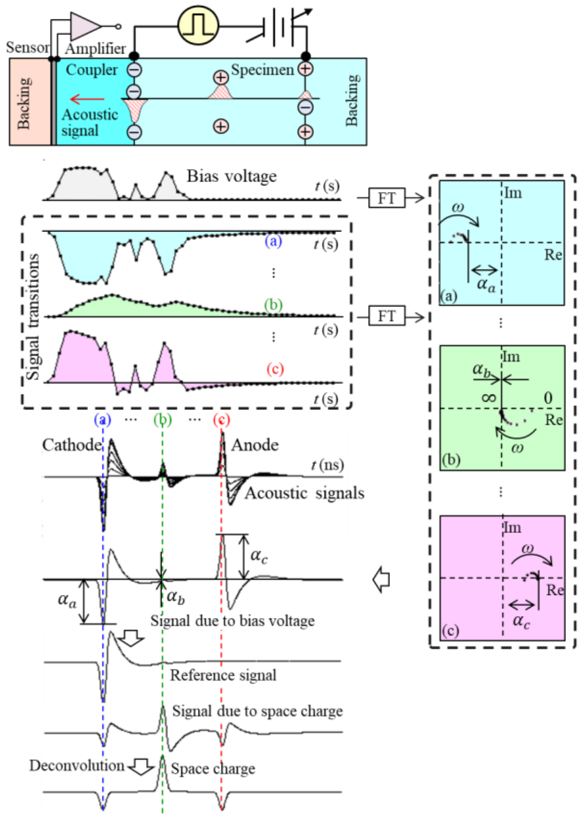

Fig. 5-1 Illustration of the analysis.

5.2 Experiment method

AC cross-linked polyethylene cables with an insulation thickness of 10 mm and a conductor radius of about 9.5 mm (including the internal semi-conductive electrodes) were used as test material. As shown in Fig. 5-2, the measurement loop was configured with a measurement loop and a dummy loop and the two loops were heated equivalently using a current transformer at currents up to 1500 A. the dummy loop was not applied with the DC voltage in order to monitor the temperature of the conductor by using a thermocouple. The temperature of conductor was maintained either at room temperature or 90 C referring to the conductor temperature of dummy loop. The measurement loop was fitted with a temperature sensor only on the surface, whereas the dummy loop was fitted with a temperature sensor on the inner layer of the conductor in addition to the surface. Under high-temperature measurement conditions, the temperature was controlled by directly detecting the conductor temperature of the dummy loop, which is assumed to be equal to the conductor temperature of the measurement loop [5]. The acoustic signals were detected by piezoelectric transducer through an amplifier and electro-optical converter with a bandwidth from DC to 10 MHz. In the experiment, the bias voltage and acoustic waveforms were recorded simultaneously while the bias voltage was varied. The measurements were carried out at room temperature and at a conductor temperature of 90 °C.

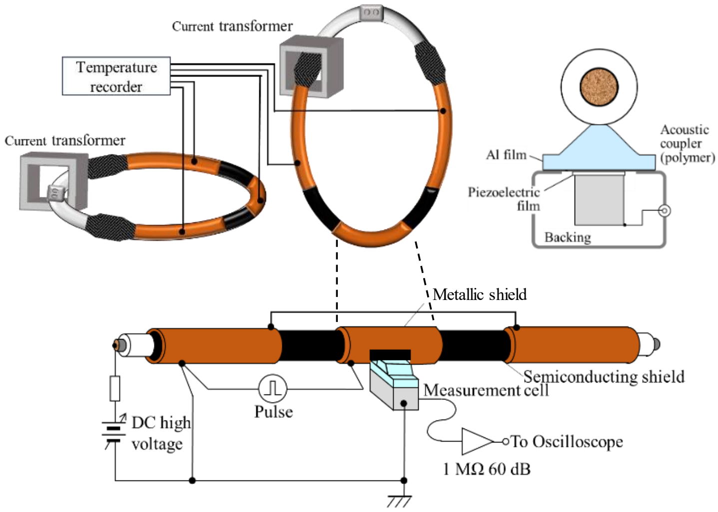

Fig. 5-2 Overview of experimental method.

5.3 Result and analysis

5.3.1 90℃

Figure 5-3 shows a bias voltage with a finite rise time applied at a conductor temperature of 90°C and its corresponding acoustic signals. The bias voltage (I) records 250 points every 2 seconds. The number of the corresponding response signals (III) is also 250, but the waveforms have been thinned out for ease of reading. Figure (II) shows the signal intensity at sampling points (a) and (b) near the electrodes. The specimen has a charging history and preliminary measurements indicate that a stable space charge already exists at the time of reception, and this can explain the offset appear in the figure (II) before the voltage application. The offset of the signal represents that the space charge was already existent when the measurement has been started. Since this component is independent of the bias voltage change, frequency analysis is performed after removing this component from the response signal.

Under this temperature conditions, space charge is generated and moves with the application of the bias voltage. At the sampling point (a), corresponding to the inner electrode, an imaginary component can be observed in the normalized spectrum and appears as a trajectory close to a semicircle. Since it is not an exact semicircle, the dielectric spectrum is treated as a multiple relaxation system.

The temporal variation of space charge is more pronounced on the side of the inner electrode where the temperature is higher and the electric field is stronger, which is thought to be due to the complex space charge polarization that occurs. This means that the polarization cannot be described by a single relaxation, but given that the space charge change in an insulator is always slower than the change in the bias voltage, it is possible to extract a reference signal from a band with no imaginary component on its high-frequency range, regardless of the shape of the semicircle. Above a frequency of about 7 mHz, there is almost no imaginary component, indicating that the fluctuations of the space charge do not follow the fluctuations of the bias voltage in this frequency range. The trajectory of the sampling point (b) on the side of the external electrode is almost centered on a single point and has almost no imaginary component. This indicates that the space charge fluctuations occur mainly on the side close to the inner electrode.

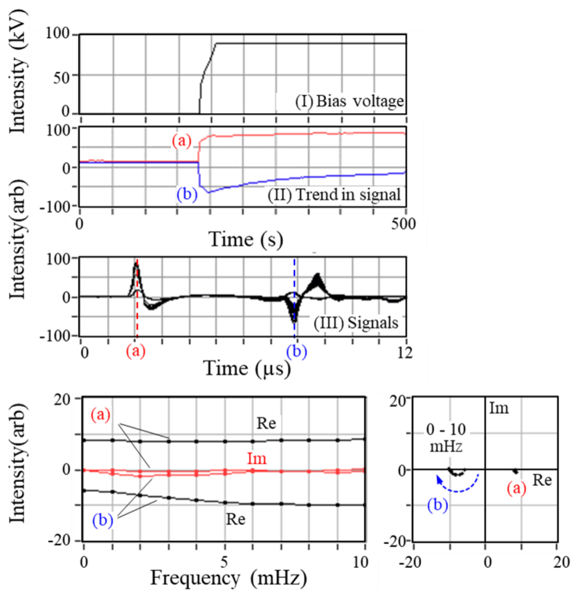

(IV) Frequency spectrum and trajectory

Fig. 5-3 Measurement results at conductor temperature 90°C.

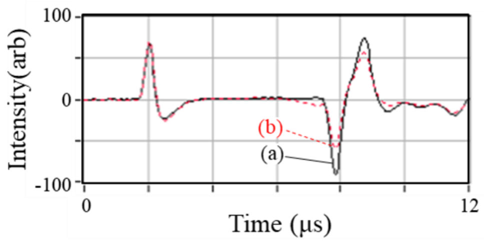

Fig. 5-4 Extracted calibration signals.

(a): components above 10 mHz are used; (b): components at 1 mHz are used.

Measurement results at conductor temperature of 90°C.

The signal reconstructed by averaging the normalized spectral intensities from 9 mHz to 10 mHz, where the frequency is relatively high, is shown in Fig 5-4(a). The reconstructed signal (b), based on the normalized spectral intensity at 1 mHz, is affected by space charge and shows a different shape from (a). This signal is not appropriate as a reference signal.

A schematic of the deconvolution process is shown in Fig. 5-5 [6]. S_{0_ref} representing the signal obtained by the above correlation algorithm. The signal $S_0(r_o, t)$ on the left side of the reference signal S_{0_ref} shown in (a) can be considered as the induced charge generated on the left (outer) electrode surface by the bias voltage, so the signal S_{1_ref} shown in (b) is obtained when the whole system is deconvolved with this as the impulse response (transfer function) of the system. Comparing $S_1(r_o, t)$ and $S_1(r_i, t)$, corresponding to the charges on the external and internal electrodes respectively, the frequency dependence of the sound velocity dispersion and acoustic attenuation over the specimen thickness can be determined. Note that $S_1(r_i, t)$ is the component from the inner electrode and was inversed into positive value to fit the calculation. This is interpolated to obtain the transfer function of the signal from the source at each point in the insulation layer to the electrode outside the sensor. These are enumerated to form the transfer matrix (c). The representation in diagram (c) is thinned out for clarity. The reconstructed signal (d) based on the transfer matrix represents the charge distribution. As the reference signal is not affected by space charge, signal (d) is a Laplace solution showing only the charges on the electrodes.

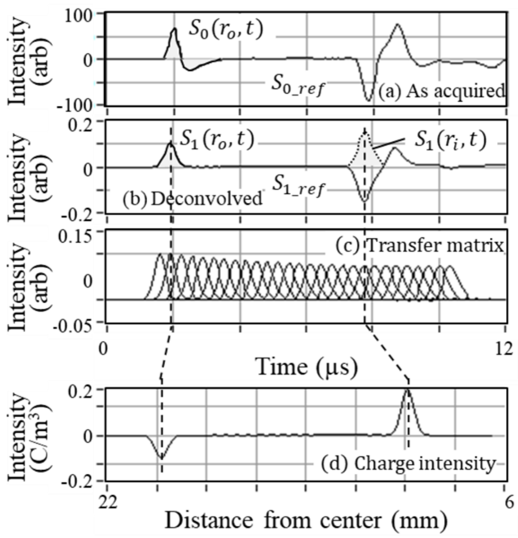

Fig. 5-5 Correction of acoustic signal propagation in the measurement and specimen system.

Figure 5-6 shows the result of using this transfer matrix for the signal (a) obtained after applying a 90 kV bias voltage for about 300 seconds. In the region of higher temperature, near the inner electrode, space charge of the same polarity (positive) is observed. Therefore, the electric field on the inner electrode side (d) is much lower than the Laplace solution. The slight positive charge on the outer electrode side was observed before the bias voltage was applied and is presumed to be a space charge stabilized by the charging history of the specimen.

At a conductor temperature of 90°C, the insulator has a temperature distribution and the acoustic characteristics vary with the distance from the center. Since the signal on the inner electrode side is the integral of this transfer function over the entire thickness of the insulator, it is necessary to correct for the temperature dependence of the acoustic properties to obtain an accurate transfer matrix [5]. Although this correction has not yet been made, the transfer functions of the signals originating from the bilateral electrode positions have been calculated, and since they are constrained (i.e., the transfer functions corresponding to the start and end points of the transfer matrix), the results calculated assuming uniformity of the acoustic properties (i.e., the results obtained in this report) do not differ significantly from those obtained by taking into account the temperature dependence. This will be discussed in more detail in the future.

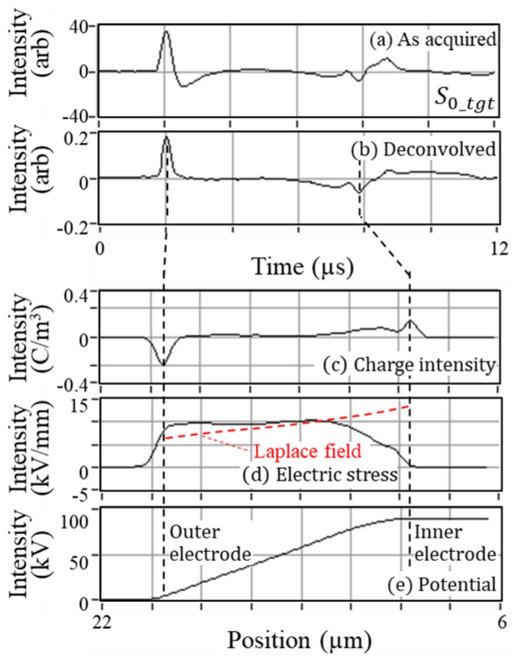

Fig. 5-6 Calculated results of charge, electric field and potential distributions at 90°C conductor temperature.

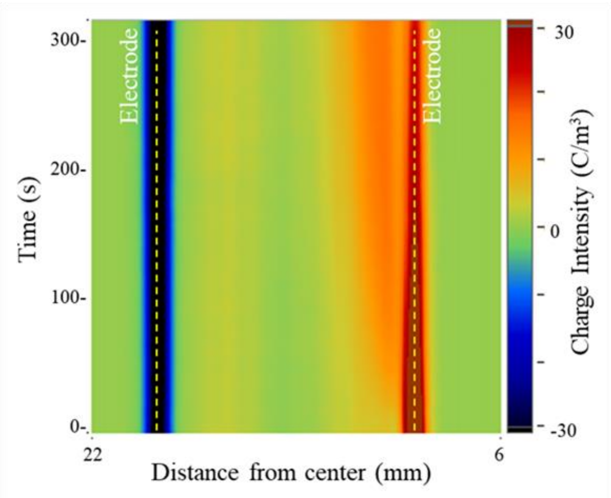

Fig. 5-7 Time variation of charge distribution when conductor temperature is 90°C and 90 kV is applied to the conductor. The bias voltage is considered to reach to its final value (90 kV) at 0 s.

Figure. 5-7 shows the change in time of the charge distribution after the bias voltage reached 90 kV, with the process of space charge formation starting from the warmer side of the inner electrode evident. It can also be seen that a stable space charge exists on the left side of the figure.

5.3.2 Ambient

Figure 5-8 shows the measurement results at room temperature (no loop current). The spectrum of the transition at points (a) and (b), which correspond to the electrode position, normalized by the transition of the bias voltage shows that almost no imaginary components are observed over a wide frequency range at any sampling point. This indicates that the intrinsic space charge is very stable and no new space charge is generated regardless of the bias voltage.

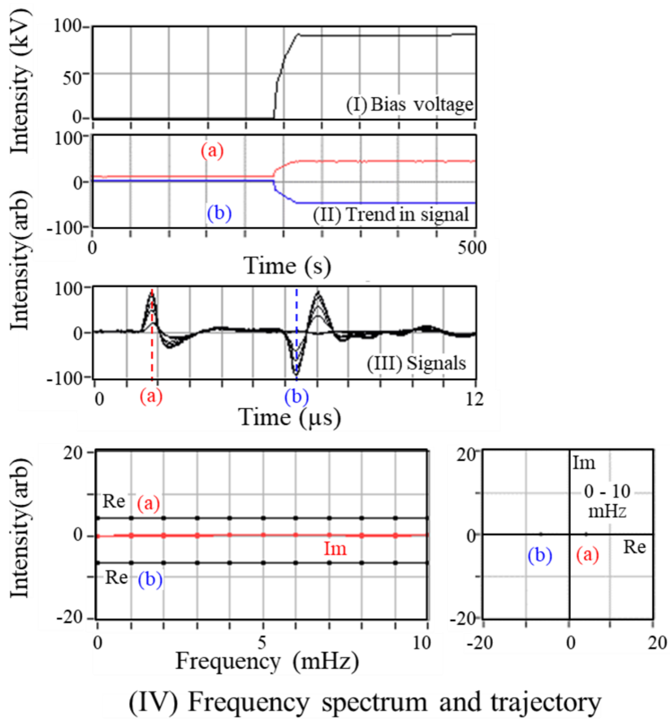

Fig. 5-8 Measurement results at ambient conductor temperature.

Under such conditions, the signal extracted from any frequency component is the same and can be used as a reference signal. The noise can sometimes be reduced by extracting an average signal weighted by spectral intensity. Figure 5-9 shows the results of charge and electric field distribution calculations based on the reference signal obtained, using a process similar to that shown in Fig. 5-5 and 5-6. The signals obtained immediately after the bias voltage reaches 90 kV and 240 seconds later are completely identical (Fig. 5-9 (a)), and the charge and field distributions are unchanged. The slight positive charge seen on the left side was generated by the history of voltage application before the specimen was received and remained stable.

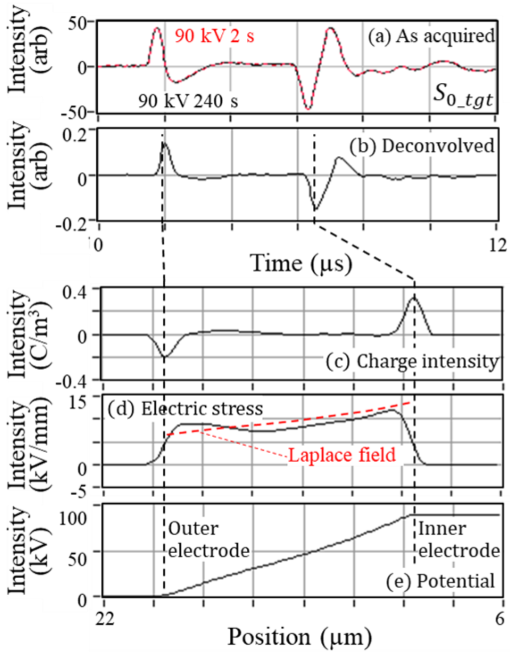

Fig. 5-9 Calculated results of charge, electric field and potential distributions at ambient conductor temperature.

5.4 Summary

Assuming a situation in which space charge tends to move in space charge measurement by the pulsed electroacoustic method, a method for acquiring a reference signal that is not affected by space charge, which is necessary for calibration, was studied.

While changing the bias voltage, the voltage and the response signal by the pulse electroacoustic method are sequentially acquired. When the space charge fluctuates in response to changes in the bias voltage, there is a delay in the response. When the spectrum of the response variation is normalized by the spectrum of the bias variation, a frequency trajectory similar to a semicircle associated with space-charge polarization is drawn.

In the frequency region where there is no imaginary component on the high-frequency side of the semicircle, the space charge fluctuation does not follow the bias voltage fluctuation, so the frequency component represents only the induced charge on the electrode caused by the bias voltage. It is extracted and used as the reference signal.

Using a cable specimen with an insulation thickness of 10 mm, measurements were made at room temperature, where there is almost no movement of space charge, and at conductor temperature of 90°C, where the space charge moves relatively quickly, to show that the above calibration method is applicable.

5.5 References

[1] K. Fukunaga, H. Miyata, M. Sugimori and T. Takada, “Measurement of Charge Distribution in the Insulation of Cables using Pulsed Electroacoustic Method”. IEEJ Trans. Fundam. Mater., 110, 647–648, 1990.

[2] C. Chen, C. Cheng, X. Wang and K. Wu, "Space Charge Characteristics for XLPE Coaxial Cable Insulation Under Electrothermal Accelerated Aging," IEEE Transactions on Dielectrics and Electrical Insulation, vol. 29, no. 2, pp. 727-736, 2022.

[3] X. Li, T. Kawashima, Y. Murakami and N. Hozumi. “Basic study on calibration using waveform variation in space charge measurement by pulsed electroacoustic method[J]”. Electrical Engineering in Japan, 2023, 216(2): e23436.

[4] N. Hozumi, X. Li, T. Kawashima and Y. Murakami, "Fundamental Study on Calibration of Space Charge Distribution by Frequency-resolved Analysis," 2022 9th International Conference on Condition Monitoring and Diagnosis (CMD), pp. 142-145, 2022.

[5] S. Morita, N. Fuse, T. Takahashi, T. Takahashi, S. Zahra and N. Hozumi, "Space Charge Measurement of 23-mm-Thick XLPE Cable at Ambient and High Temperatures," IEEE Transactions on Dielectrics and Electrical Insulation, vol. 29, no. 4, pp. 1491-1497, 2022.

[6] S. Zahra; S. Morita; M. Utagawa; T. Kawashima; Y. Murakami; N. Hozumi, P. Morshuis, Young-II Cho and Yoon-Hyoung Kim."Space Charge Measurement Equipment for Full-Scale HVDC Cables Using Electrically Insulating Polymeric Acoustic Coupler," IEEE Transactions on Dielectrics and Electrical Insulation, vol. 29, no., pp. 1053-10613, June 2022.

Chapter VI

Engineering Application Development

In this chapter, an overall summary of the research work is given. Further, an outlook for future research will be described.

6.1 Summary

In the following, the thesis work is summarized.

The main objective of space charge measurements in insulators is to observe charge behavior, while measuring and analyzing the spatial distribution and temporal variation of the resulting charge density is the most important focus of attention. The samples for space charge measurement experiments are mainly in the form of thin films with the aim of evaluating the fundamental properties of the material.

In the design of insulating systems, the maximum value of the electric field distribution distorted by space charge cannot exceed the maximum electric field allowed for practical insulating systems at high or very high voltages, but calculations based on the assumption of temperature dependence of the electric field and conductivity have been the main method of evaluation so far. Most researchers in prior studies have utilized measurements of thin film samples for their calculations, but it is difficult to obtain reliable results by applying thin film measurements directly to thick insulating systems because the similarity law is usually not valid for insulating systems. The author has therefore constructed devices capable of making direct measurements on materials with thicknesses similar to those of actual insulating systems by using polymer acoustic coupler with a metallic material as a backing.

And for a single test material that has been internally charged during the manufacturing process, lock-in calibration method is proposed that allows space charge measurements to be made even if there is only one sample. This method can be used to measure extra-high voltage insulation systems with charge histories.

In addition, the accuracy of the measurement is degraded due to the possibility that the distribution of space charge may change during the process before the varying measurement voltage reaches a stabilized state in real high-voltage insulation systems. In this regard, in this study, we have proposed the waveform correlation method to obtain the reference signal required for calibration by simply varying the bias voltage over time, which is calibrated by varying the bias voltage and correlating it with the change in the acoustic signal. By obtaining the reference signal after removing the effects of space charge and Maxwell stress, the distributions of charge, electric field and potential can be calibrated. Even with ultra-high voltage source biasing, no additional data sampling functions are required. In addition, the calibration signal can be acquired without changing the sample and measurement system conditions, even if the temperature distribution changes or a charging history exists.

Therefore, in this study, we propose the waveform correlation method, which can be used to obtain the reference signal required for calibration by simply varying the bias voltage over time, is calibrated by varying the bias voltage and correlating it with changes in the acoustic signal. Obtaining the reference signal after removing the effects of space charge and Maxwell stresses makes it possible to calibrate the distribution of charge, electric field and potential. No additional functions are required for data sampling, even when an ultra-high voltage source bias is used. In addition, even if the temperature distribution changes or a charging history exists, calibration signals can be acquired without changing the conditions of the sample and the measurement system.

Meanwhile, the time variation of space charge cannot be neglected in real insulating systems. Due to various factors such as the application of high-voltage DC field and high temperature, the condition of rapid movement of space charge with changing voltage occurs from time to time. Considering the situation, the author propose a frequency-resolved analysis method, which enables measurements in the case of space charge movement through simulations and practical experiments. In this method, the relationship between the bias voltage and the response signal change time is analyzed by Fourier transform to obtain the response spectrum. In the low-frequency region, an imaginary part of the spectrum appears due to the delay of the space charge with the bias voltage, whereas in the high-frequency region, the spectrum contains only the real part, indicating that the induced charge on the electrodes varies with the bias voltage without any delay. This reference signal is used to deconvolve the target signal to obtain a profile of the charge distribution.

It is also shown that in thick insulated systems, the charge density is integrated along the thickness direction when determining the electric field distribution, and therefore the computational errors propagate backwards, leading to large errors. In particular, it is noted that baseline and sensitivity fluctuations are not a major problem in thin-film measurements, but cause large errors in the electric field distribution in thick insulators, and therefore a method is proposed to address this problem with electromagnetically consistent calibration.

The method proposed above allows multiple calibrations to be performed at any time by applying small perturbations to the bias voltage as required, even when the signal transmission characteristics in the sample change during long-term pre-qualification tests (mainly due to temperature variations), so that accurate calibration can be performed at any stage during the test. This makes it possible to obtain an accurate electric field distribution at any stage of the test. This has been verified in experiments using power cables.

6.2 Engineering Applications

In the future outlook of the master's thesis, the researcher suggests that the future direction of research will be the size and complexity of insulators. Space charge measurements close to the actual full size of solid insulators have become a reality through the Ph.D. program phase of the research. As for the measurement of space charge distribution of insulating materials in cables, researchers in the same field have proposed the use of polymer materials as a sound coupler in the measurement system, and have fabricated devices that can be used for actual measurements [1]. Meanwhile, for actual cable under different voltage conditions for long periods of time in high-temperature environments, measurements of AC cross-linked polyethylene cables with an insulation thickness of 10 mm have also been obtained through a joint study with the Central Research Institute of Electric Power Industry, the experimental setup and conditions are shown in Fig. 6-1 [2]. However, there are still several pressing problems, as follows.

1. The upgrading of high-voltage insulation systems requires an in-depth study of various parameters of the insulation material, for which higher accuracy measurements of actual cables are required. The current proposal's correction method, which already allows for electromagnetic consistent calibration, does not yet provide an accurate

assessment of accuracy, which will need to be evaluated when the measurement analysis method is proposed as a standard.

2. At present, there is still a lack of standardized specimen for high-voltage insulation systems, i.e., “touchstones” against which other materials can be compared and evaluated by means of their measurement data. To find or produce such standard materials, a sufficient wealth of measurement data is required. At the same time, there is a demand for more accurate corrective methods and reliable measurement systems.

3. Most of the results obtained by the calibration method proposed and the measurement equipment constructed in the PhD project were obtained in a laboratory environment. In order to use the proposed correction method as an international standard measurement method, it is necessary to develop standard samples with known intrinsic space charge distributions and to carry out a comparison activity of the measurement results, i.e. a round robin test, at various institutes as part of the process.

4. At the same time, to ensure that the proposed space charge measurement device can be adapted to the needs of actual field measurements, further modifications to the carrier material of the device are needed to achieve portability, sensitivity and accuracy. The combination of polymer material and air layer used in this paper basically realizes the miniaturization of the measurement device while ensuring the sensitivity of the measurement signal. However, the large oscillation of the signal in the structure inevitably results in the loss of the low-frequency components required for signal analysis and processing. Therefore, as a future research direction, it is necessary to conduct the necessary research toward realizing miniaturization of the measurement device while using metallic backing materials.

The aim of this study is to achieve quality assurance testing of, for example, extra-high voltage DC power cables by means of a proposed measurement analysis method. The measurement analysis method is flexible and allows calibration by applying slight disturbances to the bias voltage at any time during the test, thus ensuring the accuracy and reliability of the test results. The strategy of monitoring quality changes during actual operation was therefore also found to be practical. The sampling technique used in the measurements, on the other hand, can provide a strong support for the continuous monitoring of high-voltage insulation systems.

In addition to this, the potential for application of the research in the field of engineering is extensive.

Firstly, CRIEPI plans to build a long-term current test system that continuously monitors the electric field in order to track the performance of UHV DC cables in real time. In addition, 2D and 3D measurement techniques of space charge will be used to analyze cable connections, power electronics, etc., helping to gain a deeper understanding of their operating conditions. The introduction of charge microscopy will make it possible to measure the electric field around ultra-thin and ultra-small printed circuits, thus providing important data to support the development of micro-electronic devices.

In addition, for practical oil-immersed insulation systems, such as high-viscosity oil-immersed insulated cables, electric field measurements will be able to be monitored with high sensitivity in environments with high acoustic attenuation. The realization of this capability will depend on further improvements in measurement and analysis systems. The development of government standards for measurement and analysis methods is being undertaken in the IEEE DEIS Technical Committee ‘High Voltage DC Cable Systems (Cables, joints and terminations)’to ensure that the technology is standardized and scientifically sound. This series of research and practice will provide an important guarantee of safety and efficiency in the field of power transmission.

Fig. 6-1 The experimental setup and conditions of actual cable.

6.3 References

[1] S. Zahra, S. Morita, M. Utagawa, T. Kawashima; Y. Murakami and N. Hozumi, "Space Charge Measurement Equipment for Full-Scale HVDC Cables Using Electrically Insulating Polymeric Acoustic Coupler," in IEEE Transactions on Dielectrics and Electrical Insulation, vol. 29, no. 3, pp. 1053-1061, June 2022.

[2] S. Morita, N. Fuse, T. Takahashi, T. Takahashi, S. Zahra and N. Hozumi, "Space Charge Measurement of 23-mm-Thick XLPE Cable at Ambient and High Temperatures," in IEEE Transactions on Dielectrics and Electrical Insulation, vol. 29, no. 4, pp. 1491-1497, Aug. 2022.

Acknowledgements

I would like to express my sincere gratitude to the following people, thanks to whose support this thesis was completed:

Professor Hirofumi Takikawa, Professor Inada Ryoji and Professor Hironaga Uchida

For your constructive comments and suggestions.

Professor Yoshinobu Murakami

For the precious comments and all the helping especially during the presentation.

Associate Professor Tomohiro Kawashima and Laboratory Members

For all the commonplace days we spent together.

Professor Naohiro Hozumi

For your encouragement and selfless guidance, without which all these achievements would not have been possible. I have benefited greatly from your profound knowledge and rigorous style of governance. In addition, as the great moral support you have given me has given me the same confidence in facing the stage of life. I would also like to thank you for your kindness, which has enabled me not to feel lonely even when I am far away from my motherland.

Dr. Peter Morshuis

For your excellent guidance. You are the best guide both in research and travelling. I have benefited from your words and have learnt that the world is much wider than I thought.

Professor JUNE-HO LEE

For your care at the Academic Society. I am deeply touched and motivated by your passionate approach to research and life.

Professor Boxue Du

For all the warm encouragement and precious guidance.

Dr. Kazuto Kobayashi Honda Electronics' Team

For all the experience and kindness I received and making me feel at home.

Mom and Dad

For all the unreserved love and unconditional support. For all the days mom waiting and praying at home alone and all the motivation dad had given, making me go through all these.

Julie the emotional support Felis catus

As a precious little family member, you do bring me many beautiful moments. Your little purrs, silky touch of fur, and energetic figure are so precious and always make me feel truly pleasure and peace. Hope you will be with us long and healthy in the future.

All my lovely friends

Especially Shun Huang, Yingying Wu and Yixin Pan, for all the moments we have shared and will share together, even not at the same place I never feel apart. You are family members I chose on my own will.

研究実績

査読付学術論文

[1] 李暁欣，川島朋裕，村上義信，穂積直裕，「パルス静電応力法による空間電荷測定における波形変動を利用した較正手法の基礎検討」，電気学会論文誌 A（基礎・材料・共通部門誌），Vol.143, No.4, pp.136-141, 2023. (Chapter III Section 3.3)

[2] X. Li, T. Kawashima, Y. Murakami, N. Hozumi and P. Morshuis, "Calibration for Pulsed Electroacoustic Space Charge Measurement Using Frequency-Resolved Analysis," in IEEE Transactions on Dielectrics and Electrical Insulation, doi: 10.1109/TDEI.2024.3449269. (Chapter III Section 3.4)

[3] 李暁欣，川島朋裕，村上義信，穂積直裕，「パルス静電応力法による空間電荷測定におけるノイズのゆらぎによる計算誤差の低減」，電気学会論文誌 A（基礎・材料・共通部門誌）（Accepted）. (Chapter IV)

国際会議論文

[1] X. Li, S. Zahra, T. Kawashima, Y. Murakami and N. Hozumi, "Lock-in Calibration for Space Charge Measurement," 2020 IEEE 3rd International Conference on Dielectrics (ICD), Valencia, Spain, pp.391-394, 2020. (Chapter III Section 3.2)

[2] X. Li, M. Utagawa, Y. G. An, T. Kawashima, Y. Murakami and N. Hozumi, "Space Charge Measurement of Thick Insulating Materials," 2022 IEEE 4th International Conference on Dielectrics (ICD), Palermo, Italy, pp.502-505, 2022. (Chapter II)

[3] X. Li, Y. An, T. Kawashima, Y. Murakami and N. Hozumi, "Transfer Matrix for Space-charge Analysis of Insulating Systems with Complex Geometries," 2023 IEEE 4th International Conference on Electrical Materials and Power Equipment (ICEMPE), Shanghai, China, pp.1-4, 2023. (Chapter III Section 3.4)

[4] X. Li, S. Morita, T. Kawashima, Y. Murakami and N. Hozumi, " Correlative Calibration for Space Charge Measurement in Cables Using PEA Method," 2024 IEEE 5th International Conference on Dielectrics (ICD), Toulouse, France, 3C-12, 4 pages, 2024. (Chapter V)

国内会議

[1] 李暁欣，川島朋裕，村上義信，穂積直裕,「超音波顕微鏡を利用した三次元空間電荷観測の基礎検討」. 電気学会研究会資料（誘電・絶縁材料／電線・ケーブル合同研究会）, pp:17-21, 2021.

[2] 李暁欣，Shafira Zahra，歌川真生，川島朋裕，村上義信，穂積直裕,「厚い絶縁材料のための空間電荷測定システム」. 第 52 回電気電子絶縁材料システムシンポジウム, No. MVP-19, pp. 198-200, 2021.

[3] 李暁欣，Shafira Zahra，歌川真生，川島朋裕，村上義信，穂積直裕,「厚い絶縁材料のための空間電荷測定システム」. 電気学会研究会，pp. 72-78, 2021.

[4] 李暁欣, 歌川真生，安永国， 川島朋裕，村上義信，穂積直裕,「厚い絶縁体の空間電荷測定を目的とした音響伝搬路の検討」. 電気学会研究会資料（誘電・絶縁材料／電線・ケーブル合同研究会）pp. 41-46, 2021.

[5] 李暁欣, 川島朋裕，村上義信，穂積直裕,「超音波顕微鏡を利用した三次元空間電荷観測の基礎検討」. 令和 3 年度 電気学会全国大会, pp. 37, 2021.

[6] 李暁欣, 川島朋裕，村上義信，穂積直裕,「Fourier 解析を応用した空間電荷の較正」. 第 53 回電気電子絶縁材料システムシンポジウム, No. MVP3-4, pp. 208-210, 2022.

[7] 李暁欣, 川島朋裕，村上義信，穂積直裕,「誘電スペクトルを参照した空間電荷の較正とケーブル試料への適用」. 誘電・絶縁材料研究会/電線・ケーブル研究会, pp: 27-31, 2024.